

**DSPACE IMPLEMENTATION OF A GENERALIZED METHOD OF  
HARMONIC ELIMINATION FOR PWM BOOST TYPE RECTIFIER  
UNDER UNBALANCED OPERATING CONDITIONS**

KE CHEN

Bachelor of Electrical Engineering

Tsinghua University

July, 2005

submitted in partial fulfillment of requirements for the degree

MASTER OF SCIENCE IN ELECTRICAL ENGINEERING

at the

CLEVELAND STATE UNIVERSITY

November, 2008

This thesis has been approved  
for the Department of Electrical and Computer Engineering  
and the College of Graduate Studies by

---

Thesis Chairperson, Dr. Ana V. Stankovic

---

Department & Date

---

Committee Member, Dr. Lili Dong

---

Department & Date

---

Committee Member, Dr. Jerzy T. Sawicki

---

Department & Date

## **ACKNOWLEDGEMENTS**

I would like to thank my advisor, Dr. Ana V Stankovic, without whose guidance and involvement this work would not have been possible. Her enthusiasm and inspiration were extremely helpful in successfully pursuing this research work.

Special thanks to Ms. Adrienne B. Fox for taking care of countless numbers of things so well during my study in the department.

Thank you to my family and friends for standing by me while I was in the graduate program and working on the thesis. My deepest gratitude goes to my dear wife for her constant love and support.

**DSPACE IMPLEMENTATION OF A GENERALIZED METHOD OF  
HARMONIC ELIMINATION FOR PWM BOOST TYPE RECTIFIER  
UNDER UNBALANCED OPERATING CONDITIONS**

KE CHEN

**ABSTRACT**

In this thesis, the implementation of a generalized method of harmonic elimination for the PWM boost type rectifier under severe fault conditions in the power system is presented. This method has been implemented by using DSPACE RT1104 digital control system. Control loop has been designed for real-time DC link voltage regulation. The simulation and experimental results verify the feasibility of the control scheme for input-output harmonic elimination. With the proposed method, unity power factor can be achieved as well as low-order harmonic elimination. High quality input and output waveforms of the three-phase PWM boost type rectifier are obtained under extremely unbalanced operating conditions.

# TABLE OF CONTENTS

	<b>Page</b>
<b>NOMENCLATURE.....</b>	<b>VII</b>
<b>LIST OF TABLES.....</b>	<b>VIII</b>
<b>LIST OF FIGURES.....</b>	<b>IX</b>
<b>CHAPTER</b>	
<b>I. INTRODUCTION AND LITERATURE SURVEY.....</b>	<b>1</b>
1.1 Introduction.....	1
1.2 Literature Survey.....	5
<b>II. THEORETICAL ANALYSIS.....</b>	<b>12</b>
2.1 Unbalanced Operation of the PWM Boost Type Rectifier.....	12
2.2 Harmonic Elimination Method.....	15
2.3 Constraints of the Solutions.....	20
2.4 Solutions under Unbalanced Conditions.....	23
<b>III. SIMULATION RESULTS.....</b>	<b>28</b>
3.1 Control Strategy.....	29
3.2 Simulation Results.....	35
<b>IV. EXPERIMENTAL RESULTS.....</b>	<b>42</b>
4.1 Hardware Implementation.....	43

4.2	Experimental Results .....	54
<b>V.</b>	<b>CONCLUSIONS AND FUTURE WORK.....</b>	<b>78</b>
	<b>REFERENCES.....</b>	<b>80</b>
	<b>APPENDICES.....</b>	<b>82</b>
A.	MATLAB Program for Reference Calculation (open-loop operation).....	83
B.	MATLAB Program for Reference Calculation (closed-loop operation) ...	84
C.	Simulink Model of DC Link Voltage Control .....	85

## **NOMENCLATURE**

PWM: Pulse width modulation

THD: Total harmonic distortion

IGBT: Insulated-gate bipolar transistor

SRF: Synchronous Rotating Frame

## LIST OF TABLES

<b>Table</b>	<b>Page</b>
TABLE I: Comparison of Different Control Methods.....	11
TABLE II: Base Case Parameters .....	23
TABLE III: Simulation Cases.....	35
TABLE IV: Simulation Parameters .....	35
TABLE V: Simulation Currents and DC Link Voltage.....	40
TABLE VI: Efficiency of Simulation Results .....	40
TABLE VII: List of Apparatus and Equipment .....	49
TABLE VIII: Experiment Cases on Lab-Volt IGBT Bridge.....	55
TABLE IX: Measurement Setting .....	55
TABLE X: Comparison Simulation and Experimental Currents (Magnitude) .....	60
TABLE XI: Comparison of Reference, Simulation and Experimental Voltages .....	60
TABLE XII: Comparison of Simulation and Experimental Efficiency .....	61
TABLE XIII: List of Total Harmonic Distortion of Line Currents.....	73
TABLE XIV: Function Block Time Consumption.....	76



## LIST OF FIGURES

<b>Figure</b>		<b>Page</b>
Figure 1:	The boost type rectifier .....	2
Figure 2:	Structure and power flow of PWM boost type rectifier [18] .....	6
Figure 3:	Dual current control system block diagram [17] .....	7
Figure 4:	Input voltages variation of PWM boost type rectifier .....	13
Figure 5:	Input currents and DC link voltage with unbalanced input voltages .....	14
Figure 6:	PWM boost type rectifier under unbalanced voltages and impedances ...	15
Figure 7:	Phasor representation of balanced input voltages .....	17
Figure 8:	Program flow chart .....	22
Figure 9:	Reference currents of balanced case .....	23
Figure 10:	Reference currents when the magnitude of $U_3$ decreases .....	24
Figure 11:	Reference currents when the angle of $U_3$ decreases .....	25
Figure 12:	Reference currents when the angle of $U_3$ increases .....	25
Figure 13:	Reference currents when $Z_3$ varies .....	26
Figure 14:	Diagram of simulation circuit and a current controller .....	29
Figure 15:	Diagram of current control loop (open-loop operation) .....	30
Figure 16:	Reference currents generation in open-loop mode .....	31

Figure 17:	Diagram of DC voltage control loop ( the outer loop).....	32
Figure 18:	Diagram of current controller ( closed-loop operation).....	33
Figure 19:	Reference generation in open-loop mode .....	34
Figure 20:	DC link voltage and line currents of case 1 .....	36
Figure 21:	DC link voltage and line currents of case 2 .....	37
Figure 22:	DC link voltage and line currents of case 3 .....	37
Figure 23:	DC link voltage and line currents of case 4 .....	38
Figure 24:	DC link voltage and line currents of case 5 .....	38
Figure 25:	DC link voltage and line currents of case 6 .....	39
Figure 26:	DC link voltage and line currents of case 7 .....	39
Figure 27:	Simulation result of closed-loop operation, based on case 3 .....	41
Figure 28:	DSPACE DSP controller board .....	43
Figure 29:	Diagram of PWM boost type rectifier with harmonic elimination .....	44
Figure 30:	Diagram of hardware configuration.....	47
Figure 31:	Dead time waveform definition .....	48
Figure 32:	Schematic of one phase IGBT drive circuit.....	48
Figure 33:	Designed IGBT drive board.....	49
Figure 34:	Diagram of Simulink model for open-loop operation.....	50
Figure 35:	Diagram of Simulink model for closed-loop operation .....	51

Figure 36:	Digital hysteresis controllers in Simulink.....	52
Figure 37:	Diagram of the DSPACE control desk .....	53
Figure 38:	Line currents and DC link voltage of case 1 .....	56
Figure 39:	Input voltages, DC link voltage and line currents of case 2 .....	56
Figure 40:	Input voltages, DC link voltage and line currents of case 3 .....	57
Figure 41:	Input voltages, DC link voltage and line currents of case 4 .....	57
Figure 42:	Input voltages, DC link voltage and line currents of case 5 .....	58
Figure 43:	Input voltages, DC link voltage and line currents of case 6 .....	58
Figure 44:	Input voltages, DC link voltage and line currents of case 7 .....	59
Figure 45:	Measured switching frequency in open-loop operation.....	59
Figure 46:	Angle between phase A voltage and current.....	62
Figure 47:	Angle between phase B voltage and current.....	62
Figure 48:	Spectrum of phase A current of case 1 .....	63
Figure 49:	Spectrum of phase B current of case 1.....	63
Figure 50:	Spectrum of phase C current of case 1.....	64
Figure 51:	Spectrum of phase A current of case 2 .....	64
Figure 52:	Spectrum of phase B current of case 2.....	65
Figure 53:	Spectrum of phase C current of case 2.....	65
Figure 54:	Spectrum of phase A current of case 3 .....	66

Figure 55:	Spectrum of phase B current of case 3.....	66
Figure 56:	Spectrum of phase C current of case 3.....	67
Figure 57:	Spectrum of phase A current of case 4 .....	67
Figure 58:	Spectrum of phase B current of case 4.....	68
Figure 59:	Spectrum of phase C current of case 4.....	68
Figure 60:	Spectrum of phase A current of case 5 .....	69
Figure 61:	Spectrum of phase B current of case 5.....	69
Figure 62:	Spectrum of phase C current of case 5.....	70
Figure 63:	Spectrum of phase A current of case 6 .....	70
Figure 64:	Spectrum of phase B current of case 6.....	71
Figure 65:	Spectrum of phase C current of case 6.....	71
Figure 66:	Spectrum of phase A current of case 7 .....	72
Figure 67:	Spectrum of phase B current of case 7.....	72
Figure 68:	Spectrum of phase C current of case 7.....	73
Figure 69:	Experimental result of closed-loop operation, 20V voltage change .....	74
Figure 70:	Experimental result of closed-loop operation, first step change.....	75
Figure 71:	Experimental result of closed-loop operation, second step change .....	75
Figure 72:	Measured switching frequency in closed-loop operation .....	76
Figure 73:	Diagram of main model for DC link voltage control.....	85

Figure 74:	Diagram of DC voltage error feedback block.....	85
Figure 75:	Diagram of real-time reference calculation block .....	86
Figure 76:	Diagram of real-time reference currents generation block .....	86

# **CHAPTER I**

## **INTRODUCTION AND LITERATURE SURVEY**

### **1.1 Introduction**

The AC/DC converters, also known as rectifiers, are very common and vital to the industry and people's daily lives, because a large portion of generated electric power is to serve DC type load. Almost all applications have rectifiers, with the exception of motors, heaters and lighting which are operated at the power-line frequency [1]. However, traditional diode and thyristor rectifiers create a series of problems during their operation: low displacement power factor due to excessive reactive power on AC side, AC side power lines pollution caused by line current distortions, EM interference, etc.

Compared with conventional rectifiers, PWM switched mode rectifiers gain more attentions from both academic researchers and industrial users. The boost type rectifier has been increasingly employed for high performance applications [2]. Fig.1 illustrates its basic circuit diagram. The PWM boost type rectifier can provide sinusoidal input line current with unity power factor and high quality DC output voltage with a small output

filter capacitor. It also offers the capability for nearly instantaneous reversal of power flow and power factor management. These advantages lead to the reduction of current ripples and voltage distortion, smaller size of input and output filters, reduced losses and magnetic noise. Thus, overall system performance is improved. The input-output characteristics of the PWM rectifier make it suitable for applications like magnet power supplies [3], DC motor drives [4], front end DC link of voltage source and current source inverters [5], reactive power control, harmonic compensation, and utility interactive photovoltaic systems [6].

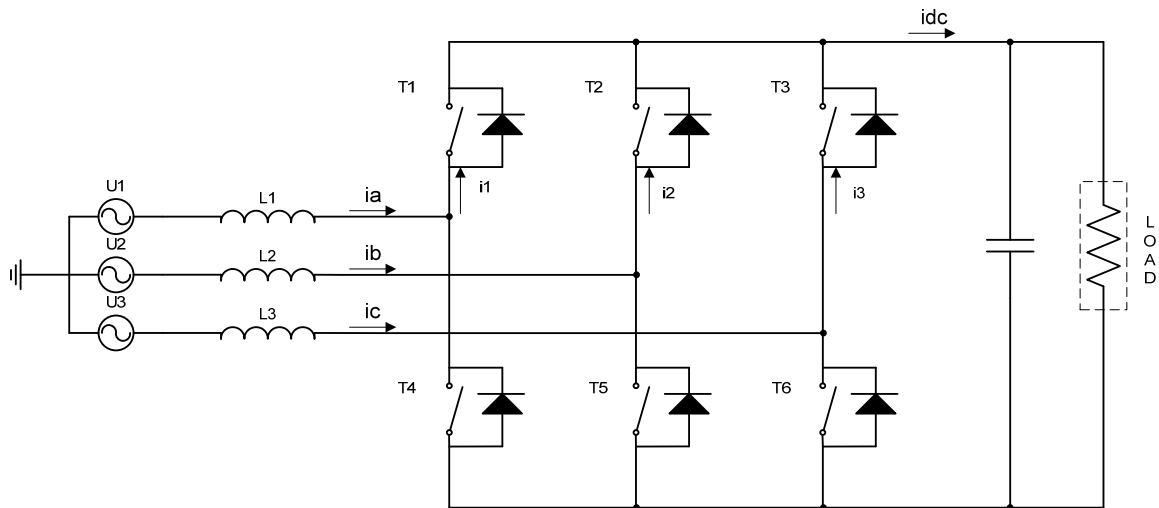


Figure 1: The boost type rectifier

However, all of these advantages of the PWM boost type rectifier can only be obtained under balanced input conditions. When the input supply is unbalanced, the performance is not necessarily improved. Such an unbalanced condition occurs frequently, especially in weak AC systems. A major cause of voltage imbalance is the non-uniform distribution of load in a three-phase system. This is particularly true for rural distribution systems or large urban systems which have heavy single-phase demand [7].

An unbalanced condition can also be caused by asymmetric transformer windings or transmission impedances. Regardless of the causes, unbalanced voltage inputs can drastically influence the performance of PWM boost type rectifiers. Particularly, abnormal low frequency harmonics appear at both input and output sides under unbalanced operating conditions. It has been shown in [8] that unbalanced input supply leads to large even-order harmonics at the output voltage. This in turn results in odd-order harmonics at the input line current and pollutes the utility. Such harmonic pollution has been a growing concern in recent years.

Two approaches can be applied to eliminate the harmonics of the DC link voltage and AC side line currents. One approach is to use bulky filters to remove ripples in output voltage and input currents. But this would slow down the dynamic response of the PWM boost type rectifier [9]. The other approach is to use active control schemes to minimize the harmonics. In this case, smaller filters can be applied to improve rectifier dynamic response. There are numerous papers about the PWM boost type rectifier, and several control schemes have been proposed based on the stationary frame and rotating frame methods [9]-[21]. However, most of them only consider regulation of PWM boost type rectifier under slight to medium levels of imbalance. Moreover, no implementations under extremely unbalanced conditions are obtained. In [13], the authors propose a completely new strategy for input-output harmonic elimination under extremely unbalanced operating conditions. The power factor can be adjusted at the same time when harmonics are eliminated. However, it has not been implemented after being published.

This thesis project uses DSPACE RT1104 digital control system to implement the control scheme in [13]. The results verify the feasibility of the proposed control method



for input-output harmonic elimination for the PWM boost type rectifier with extremely unbalanced input voltages and impedances.

Chapter II presents the derivation for harmonic elimination under unbalanced input voltages and unbalanced input impedances. This generalized control method is initially proposed in [14]. An analytical solution is obtained in the complex domain. The references for three-phase input currents are generated to eliminate undesirable low-order harmonics of the input and output at the rectifier. Some constraints are applied to the solution. And the impacts of imbalance in voltages and impedances are discussed.

Chapter III presents the simulation model in Simulink using the SimPowerSystems toolbox. The simulation is performed in both open-loop and closed-loop operation modes. Results are given to validate the proposed control method.

Chapter IV presents the configuration of the PWM boost type rectifier prototype and the implementation of the control scheme on DSPACE control system. Hardware devices and control diagrams are described in detail. Seven cases with different levels of unbalanced input voltages and impedances are studied.

Chapter V provides conclusions and suggestions for future study.

## 1.2 Literature Survey

### 1.2.1 Recent Studies on Harmonic Elimination of PWM Boost Type Rectifier

Rioual *et al.* [11] proposed a generalized model in d-q synchronous rotating frames (SRF) to regulate the instantaneous power for PWM rectifier under unbalanced supply voltages. Song and Nam [12] proposed a dual current control scheme in which positive and negative sequence currents are regulated separately by four PI controllers in positive and negative sequence SRFs.

In the past decade, most of studies [15] – [19] about PWM boost type rectifier under unbalanced operating conditions are based on the control scheme in [11] and [12]. The rectifier is analyzed in positive and negative d-q SRFs. Reference currents in positive and negative SRFs are obtained by solving a set of non-linear equations. A generalized matrix expression is shown in (1.1).

$$\begin{bmatrix} I_{dq} \end{bmatrix} = \begin{bmatrix} E_{dq} \end{bmatrix}^{-1} \begin{bmatrix} S_{in} \end{bmatrix} \quad (1.1)$$

$\begin{bmatrix} S_{in} \end{bmatrix}$  contains the setting of transferred power. The elements in  $\begin{bmatrix} E_{dq} \end{bmatrix}$  are non-linear combinations of voltage signals in positive and negative SRFs.  $\begin{bmatrix} I_{dq} \end{bmatrix}$  are calculated reference currents which are used to regulate actual three-phase currents of PWM boost type rectifier.

Suh *et al.* [15] [16] proposed a control scheme to eliminate harmonics in the output DC voltage under generalized unbalanced operating conditions. The proposed

technique nullifies the instantaneous ripple power at the rectifier input terminals (BB'). Zero average reactive power is maintained at the supply input terminal (AA') to obtain a unity power factor. Fig. 2 shows the structure and power flow of PWM boost type rectifier.

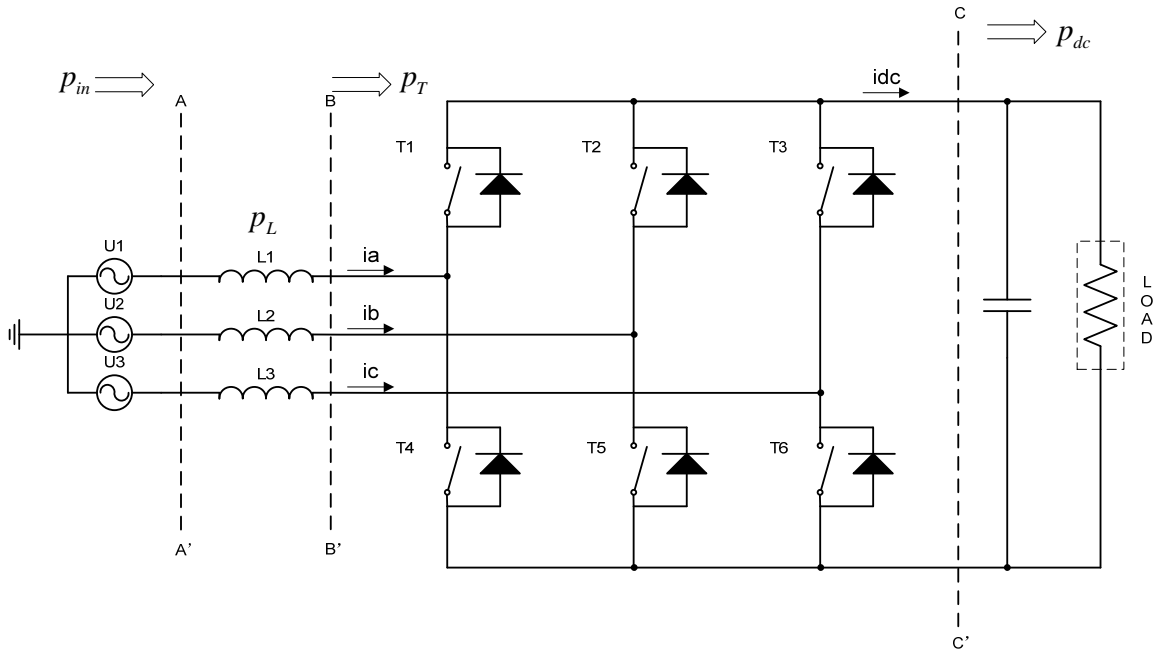


Figure 2: Structure and power flow of PWM boost type rectifier [18]

In [17], the authors linearized the equations by employing the rectifier terminal voltages as known variables to simplify the reference current calculating block. Furthermore, detailed discussion about the design of dual current controller is provided to improve the transient response of the PWM boost type rectifier.

The strategies proposed in [15], [16] and [17] have addressed the main issues in the control of PWM rectifier system. However, this approach requires a series of frame transformation and calculation which increase the complexity of its implementation. Fig. 3 shows the control block diagram of this method.

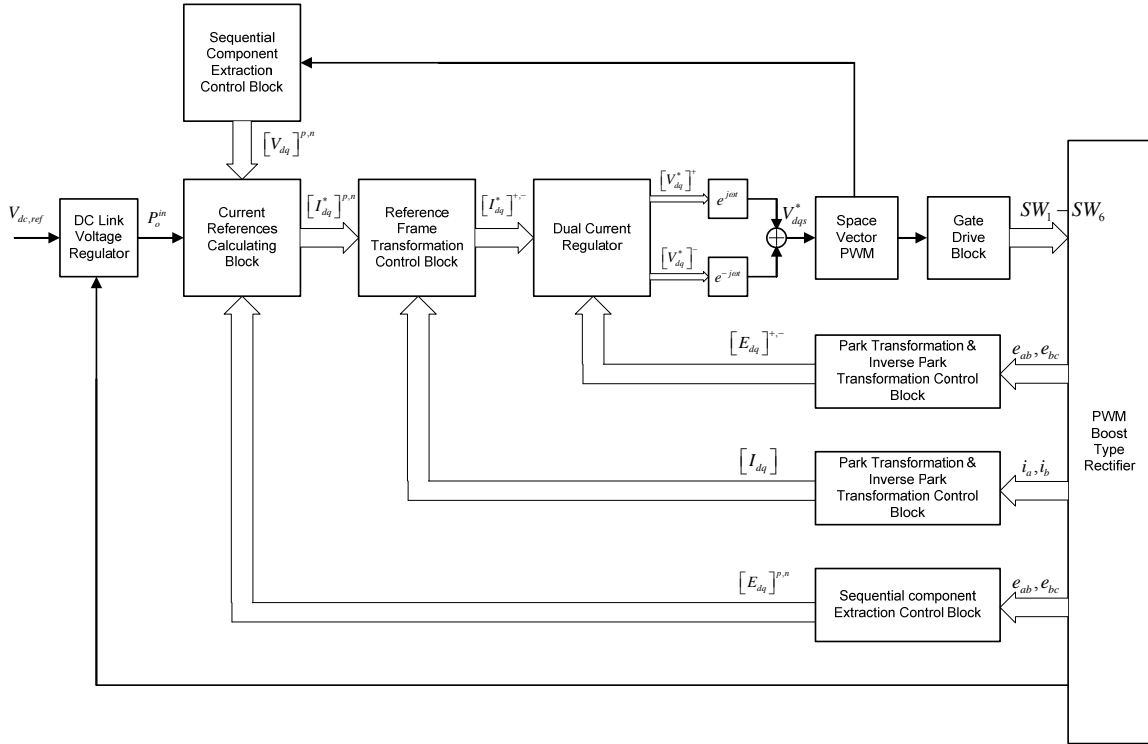


Figure 3: Dual current control system block diagram [17]

Although simulation and experimental results demonstrate the effectiveness of the proposed control method for harmonic elimination, no result under extremely unbalanced operating conditions is provided.

Yin *et al.* [18] further developed the ideas in [15], [16] and [17] and proposed an output-power-control strategy which can achieve good performance on both input and output sides of the rectifier. In this method, constant instantaneous power and zero reactive power are both maintained at the rectifier input terminals (BB'). Delivering constant power to DC side ensures a constant DC voltages with no or negligible low-order harmonics. However, the power factor cannot be directly controlled. And there is no result obtained under extremely unbalanced cases.

Wu *et al.* [19] presented a new mathematical model of a three-phase PWM boost type rectifier in the positive and negative SRFs, which can be used to accurately describe the dynamic behavior of PWM rectifier under the balanced and unbalanced operating conditions. However, the control scheme for harmonic elimination and its implementation are still the same as the method in [17].

Xiao *et al.* [20] presented a control scheme which decouples DC voltage and power factor control with fixed switching frequency. This method can provide balanced input line currents under the conditions of unbalanced and/or distorted supply voltages. A near-synchronous reference frame is used to avoid frame transformation. A predictive method is implemented to compensate computational delay. However, when the supply voltages are not balanced, the DC link voltage still contains even-order harmonics. Although simulation results indicate that the method can eliminate the harmonics in input currents, further experimental results are needed.

While most recent work about PWM boost type rectifier under unbalanced operating conditions uses positive and negative synchronous rotating frames, O. Ojo and Z. Wu [21] proposed a control method using untransformed state variables in abc frame. This method does not require synchronous reference transformation. However, the simulation and experimental results are only based on the condition of unbalanced impedances with balanced voltages. There is no unbalanced input voltages result to validate the generality of this method.

## 1.2.2 Comparison of This Thesis and Recent Studies

In this thesis, a generalized method of input-output harmonic elimination for PWM boost type rectifier [13] is implemented on a laboratory prototype using DSPACE RT1104 digital control system. The proposed method is general and can be used for all levels of imbalance in input voltages and input impedances. Its performance is verified by experimental results.

In contrast to most of the recent studies about PWM boost type rectifier [15] – [19], the method used in this thesis is using a rectifier model in abc frame. In the analysis and calculations, all variables are using phasor representation without any frame transformation or sequence conversion. This straightforward approach makes the control strategy easy to understand. It also saves calculation time of the control system in real-time implementation. Furthermore, there is no consequence error that may occur during reference frame transformation and degrade the operation of the controller.

In other studies, voltage vector space PWM controller is used, which requires the current references to be converted into proper voltage signals. In this thesis, hysteresis current controllers are used to regulate the actual three-phase currents. Three-phase current references are obtained through calculation. The hysteresis current controller can directly make the actual current track the reference. It is effective and easy to implement. However, there is one disadvantage of hysteresis current controller compared with voltage vector space PWM controller. The hysteresis current controller has a variable switching frequency while the voltage space vector PWM controller has a constant switching frequency, and this frequency may become very high under some particular

circumstances [22]. Fortunately, when the hysteresis controller is implemented on DSPACE digital control system in this thesis, the discrete sampling time performs as an inherent limit of the switching frequency.

Applying the proposed method in this thesis, the power factor can be adjusted in addition to the harmonic elimination. High quality input currents and output DC link voltage are obtained even under extremely unbalanced operating conditions. The experimental results demonstrate the feasibility of operating the three-phase PWM boost type rectifier from single phase supply without input-output harmonics. Such results are not provided in any previous study.

To conclude, the proposed control scheme in this thesis is a generalized method of input-output harmonic elimination for the PWM boost type rectifier. The analysis and calculation are based on the rectifier model in abc frame. After a set of current references are obtained, the hysteresis current PWM controllers directly regulate the actual currents to track the references. It requires less calculation or transformation in the control loop and reduces the calculation time of DSP (shown in Chapter IV). This method can be applied for all levels of imbalance in input voltages and input impedances. Effective harmonic elimination and power factor control are achieved. High quality input currents and output DC link voltage are obtained under extremely unbalanced cases. The results of extreme cases are not provided in previous studies

Table I provides a summary of the features of the proposed method in this thesis and other control schemes.

TABLE I: COMPARISON OF DIFFERENT CONTROL METHODS

	<b>Generalized Method in This Thesis</b>	<b>Power Control Method in [15]-[19]</b>	<b>Control Method in [21]</b>
<b>Model Frame</b>	abc Frame	d-q Synchronous Rotating Frame	abc Frame
<b>Current Regulation</b>	Current references in abc frame; actual currents directly track the references	Dual SRF current references; converted to voltage signal for current control	Current references in abc frame; converted to voltage signal for current control
<b>PWM Controller</b>	Hysteresis current controller; variable switching frequency	Voltage space vector controller; constant switching frequency	Voltage Sine-Triangle PWM controller; constant switching frequency
<b>Harmonic Elimination</b>	Good	Good	Good
<b>Power Factor Control</b>	Controllable power factor	Controllable power factor [13]- [17]; No direct power factor control in [18]	Controllable power factor
<b>Implementation</b>	Easy and straightforward; with fewer calculation blocks	Several frame transformation blocks are required	Extra controllers are required for current regulation
<b>Experimental Result</b>	Generalized method; results of extreme cases are provided	Unbalanced voltages and impedances cases are tested; No extreme case result	Only unbalanced impedance results are provided



## **CHAPTER II**

### **THEORETICAL ANALYSIS**

#### **2.1 Unbalanced Operation of the PWM Boost Type Rectifier**

The PWM boost type rectifier has several advantages such as approximately sinusoidal input currents, controllable power factor, and bi-directional power flow. Unfortunately, all these features can only be realized under three-phase balanced inputs. Under unbalanced operating conditions, the output DC voltage and the input currents of the PWM boost type rectifier are highly distorted.

It has been shown in [8] that unbalanced input voltages lead to an abnormal second-order harmonic in the DC link voltage which reflects back to the input, causing a third-order harmonic in the input line currents. This interaction continues back and forth and results in the appearance of even harmonics at the DC link and odd harmonics in the input currents.

Fig. 4 and Fig. 5 illustrate the operation of three-phase PWM boost type rectifier under unbalanced input voltages. Fig. 4 shows the variation of three-phase input voltages. The boost type rectifier is initially operated under three-phase balanced conditions. The magnitude of phase A voltage drops by 20% when  $t = 0.1$  sec, then the rectifier is operated under unbalanced input voltages. Assuming switching functions stay the same as for balanced conditions, low-order harmonics appear at both sides of the rectifier. Fig. 5 shows input currents and DC link voltage under unbalanced input voltages.

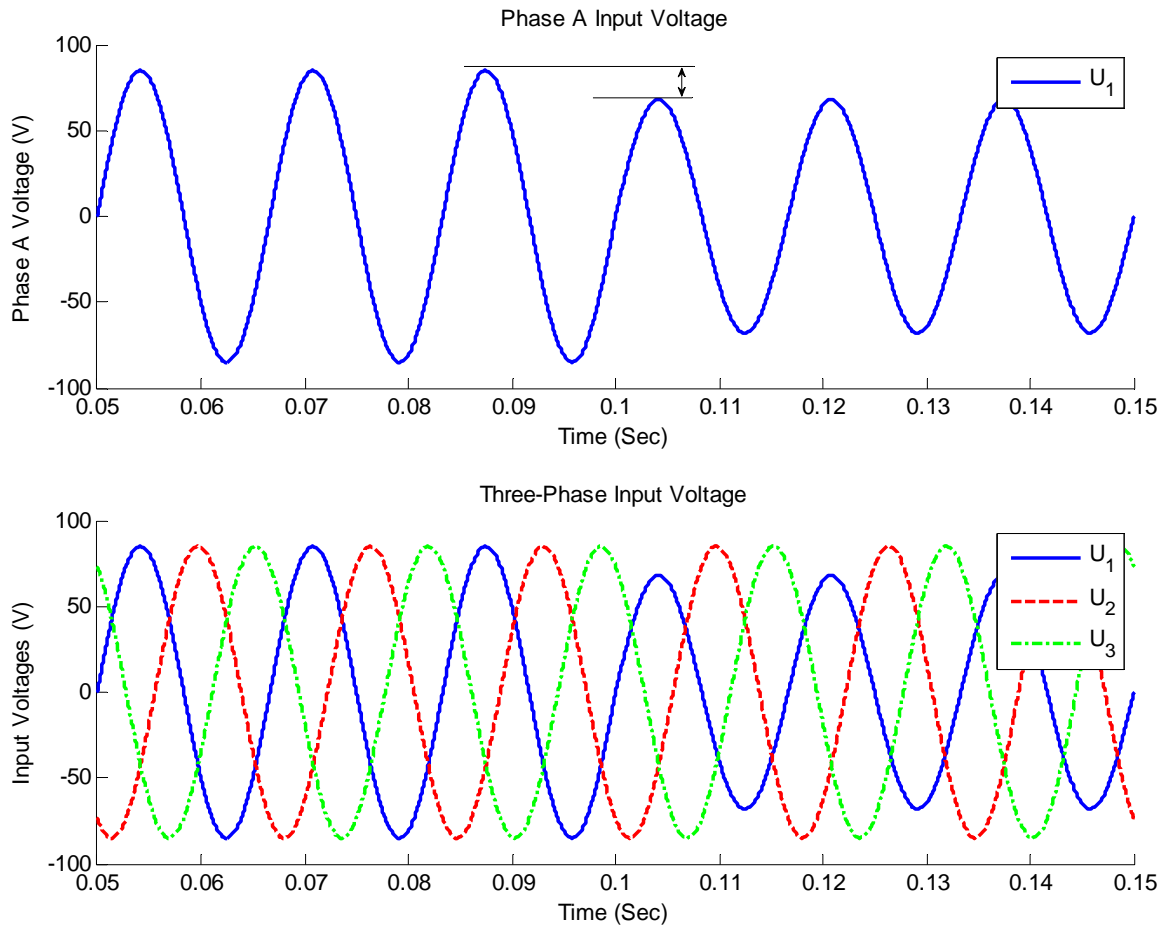


Figure 4: Input voltages variation of PWM boost type rectifier

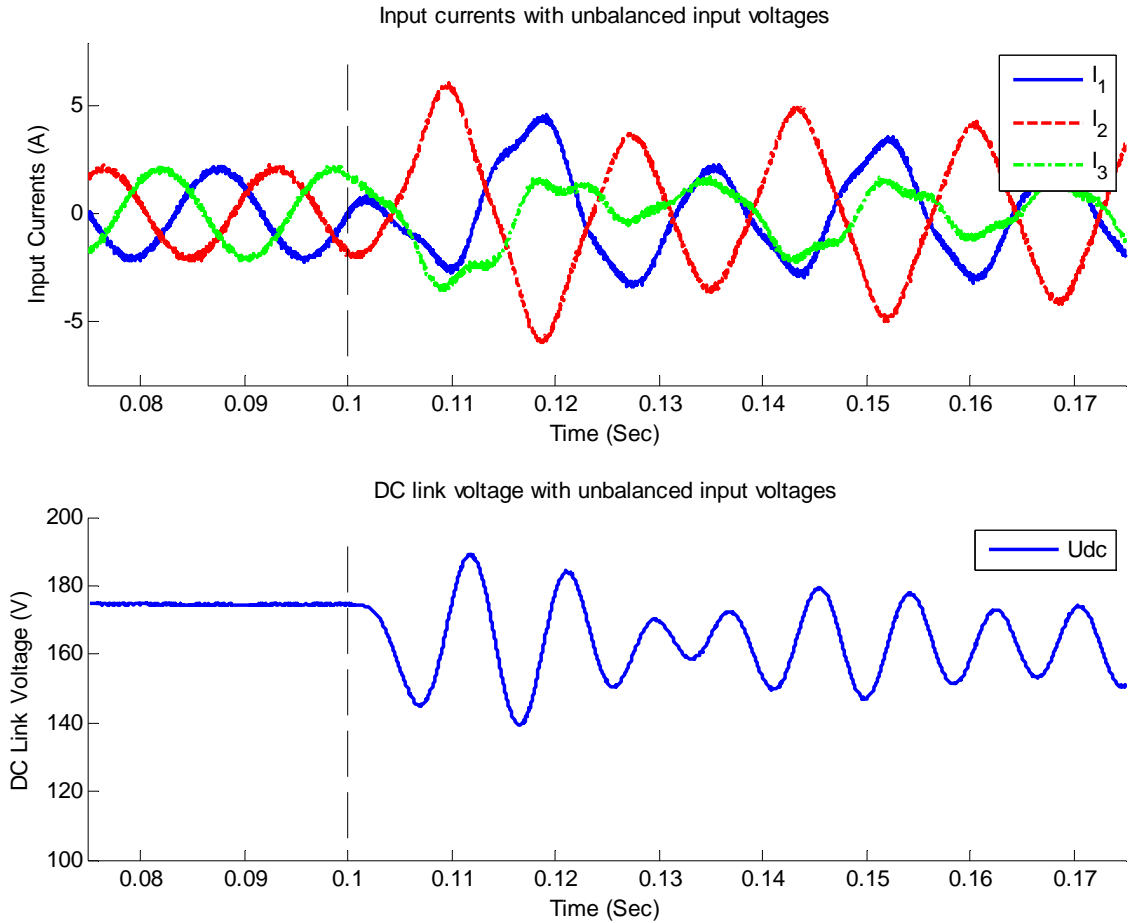


Figure 5: Input currents and DC link voltage with unbalanced input voltages

It can be seen that the PWM boost type rectifier has balanced three-phase sinusoidal input currents and ripple-free DC link voltage when input voltages are balanced. Under unbalanced operating condition, obvious second-order harmonic ripples appear in the DC link voltage. Three-phase input currents are also distorted due to the unbalanced input voltages. The magnitudes of input currents may become several times higher. This causes more conduction and switching losses, or even device damage.

## 2.2 Harmonic Elimination Method

Ana V. Stankovic and Thomas A. Lipo proposed a generalized method [13] of input-output harmonic elimination for PWM boost type rectifiers under severe fault conditions in the power system. For the circuit shown in Fig. 6, this method is derived with the following assumptions:

- Input voltages are unbalanced
- Input impedances are unbalanced
- The converter circuit is lossless

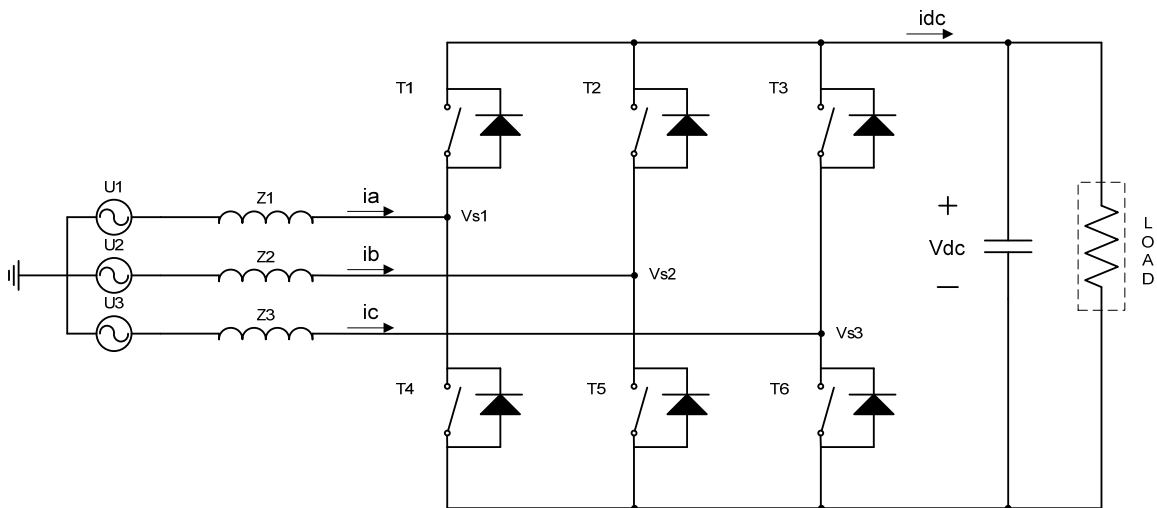


Figure 6: PWM boost type rectifier under unbalanced voltages and impedances

It has been shown in [13] that the complete harmonic elimination can be achieved under the following conditions shown in (2.1).

$$\left\{ \begin{array}{l} I_1 = -I_2 - I_3 \\ I_2 = \frac{S^* - I_3(U_3^* - U_1^*)}{U_2^* - U_1^*} \\ \left[ \frac{2z_1(U_3^* - U_1^*)}{U_2^* - U_1^*} - \frac{(z_1 + z_2)(U_3^* - U_1^*)^2}{(U_2^* - U_1^*)^2} - (z_1 + z_3) \right] I_3^2 \\ + \left[ (U_3 - U_1) - \frac{(U_3^* - U_1^*)(U_2 - U_1)}{U_2^* - U_1^*} - \frac{2z_1 S^*}{U_2^* - U_1^*} + \frac{2S^*(z_1 + z_2)(U_3^* - U_1^*)}{(U_2^* - U_1^*)^2} \right] I_3 \\ + \frac{S^*(U_2 - U_1)}{U_2^* - U_1^*} - \frac{(z_1 + z_2)S^{*2}}{(U_2^* - U_1^*)^2} = 0 \end{array} \right. \quad (2.1)$$

where  $U_1$ ,  $U_2$  and  $U_3$  are three-phase input voltages;  $z_1$ ,  $z_2$  and  $z_3$  are input line impedances;  $I_1$ ,  $I_2$  and  $I_3$  are three-phase input currents.  $S$  is the apparent power transferred from AC side to DC side.  $U_1^*$ ,  $U_2^*$ ,  $U_3^*$  and  $S^*$  are conjugates of the input voltages and apparent power.  $U_i$ ,  $z_i$ , and  $S$  are known variables whereas  $I_1$ ,  $I_2$ ,  $I_3$  are unknown variables. All these variables are using phasor representation in abc frame. The phasor magnitude is RMS value. By solving (2.1), three-phase currents can be calculated to achieve harmonic elimination.

$$\left[ \frac{2z_1(U_3^* - U_1^*)}{U_2^* - U_1^*} - \frac{(z_1 + z_2)(U_3^* - U_1^*)^2}{(U_2^* - U_1^*)^2} - (z_1 + z_3) \right] I_3^2 \\ + \left[ (U_3 - U_1) - \frac{(U_3^* - U_1^*)(U_2 - U_1)}{U_2^* - U_1^*} - \frac{2z_1 S^*}{U_2^* - U_1^*} + \frac{2S^*(z_1 + z_2)(U_3^* - U_1^*)}{(U_2^* - U_1^*)^2} \right] I_3 \\ + \frac{S^*(U_2 - U_1)}{U_2^* - U_1^*} - \frac{(z_1 + z_2)S^{*2}}{(U_2^* - U_1^*)^2} = 0 \quad (2.2)$$

The third equation of (2.1) is a quadratic equation with complex coefficients, which is re-written in (2.2). Three complex coefficients are listed below.

$$a = \frac{2z_1(U_3^* - U_1^*)}{U_2^* - U_1^*} - \frac{(z_1 + z_2)(U_3^* - U_1^*)^2}{(U_2^* - U_1^*)^2} - (z_1 + z_3) \quad (2.3)$$

$$b = (U_3 - U_1) - \frac{(U_3^* - U_1^*)(U_2 - U_1)}{U_2^* - U_1^*} - \frac{2z_1 S^*}{U_2^* - U_1^*} + \frac{2S^*(z_1 + z_2)(U_3^* - U_1^*)}{(U_2^* - U_1^*)^2} \quad (2.4)$$

$$c = \frac{S^*(U_2 - U_1)}{U_2^* - U_1^*} - \frac{(z_1 + z_2)S^{*2}}{(U_2^* - U_1^*)^2} \quad (2.5)$$

When the input voltages are balanced,  $U_1$ ,  $U_2$  and  $U_3$  have equal magnitudes and  $120^\circ$  phase shift between each other,  $U_1 = U_1^* = |U| \angle 0^\circ$ ,  $U_2 = U_3^* = |U| \angle -120^\circ$ ,  $U_3 = U_2^* = |U| \angle 120^\circ$ . Fig. 7 demonstrates the phasor representation of three-phase input voltages.

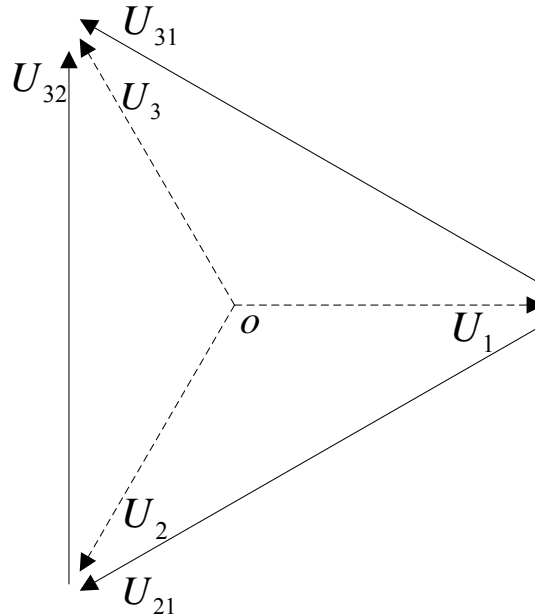


Figure 7: Phasor representation of balanced input voltages

Under balanced condition, the boost type rectifier has three equal input line impedances,  $z_1 = z_2 = z_3 = z$ . Transferred power is set to be  $S$ . The numerator of coefficient  $a$  can be simplified according to (2.3).

$$\begin{aligned}
NUM(a) &= 2z(U_2 - U_1)(U_3 - U_1) - 2z(U_2 - U_1)^2 - 2z(U_3 - U_1)^2 \\
&= 2z(U_{21} \cdot U_{31} - U_{21}^2 - U_{31}^2) \\
&= 2z(3|U|^2 \angle 0^\circ - 3|U|^2 \angle -300^\circ - 3|U|^2 \angle 300^\circ) \\
&= 0
\end{aligned} \tag{2.6}$$

The coefficient  $a$  is zero in balanced condition. Then, (2.2) becomes a linear equation, and  $I_3$  can be determined by coefficients  $b$  and  $c$ .

$$\begin{aligned}
b &= \frac{(U_3 - U_1)^3 - (U_2 - U_1)^2(U_3 - U_1) - 2zS^*(U_3 - U_1) + 4zS^*(U_2 - U_1)}{(U_3 - U_1)^2} \\
&= \frac{U_{31}^3 - U_{21}^2 U_{31} - 2zS^* U_{31} + 4zS^* U_{21}}{U_{31}^2} \\
&= \frac{-2zS^* U_{31} + 4zS^* U_{21} + 3\sqrt{3}|U|^3 \angle 90^\circ - 3\sqrt{3}|U|^3 \angle -150^\circ}{U_{31}^2} \\
&= \frac{-2zS^* U_{31} + 4zS^* U_{21} + 3|U|^2 U_{32} - 3|U|^2 U_{21}}{U_{31}^2} \\
&= \frac{-2zS^* U_{31} + 4zS^* U_{21} + 3|U|^2 (U_{31} - U_{21}) - 3|U|^2 U_{21}}{U_{31}^2} \\
&= \frac{2U_{21}(2zS^* - 3|U|^2) - U_{31}(2zS^* - 3|U|^2)}{U_{31}^2}
\end{aligned} \tag{2.7}$$

$$\begin{aligned}
c &= \frac{S^*(U_2 - U_1)(U_3 - U_1) - 2zS^{*2}}{U_{31}^2} \\
&= \frac{S^*(U_{21}U_{31} - 2zS^*)}{U_{31}^2} \\
&= -\frac{S^*(2zS^* - 3|U|^2)}{U_{31}^2}
\end{aligned} \tag{2.8}$$

$$\begin{aligned}
I_3 &= -\frac{c}{b} = \frac{(2zS^* - 3|U|^2)}{2(2zS^* - 3|U|^2) - (2zS^* - 3|U|^2)} \\
&= \frac{S^*}{2U_{21} - U_{31}} \\
&= \frac{S^*}{U_{21} - U_{23}} \\
&= \frac{S^*}{3U_3}
\end{aligned} \tag{2.9}$$

$I_2$  and  $I_3$  can be calculated from (2.1).

$$\begin{aligned}
I_2 &= \frac{S^* - I_3(U_3^* - U_1^*)}{U_2^* - U_1^*} \\
&= \frac{2S^*U_2 + S^*U_1}{3U_2(U_3 - U_1)} \\
&= \frac{S^*U_{23}}{3U_2U_{31}} \\
&= \frac{S^*}{3U_2}
\end{aligned} \tag{2.10}$$

$$\begin{aligned}
I_1 &= -I_2 - I_3 \\
&= -\frac{S^*}{3U_2} - \frac{S^*}{3U_3} \\
&= \frac{S^*(-U_2 - U_3)}{3|U|^2 \angle 0^\circ} \\
&= \frac{S^*}{3U_1}
\end{aligned} \tag{2.11}$$

Equation (2.9), (2.10) and (2.11) demonstrate the operation of boost type rectifier under balanced condition:

$$S^* = 3U_1^*I_1 = 3U_2^*I_2 = 3U_3^*I_3. \tag{2.12}$$



Under unbalanced input conditions, (2.2) is a quadratic equation with complex coefficients.  $I_3$  can be solved by the following quadratic formula:

$$I_3 = \frac{-b \pm \sqrt{b^2 - 4ac}}{2a} \quad (2.13)$$

Equation (2.13) indicates two solutions for  $I_3$ . Therefore two sets of current references can be obtained from (2.1). Some constraints are then applied to determine the applicable set of solutions.

### 2.3 Constraints of the Solutions

The most important criterion to select the current references is the phase sequence. According to the sequence of three-phase input voltages, phase B current must lag phase A current and phase C current must lead phase A current. This can be expressed as (2.14).

$$\theta_2 < \theta_1 < \theta_3, \quad \theta_1, \theta_2, \theta_3 \in [-180^\circ, 180^\circ) \quad (2.14)$$

In practical operation, the output DC link voltage is slightly higher than the peak of input line-to-line voltage:

$$V_{dc} = \hat{V}_{l-l} \sim 1.2\hat{V}_{l-l} \quad (2.15)$$

The relationship between input and output voltages is represented in (2.16).

$$U_i = z_i I_i + SW_i \frac{V_{dc}}{2\sqrt{2}} \quad (2.16)$$

The three-phase switching functions  $SW_1$ ,  $SW_2$  and  $SW_3$  must be less than or equal to one to ensure the analytical solution is practically valid for the PWM bridge. According to (2.15) and (2.16), the switching functions are close to one under balanced operating conditions.

Under unbalanced condition when one phase voltage is dropping to zero, (2.17) indicates that the angle between current and switching function is greater than  $90^\circ$ .

$$z_i I_i = U_i - SW_i \frac{V_{dc}}{2\sqrt{2}} < 0 \quad (2.17)$$

From (2.16), the input voltage and impedance in one phase should not be zero at the same time. Otherwise, the phase switching function would be zero, which means that the corresponding phase is out of operation. Hence, this method of harmonic elimination is valid if and only if (2.18) is complied.

$$|U_i| + |z_i| \neq 0, \quad i = 1, 2, 3 \quad (2.18)$$

For optimal design of the PWM boost type rectifier, the phase input impedance is selected to keep  $z_i I_i$  within a range of 10% to 15% of the input phase voltage under balanced operating condition.

$$10\% \cdot U_i \leq z_i I_i \leq 15\% \cdot U_i \quad (2.19)$$

Applying (2.14) to (2.19), a MATLAB program is used to calculate and determine a feasible set of current references. The program is listed in Appendix and Fig. 8 shows its flow chart. A warning function is added to avoid dead-loop calculation although it is unlikely to happen. This function is also useful in real-time computation when the measured data are inaccurate or missing. It can hold the output current references and

wait for input change until next computation cycle. In this way, it prevents current references from unnecessary fluctuating and provides more stable operation with fewer transients.

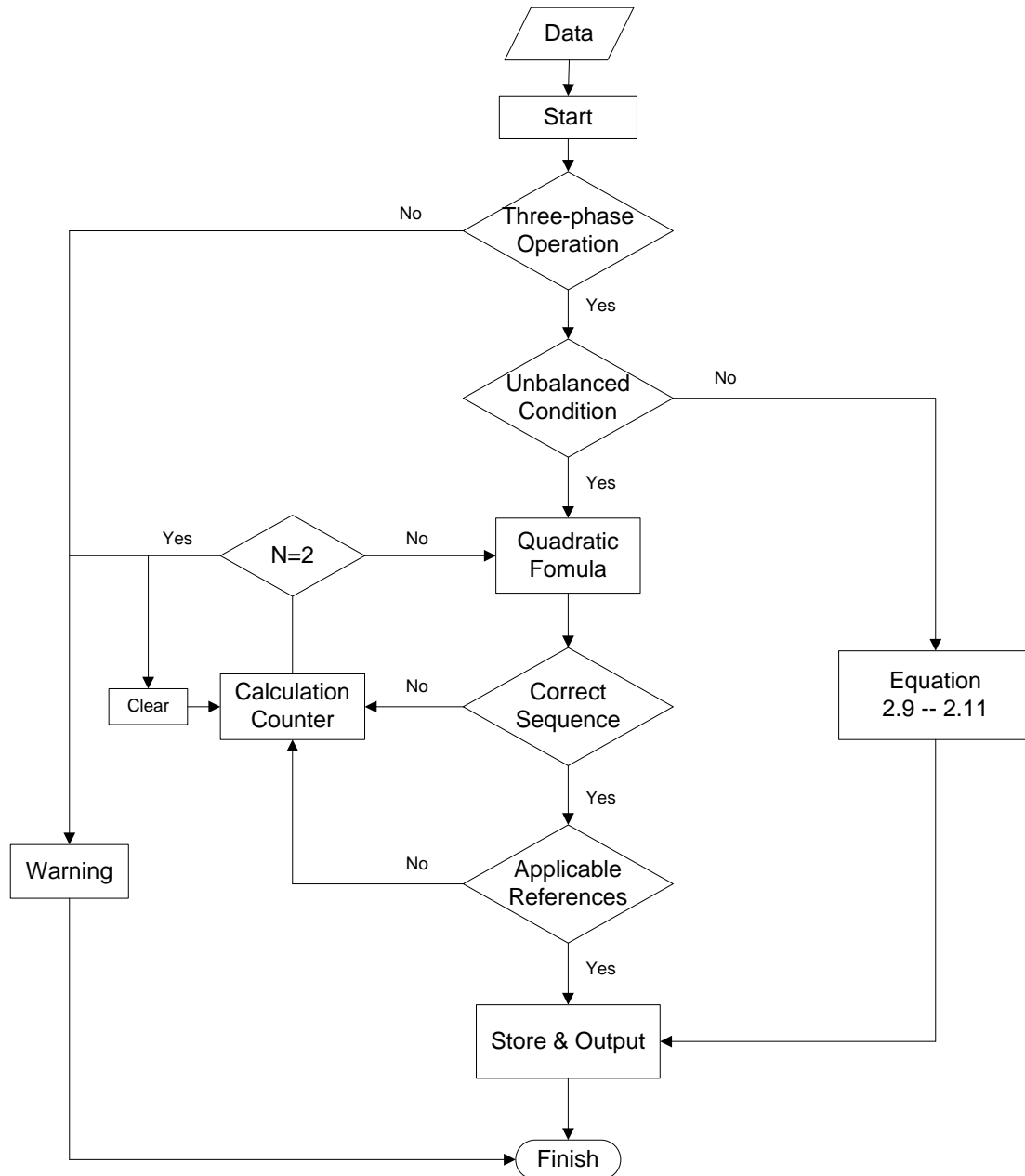


Figure 8: Program flow chart

## 2.4 Solutions under Unbalanced Conditions

First, let us consider a balanced case as specified in TABLE II. The solution of this balanced case is shown in Figure 9. Next, several unbalanced cases are solved and compared with the balanced case.

TABLE II: BASE CASE PARAMETERS

Input Voltages (V)			Input Impedances (mH)			Power Setting (W)
A	B	C	A	B	C	
$60\angle 0^\circ$	$60\angle -120^\circ$	$60\angle 120^\circ$	10	10	10	250

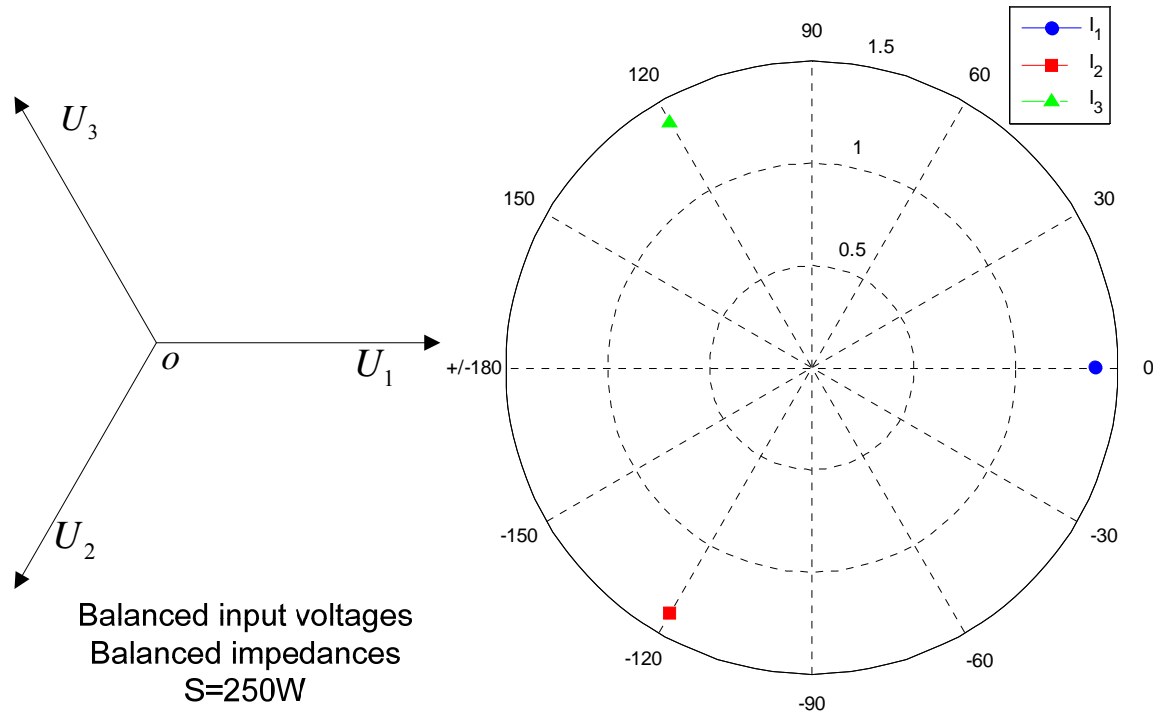


Figure 9: Reference currents of balanced case

### Unbalanced Voltage Magnitude |U|

Fig. 10 shows the solution of reference currents when the magnitude of  $U_3$  drops from 60V to 0V. The phase angle of  $U_3$  remains the same at  $120^\circ$ . The PWM boost type rectifier is supplied by only two-phase voltages when  $U_3$  becomes zero. From Fig. 10, it can be seen that one phase voltage dropping causes obvious deviation in both magnitudes and angles of reference currents.

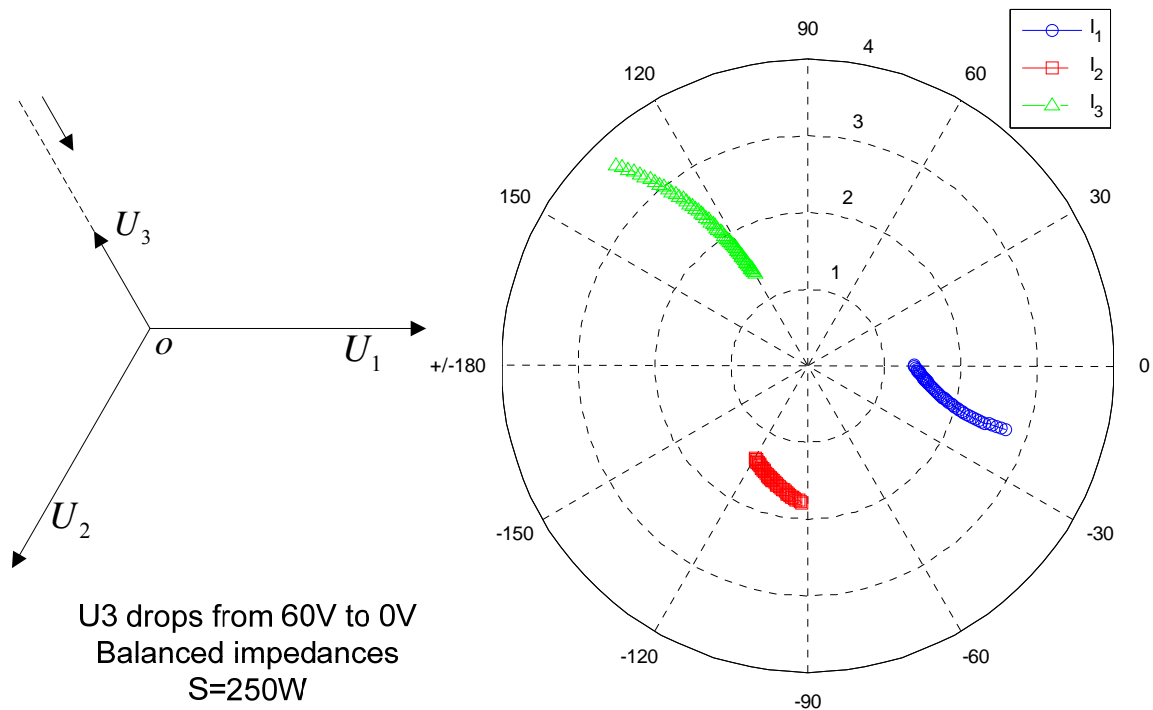


Figure 10: Reference currents when the magnitude of  $U_3$  decreases

### Unbalanced Voltage Phase Angle $\theta$

Fig. 11 and 12 show the solution of reference currents when the angle of  $U_3$  varies by  $\pm 60^\circ$ . The magnitude of  $U_3$  is kept the same at 60V. Although the circumstance of huge phase angle change is unlikely to happen in practical operation, it demonstrates that the method is generalized and solution can be obtained.

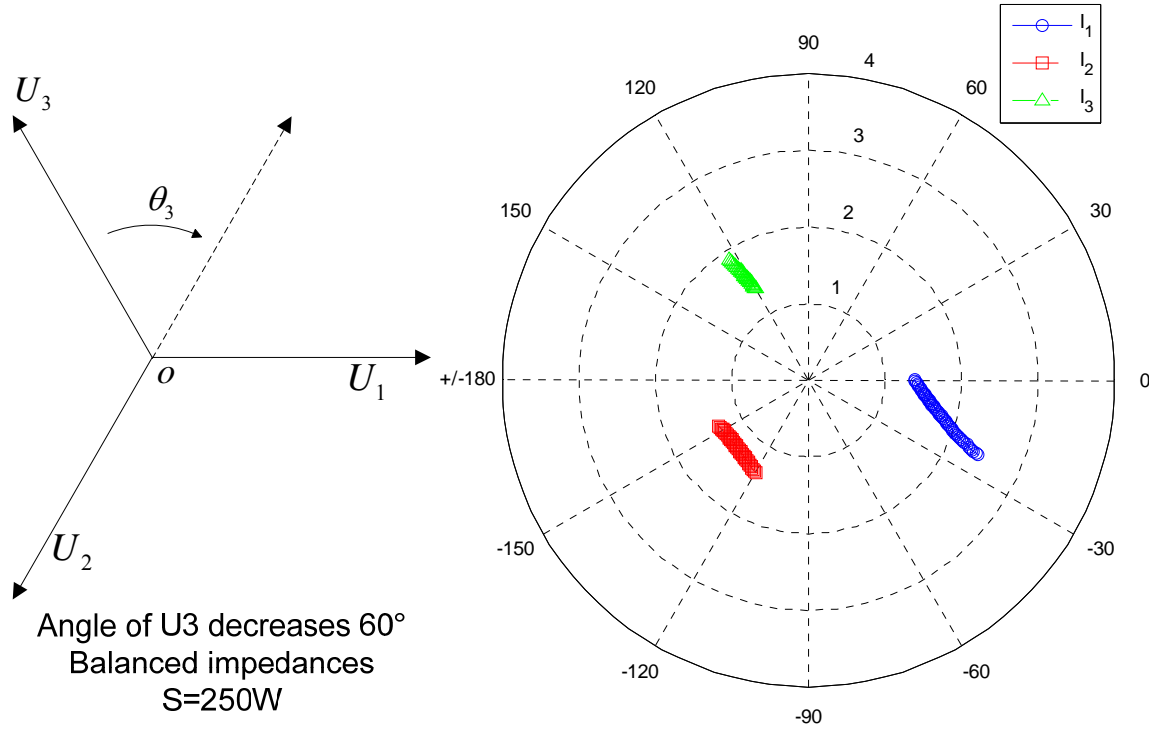


Figure 11: Reference currents when the angle of U3 decreases

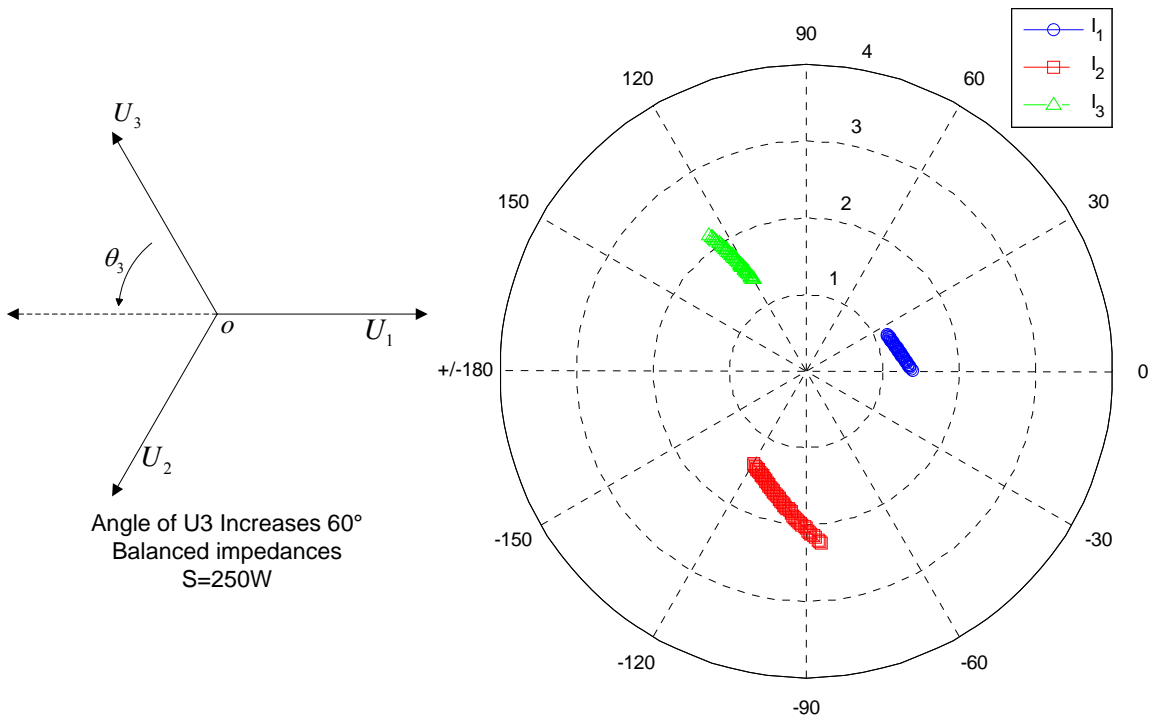


Figure 12: Reference currents when the angle of U3 increases

From Fig. 11 and 12, it can be seen that a change in one phase voltage angle has impact on both magnitudes and angles of reference currents. However, the magnitude deviation of reference currents in Fig. 11 is smaller compared to Fig. 10. Hence, the voltage magnitude drop is a more severe unbalanced situation compared to phase angle variation.

### Unbalanced input Impedance $Z$

Fig. 13 shows the solution of reference currents when the impedance of phase C increases from 0 to 20mH. Balanced three-phase input voltages are supplied. According to Fig. 13, the change of phase impedance leads to slight deviation in the magnitudes and angles of reference currents. The impedance change has less impact than voltage change in Fig 10, 11 and 12.

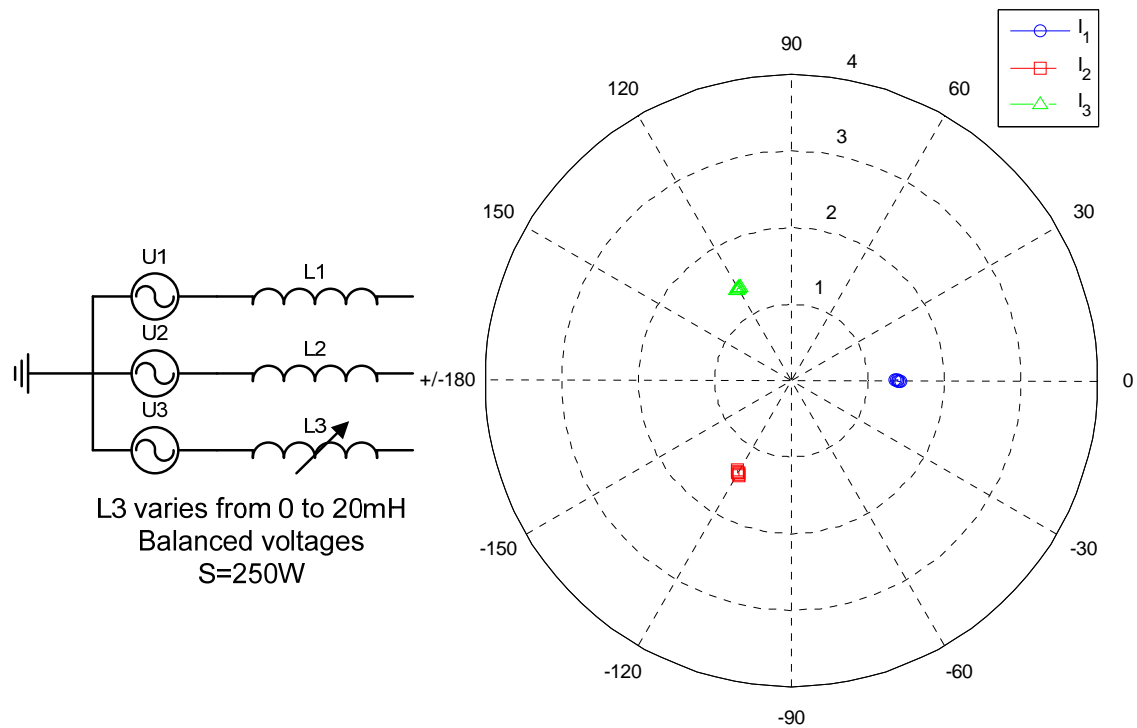


Figure 13: Reference currents when  $Z_3$  varies

To conclude, abnormal harmonic components appear at both input AC side and DC link when the PWM boost type rectifier is under unbalanced operating conditions. A generalized method of harmonic elimination was proposed in [13]. By solving a set of quadratic equations in complex domain, three-phase input reference currents can be obtained. By tracking the reference currents, the PWM boost type rectifier can operate at a desired DC link voltage and input power factor without low-order harmonic components.

In this chapter, an analytical solution of the set of three quadratic equations is derived. It is convenient to calculate the solution using computer programs. Several constraints should be considered in the calculation procedure to make sure the solution is applicable. The flow chart of the program considering these constraints is provided.

Several solutions are plotted and compared under different unbalanced conditions. The drop of voltage magnitude is the most severe unbalanced situation, which causes dramatic magnitude increase and angle shift in the reference currents. Voltage phase angle deviation will also lead to magnitude raise and angle change in reference currents, although huge unexpected voltage angle shift is unlikely to happen in practical operations. The impedance change has less impact on the currents compared to the voltage change.

This generalized method provides a straightforward way for input-output harmonic elimination. The solution exists for all levels of imbalance in voltages and impedances.



## **CHAPTER III**

### **SIMULATION RESULTS**

A feed-forward control method is proposed based on the open loop configuration analysis presented in the last chapter. Input voltages and impedances are measured as known parameters. Apparent power is determined by the DC link information and desired DC link voltage. According to (2.1), three-phase reference currents are calculated. Three independent hysteresis controllers are used to track the reference.

In this chapter, the operation of the three phase PWM boost type rectifier is simulated in MATLAB Simulink using SimPowerSystems toolbox. The proposed control method is implemented. Seven different cases, from three-phase balanced input voltages and impedances to extremely unbalanced input conditions, are selected for simulation. The closed-loop operation is also performed to control DC link voltage in real time. Simulation results verify the feasibility of the proposed control method. The rectifier operates at unity power factor with a stable behavior in spite of unbalanced input conditions.

### 3.1 Control Strategy

The operation of the PWM boost type rectifier under the proposed harmonic elimination control scheme is simulated using MATLAB Simulink SimPowerSystems toolbox. The circuit diagram and a current controller are shown in Fig. 14. Three individual AC voltage sources are used to represent three-phase input voltages. Each phase has an inductor to represent the input impedance. The PWM Boost Rectifier consists of six IGBTs and six anti-parallel diodes. A capacitor is connected at the DC link as a filter. The load is represented by a resistor.

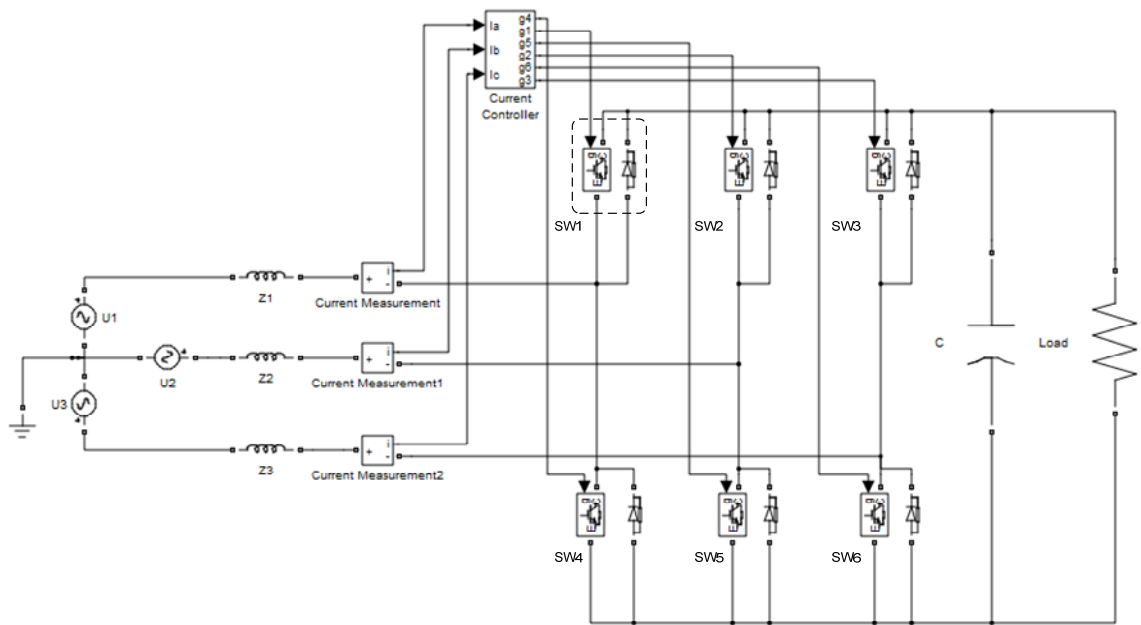


Figure 14: Diagram of simulation circuit and a current controller

### 3.1.1 Current Control Loop

The current controller is implemented by using a hysteresis controller [23]. It compares actual three-phase line currents with calculated three-phase current references. The hysteresis control method generates six gating signals and supplies them to six switches. As a result, three-phase actual currents track the reference currents. And the PWM boost type rectifier achieves input-output harmonic elimination.

The diagram of current control loop under open-loop operation mode is shown in Fig. 15. There is also a closed-loop operation mode which applies DC link voltage as a feedback signal for current control. Two operation modes have different reference calculator blocks that generate three-phase reference currents. After the generation of reference currents, the rest parts of the control loop are identical in two operation modes. Detailed description of reference generation is provided in the following sections.

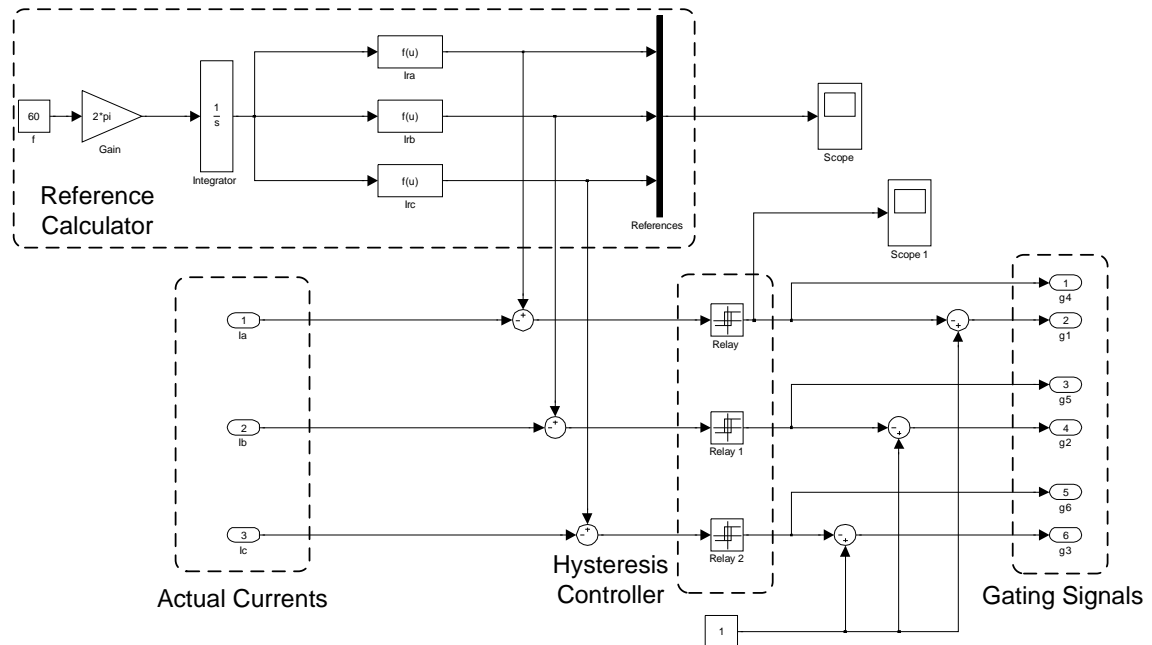


Figure 15: Diagram of current control loop (open-loop operation)

### 3.1.2 Open-loop Operation

The proposed control method can be easily implemented on a PWM boost type rectifier under its open-loop operation mode. It is a feed-forward method by assuming all known variables in (2.1) are constant. Therefore, the reference currents do not change once they are calculated.

The unbalanced three-phase input voltages and input impedances are measured in advance and assumed not to change after turning on the rectifier. The program listed in appendix A is used to calculate three-phase reference currents. The magnitudes and phase angles of the reference currents are stored into memory. MATLAB Simulink model can read those values and generate the references in real time. Fig. 16 shows the procedure of reference currents generation in open-loop mode.

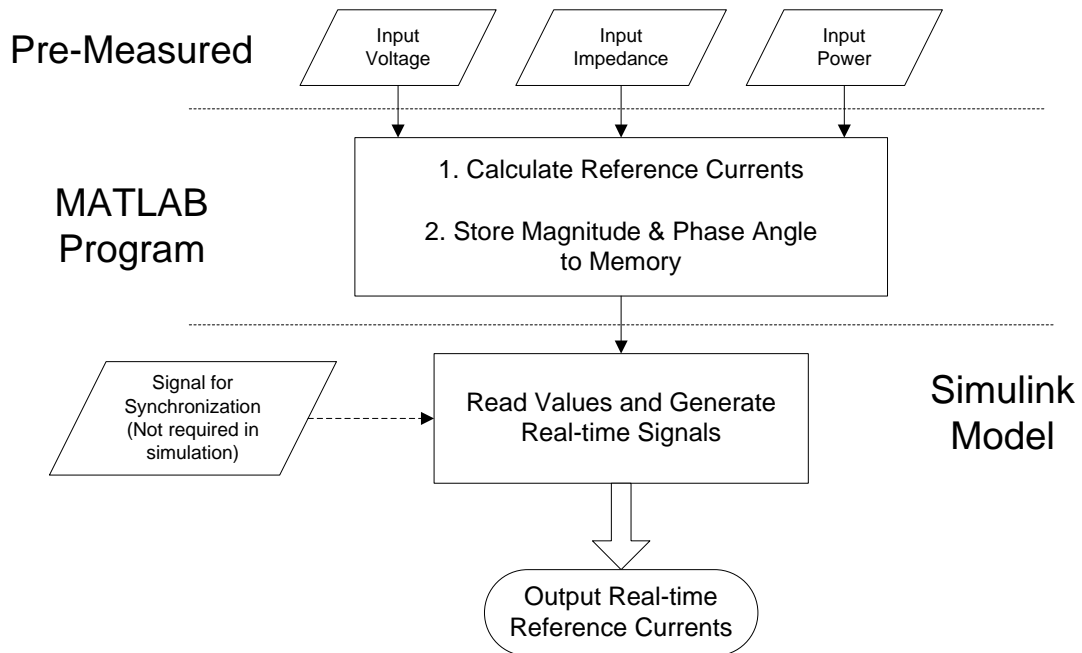


Figure 16: Reference currents generation in open-loop mode

### 3.1.3 Closed-loop Operation

Closed-loop operation of the PWM boost type rectifier makes the output DC link voltage controllable. The output of the DC voltage controller sets a reference for three-phase currents. The DC voltage control loop is shown in Fig. 17.

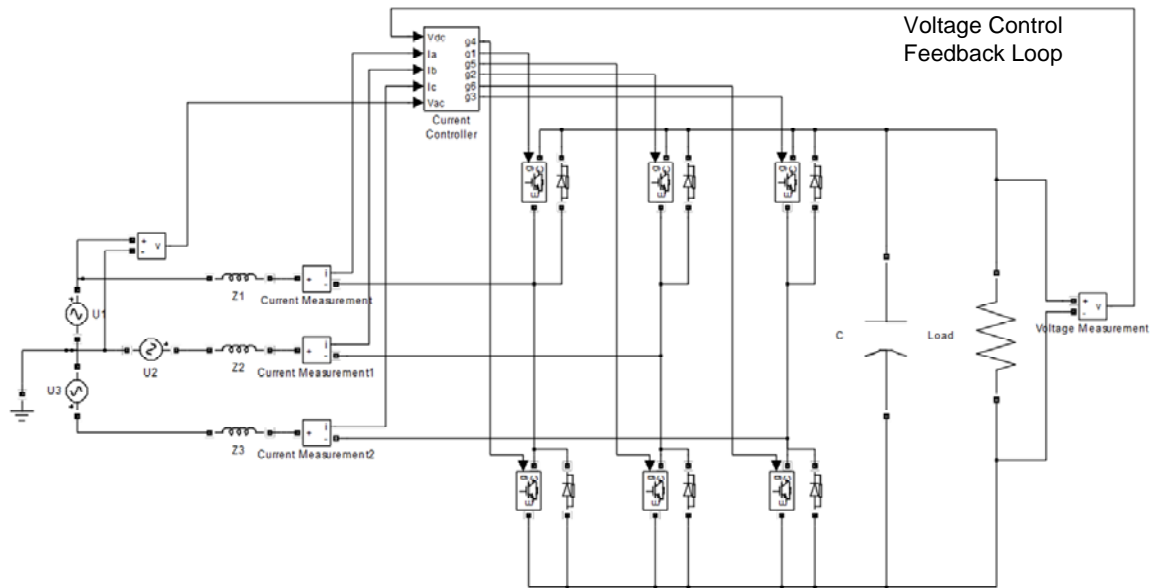


Figure 17: Diagram of DC voltage control loop ( the outer loop)

A feedback loop is designed to control the DC link voltage. Assume the three-phase input voltages and input impedances are known, therefore, the reference currents are determined by the input power  $S$  in (2.1). The DC link voltage is fed back to the current controller and compared to the reference DC voltage. The error signal is used to update the setting of the power  $S$ . Three-phase reference currents are generated in real time to control the DC link voltage. Hysteresis controllers make the input line currents track the references. Harmonic elimination is achieved at both input and output while the

DC link voltage is controllable. The diagram of current control loop in closed-loop operation is shown in Fig. 18.

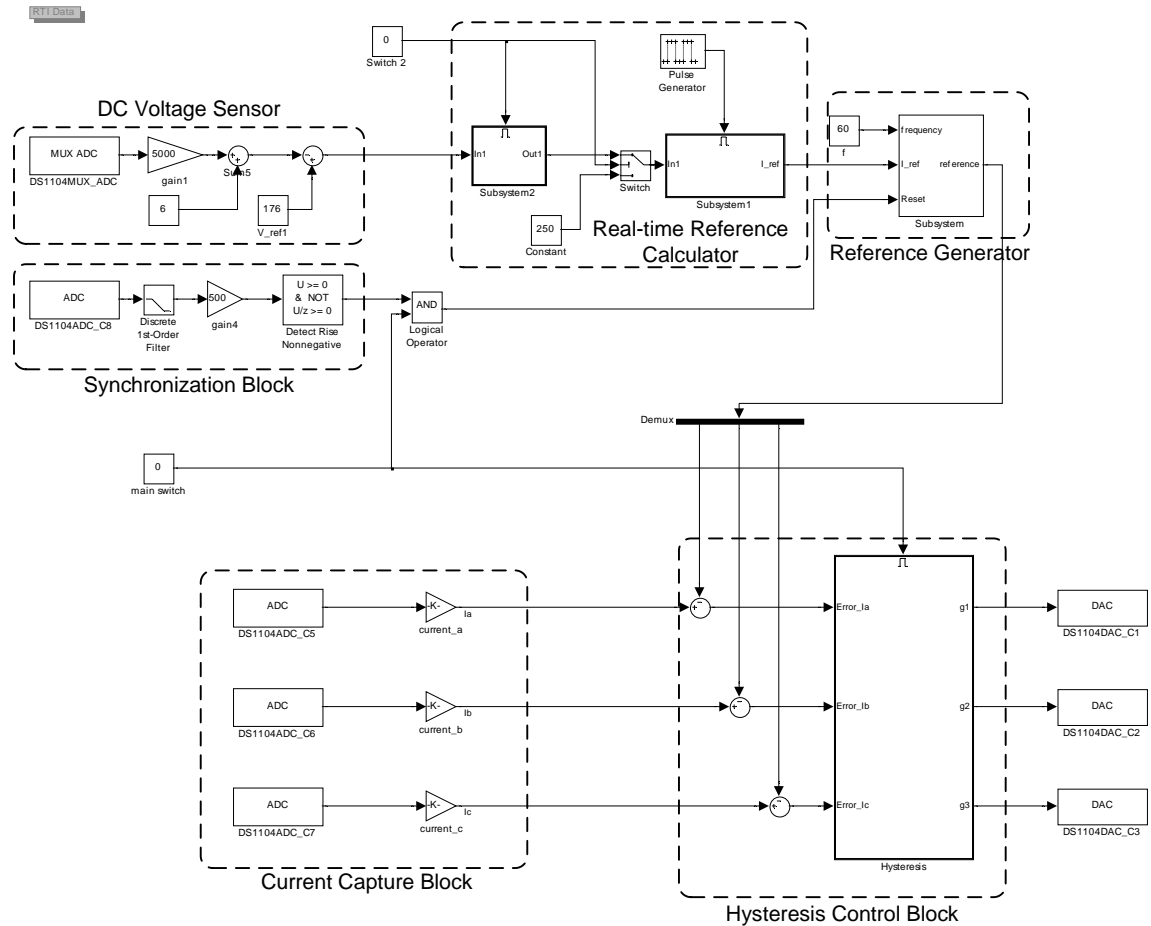


Figure 18: Diagram of current controller ( closed-loop operation)

The reference currents generation of closed-loop mode requires two types of input data. One is assumed to be constant, such as input voltages and input impedances. The other is varying in real time, the DC link voltage error. The MATLAB program in appendix B is applied to process constant data before real-time operation. This program can also be further implemented into Simulink model if the input voltages and impedances are measured in real time. The reference calculator block in Simulink model

is used to get magnitudes and phase angles of three-phase reference currents. A reference generator block reads these values and provides real-time reference signals to the hysteresis controller. Fig. 19 shows the procedure of reference currents generation in closed-loop mode.

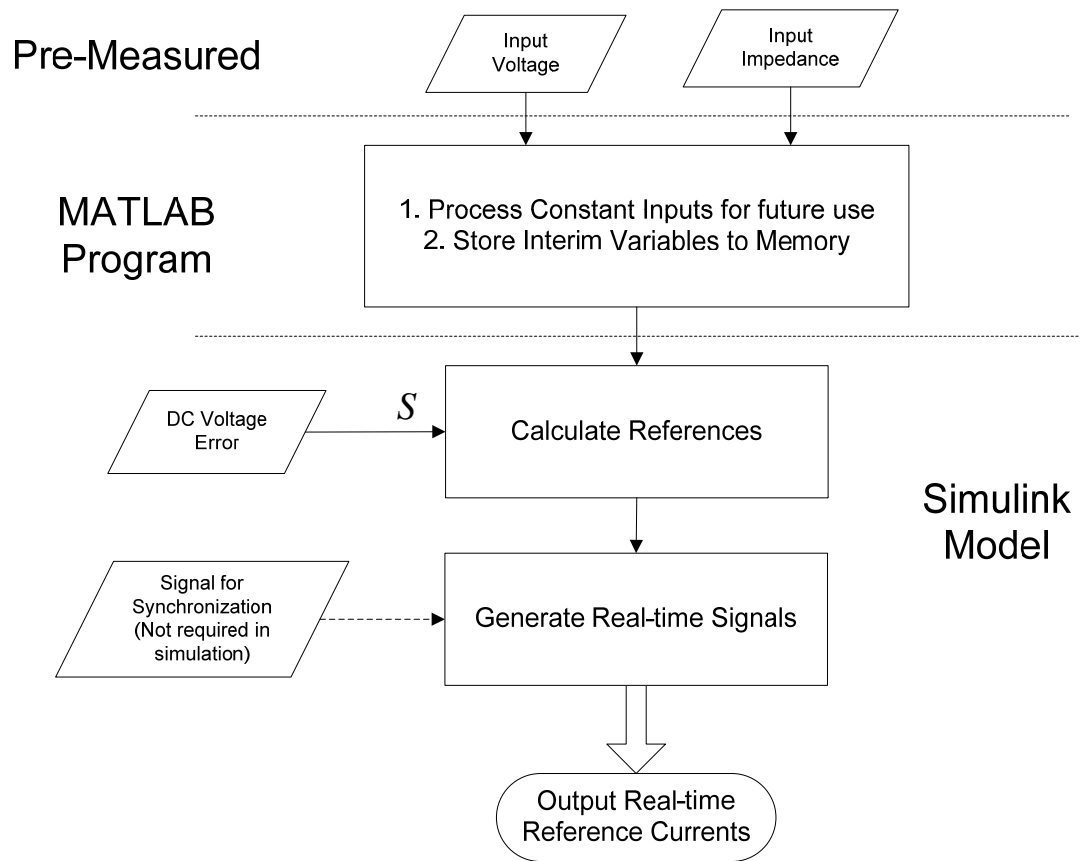


Figure 19: Reference generation in open-loop mode

### 3.2 Simulation Results

Seven different simulation cases are selected to verify the proposed harmonic elimination method. A case with balanced three-phase input voltages and impedances is performed as a reference case. Then, six cases with different levels of unbalanced three-phase input conditions are simulated. Table III shows a list of simulation cases. Parameters and the power circuit components are summarized in Table IV.

TABLE III: SIMULATION CASES

CASE	Input Conditions		Power Setting (W)	DC Load Resistance ( $\Omega$ )
	Voltage (V)	Impedance		
1	$U_1 = 60\angle 0^\circ$ $U_2 = 60\angle -120^\circ$ $U_3 = 60\angle 120^\circ$	$L_1 = L_2 = L_3 = 10\text{mH}$	250	114
2	$U_1 = 60\angle 0^\circ$ $U_2 = 60\angle -120^\circ$ $U_3 = 60\angle 120^\circ$	$L_1 = L_3 = 10\text{mH}$ $L_2 = 0$	250	114
3	$U_1 = 60\angle 0^\circ$ $U_2 = 60\angle -120^\circ$ $U_3 = 0$	$L_1 = L_2 = L_3 = 10\text{mH}$	250	114
4	$U_1 = 60\angle 0^\circ$ $U_2 = 60\angle -120^\circ$ $U_3 = 0$	$L_1 = L_3 = 10\text{mH}$ $L_2 = 0$	250	114
5	$U_1 = 60\angle 0^\circ$ $U_2 = 0$ $U_3 = 0$	$L_1 = L_2 = L_3 = 10\text{mH}$	100	342
6	$U_1 = 60\angle 0^\circ$ $U_2 = 0$ $U_3 = 0$	$L_1 = 0$ $L_2 = L_3 = 10\text{mH}$	100	342
7	$U_1 = 60\angle 0^\circ$ $U_2 = 60\angle -180^\circ$ $U_3 = 0$	$L_1 = L_2 = L_3 = 10\text{mH}$	100	400

TABLE IV: SIMULATION PARAMETERS

Parameter	Value	Parameter	Value
Fundamental frequency, $f$	60 Hz	IGBT on resistance	0.4 $\Omega$
DC link capacitor, $C$	460 $\mu\text{F}$	Diode on resistance	0.4 $\Omega$
Hysteresis band	0.02 A	IGBT forward voltage	2.5 V
Switch on inductance	$7.5 \times 10^{-9}$ H	Diode forward voltage	1.5 V



In case 1, the operation of the three-phase PWM boost type rectifier is simulated under balanced input voltages and impedances. Three-phase reference currents are calculated by solving (2.9) to (2.11). Fig. 20 shows the steady-state three-phase input currents and DC link voltage waveforms of case 1.

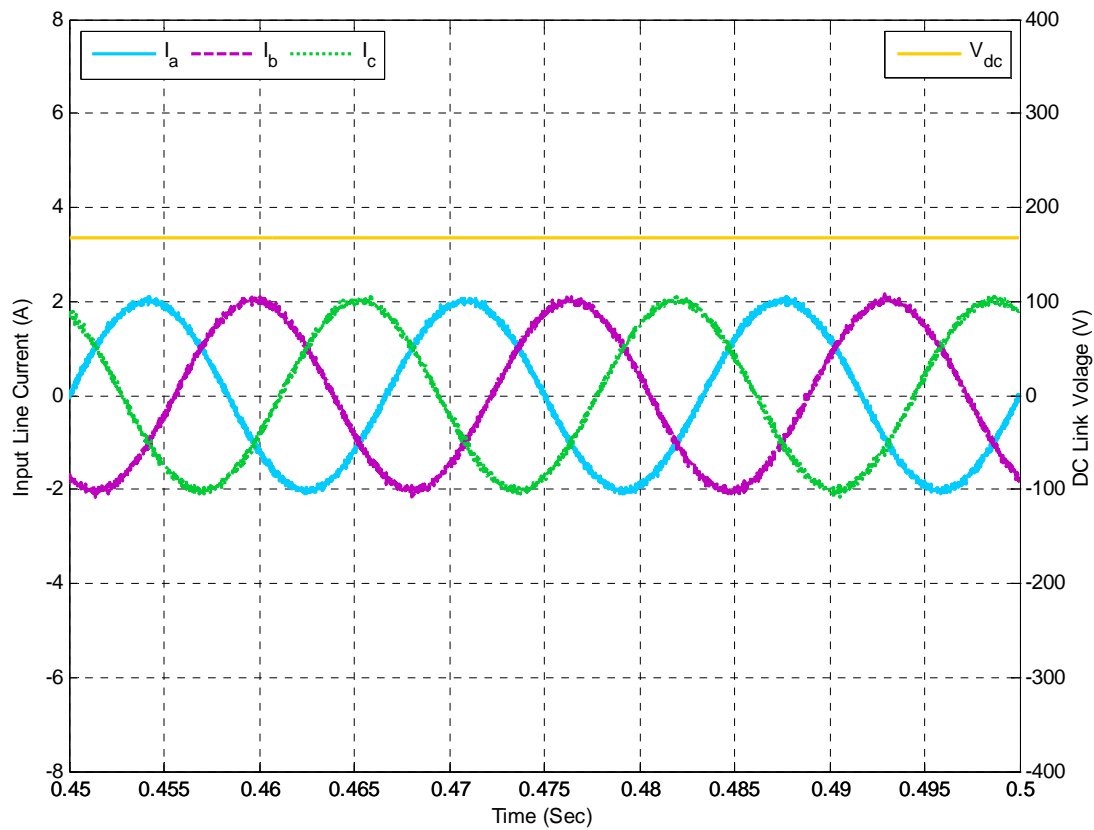


Figure 20: DC link voltage and line currents of case 1

Case 2 to 7 have different unbalanced input voltages and impedances. The simulation results are shown in Fig.21 to Fig. 26. Each plot contains three-phase input currents and output DC link voltages.

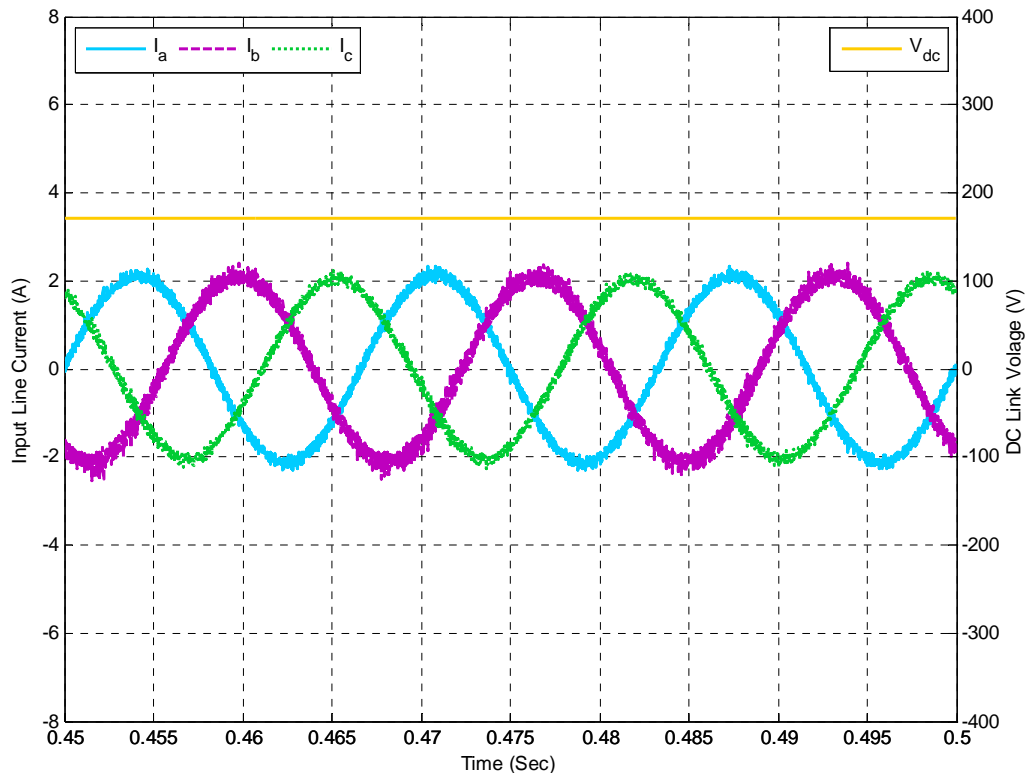


Figure 21: DC link voltage and line currents of case 2

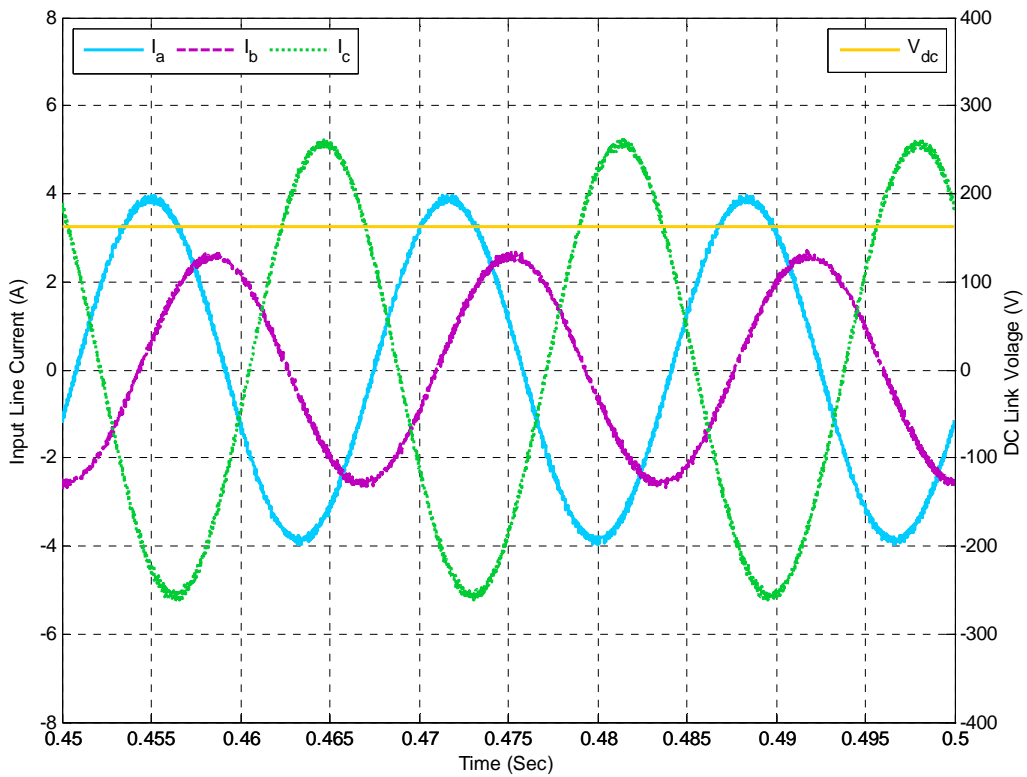


Figure 22: DC link voltage and line currents of case 3

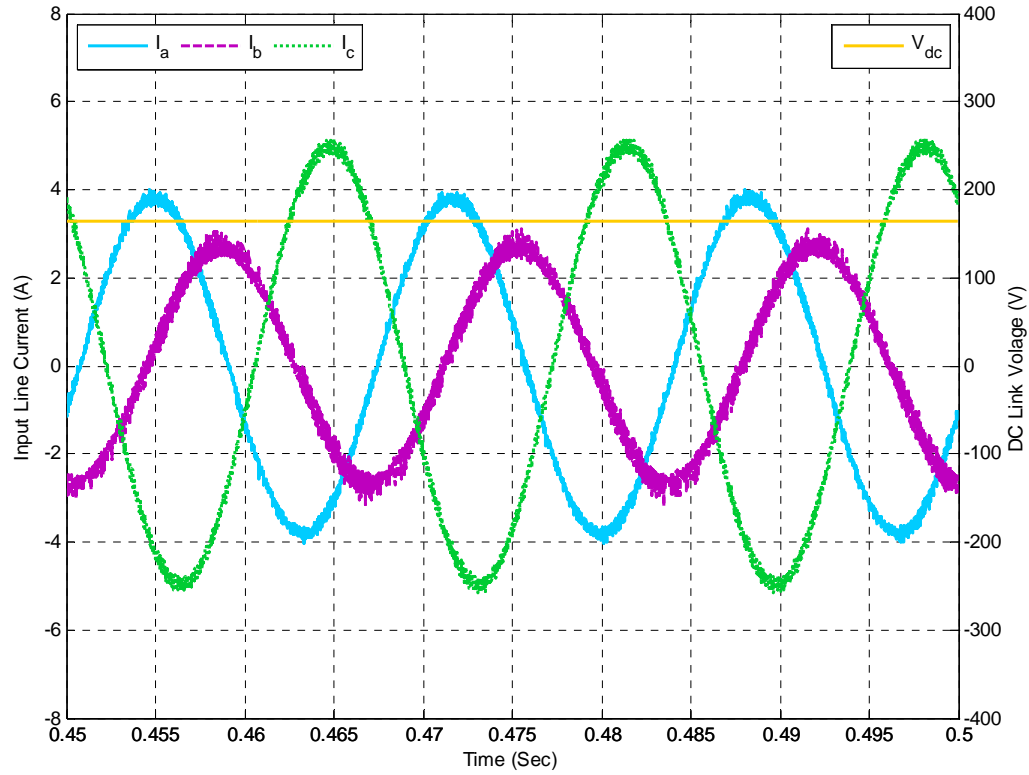


Figure 23: DC link voltage and line currents of case 4

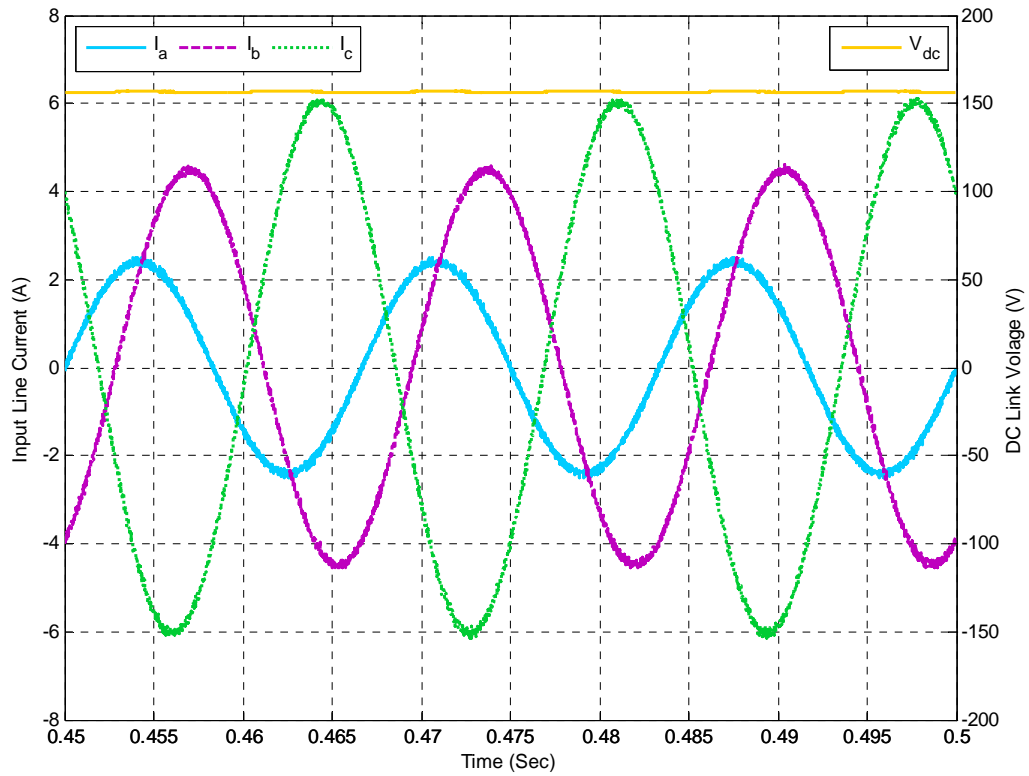


Figure 24: DC link voltage and line currents of case 5

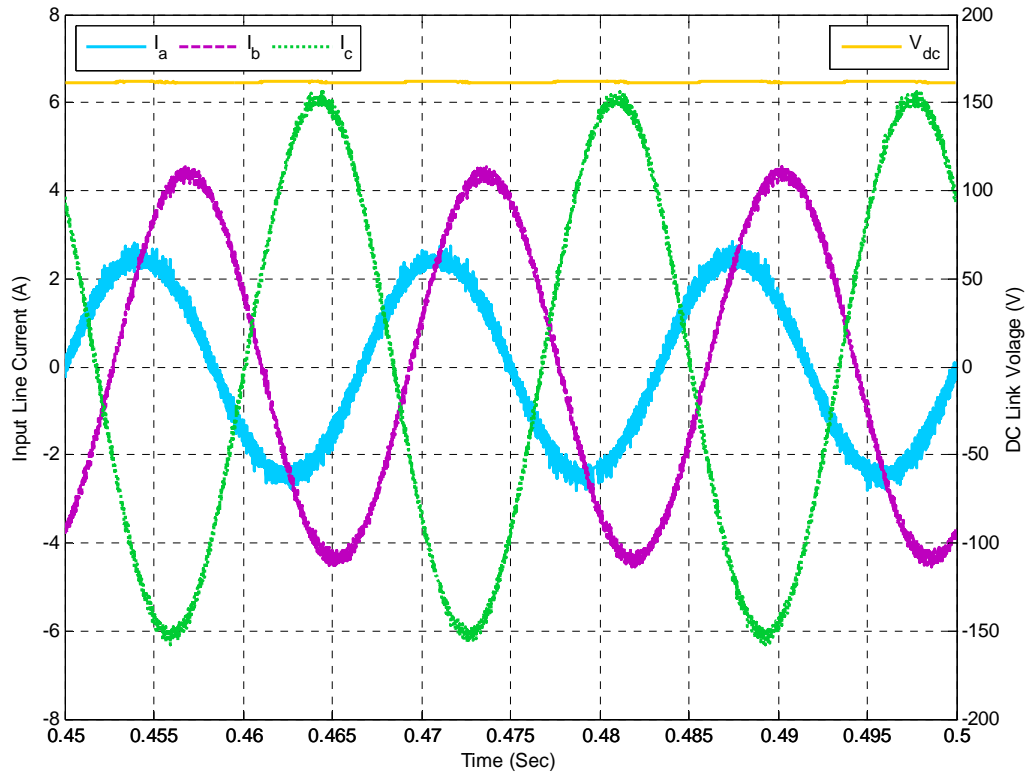


Figure 25: DC link voltage and line currents of case 6

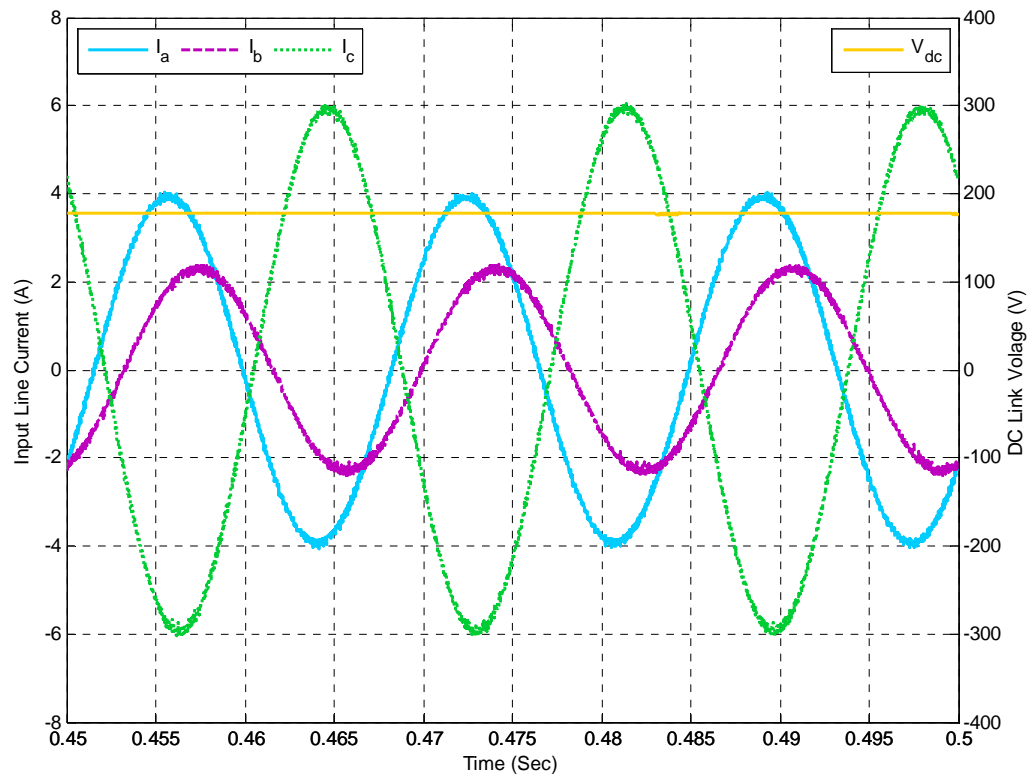


Figure 26: DC link voltage and line currents of case 7

A summary of simulation results is provided in Table V. The rms values of actual input currents and steady-state DC link voltages are listed in the table.

TABLE V: SIMULATION CURRENTS AND DC LINK VOLTAGE

CASE	Current rms (A)			DC Link Voltage (V)
	a	b	c	
1	1.429	1.429	1.43	168.2
2	1.507	1.494	1.438	171.1
3	2.737	1.815	3.626	162.3
4	2.685	1.899	3.512	164.3
5	1.699	3.171	4.257	156.2
6	1.758	3.106	4.294	161.2
7	2.779	1.625	4.199	177.4

Table VI shows the input power, output power, power factor and system efficiency of seven cases. It can be seen that unity power factor is achieved since no reactive power is set in  $S$  for all cases. Non-ideal switches are used in the simulation circuit, therefore, the power losses cause efficiency drop in the simulation results. Because the current magnitude increases dramatically under extreme cases, the efficiency is lower for more unbalanced case.

TABLE VI: EFFICIENCY OF SIMULATION RESULTS

CASE	Simulation				
	INPUT			OUTPUT	Efficiency
	P (W)	Q (Var)	pf	P (W)	
1	257.2	0.7731	1.0	248.2	96.49%
2	265.5	0.7073	1.0	256.8	96.72%
3	254.2	1.208	1.0	231.1	90.90%
4	259.5	2.11	1.0	236.8	91.25%
5	101.9	0.3532	1.0	71.3	70.01%
6	105	0.7049	1.0	76.0	72.36%
7	105.5	0.4098	1.0	78.7	74.58%

The closed-loop operation of case 3 is simulated to control the DC link voltage while harmonic elimination. The DC reference is initially set to be 180V and has a step change to 200V when  $t=0.5$  s. After one second, the DC reference changes back to 180V when  $t=1.5$  s. Fig. 27 shows the comparison of reference voltage and actual DC link voltage.

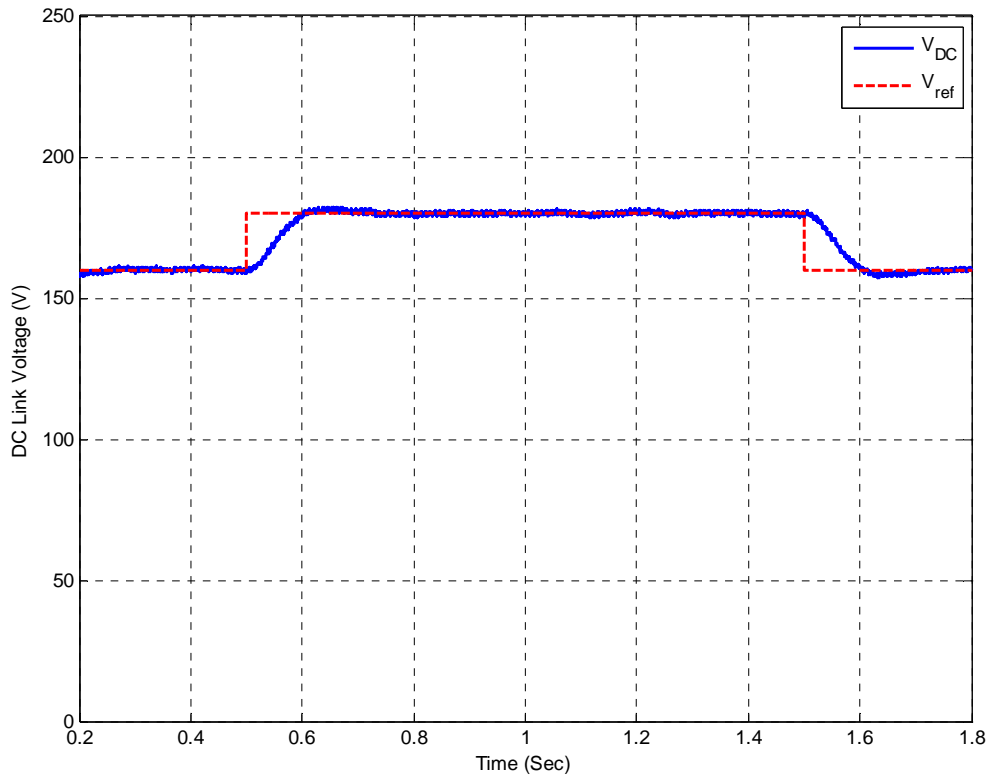


Figure 27: Simulation result of closed-loop operation, based on case 3

From the results, it can be seen the three-phase PWM boost type rectifier achieves input-output harmonic elimination by using the proposed control method. There is no obvious low-order harmonics in the input currents and DC link voltages even under extremely unbalanced operating conditions. In closed-loop operation, controllable DC link voltage is achieved as well as harmonic elimination.

## **CHAPTER IV**

### **EXPERIMENTAL RESULTS**

Based on the theoretical analysis presented in [13] a generalized control method of input-output harmonic elimination for the three-phase PWM boost type rectifier under unbalanced input voltages and unbalanced input impedances has been implemented. The DSPACE digital control system and Lab-Volt test bench have been used to implement the proposed method.

In this chapter, the hardware configuration and the DSPACE control algorithm are described in detail. Each functional block in the control loop is explained. Diagrams and parameters of the power circuit and control loop are provided. The graphical interface of the DSPACE control desk is displayed.

Finally, the experimental results are presented and compared to the simulation results. The results show that the three-phase PWM boost type rectifier can achieve low-order harmonic elimination as well as unity input power factor even under extreme operating conditions.

## 4.1 Hardware Implementation

The proposed generalized method of harmonic elimination for three-phase PWM boost type rectifier has been implemented on a laboratory prototype by using the DSPACE digital controller and the Lab-Volt test bench.

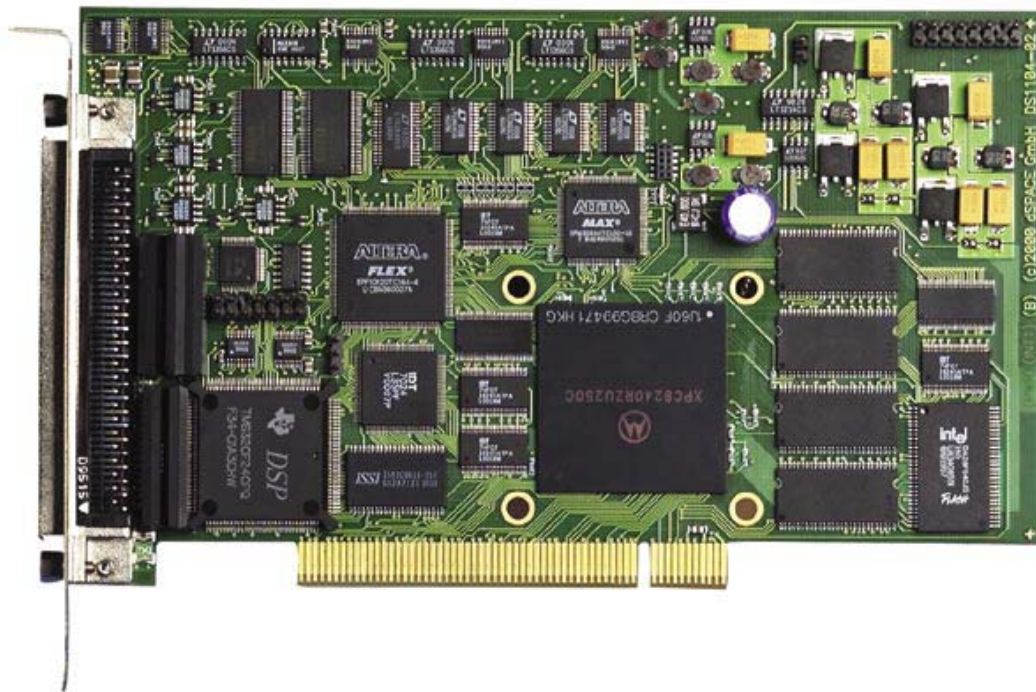


Figure 28: DSPACE DSP controller board

The DSPACE DSP controller board shown in Fig. 28 is an interface between the host computer, the driving circuit, and the converter system, including A/D and D/A converters, serial interfaces, sensors, etc. One of the best features of the DSPACE package is the ease of building real-time applications. DSPACE has a software interface to the controller board based on MATLAB Simulink. Once the Simulink model is completed, DSPACE software can convert it into real-time DSP code. Then, it downloads



the code to the controller board, and executes the program in real time. DSPACE software also has tools to display, store data, and change parameters [23].

It is very convenient to implement the proposed control method using the DSPACE control system. With its help, the powerful functions of MATLAB and Simulink can be used to overcome the complexity of the method proposed in [13].

#### 4.1.1 Overall System

The block diagram of the overall system is shown in Fig. 29.

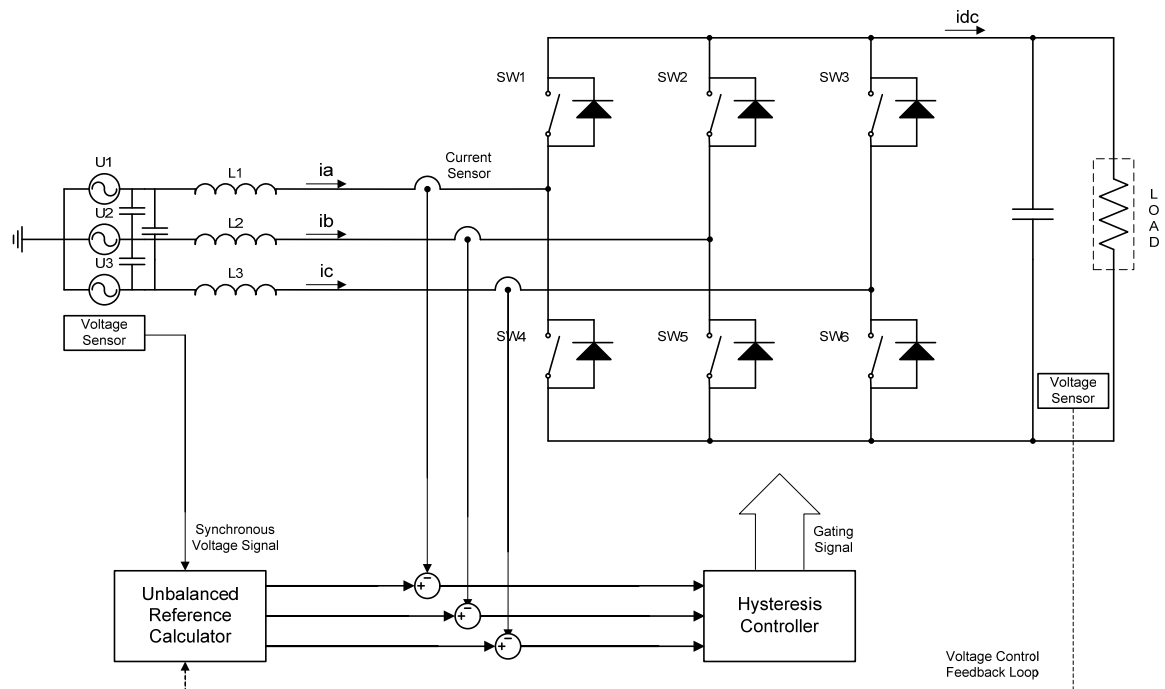


Figure 29: Diagram of PWM boost type rectifier with harmonic elimination

The power circuit contains a three-phase voltage source, three inductors on the AC side and the PWM boost type rectifier supplying a pure resistive load. Three ceramic

capacitors are placed between every two phases as a filter to ensure sinusoidal input voltages. A three-phase bridge contains of six switches with six anti-parallel diodes. The switches are controlled by using six gating signals. An electrolytic capacitor is connected in parallel with the load.

One AC voltage sensor is used to synchronize control signals with the AC input voltage (a zero crossing detector). A feedback loop is designed to control DC link voltage in the closed-loop operation. The reference calculator generates three-phase reference currents. Three independent hysteresis controllers are used to keep the actual currents tracking the references. Logic signals from the hysteresis controllers are supplied to a drive unit to provide six gating signals to six switches of the PWM converter bridge.

#### 4.1.2 Control Scheme

To eliminate harmonics on both the input and output sides of the PWM boost type rectifier under unbalanced operating conditions, both the magnitudes and phase angles of the three-phase currents need to be controlled. Three-phase reference currents are calculated from (2.1). Three equations are also rewritten below.

$$I_1 = -I_2 - I_3$$

$$I_2 = \frac{S^* - I_3(U_3^* - U_1^*)}{U_2^* - U_1^*}$$

$$\begin{aligned}
& \left[ \frac{2z_1(U_3^* - U_1^*)}{U_2^* - U_1^*} - \frac{(z_1 + z_2)(U_3^* - U_1^*)^2}{(U_2^* - U_1^*)^2} - (z_1 + z_3) \right] I_3^2 \\
& + \left[ (U_3 - U_1) - \frac{(U_3^* - U_1^*)(U_2 - U_1)}{U_2^* - U_1^*} - \frac{2z_1 S^*}{U_2^* - U_1^*} + \frac{2S^*(z_1 + z_2)(U_3^* - U_1^*)}{(U_2^* - U_1^*)^2} \right] I_3 \\
& + \frac{S^*(U_2 - U_1)}{U_2^* - U_1^*} - \frac{(z_1 + z_2)S^{*2}}{(U_2^* - U_1^*)^2} = 0
\end{aligned}$$

$U_1, U_2, U_3$  are input voltages;  $z_1, z_2, z_3$  are input impedances;  $S$  is the apparent power and  $I_1, I_2, I_3$  are input currents. All are represented in the complex domain. By solving three equations with three unknown variables,  $I_1, I_2, I_3$  can be calculated.

The scenario of unbalanced input voltages and impedances can be either pre-determined or measured online by applying a series of sensors at the input of the rectifier. In the open-loop operation mode, input parameters and transferred power are pre-fixed. The MATLAB program and DSPACE RT1104 processor are then used to calculate reference currents. By tracking the reference currents, the rectifier achieves input-output harmonic elimination. In the closed-loop operation mode, input parameters are assumed to be known. DC link voltage is measured and compared to the reference. The feedback loop is applied to adjust power setting, and then the reference currents are updated. Finally, real-time DC link voltage control is achieved as well as harmonic elimination in closed-loop operation.

### 4.1.3 Hardware Configuration

The proposed control strategy is implemented by using MATLAB Simulink and DSPACE RT1104 control system. The diagram of hardware configuration is shown in Fig. 30.

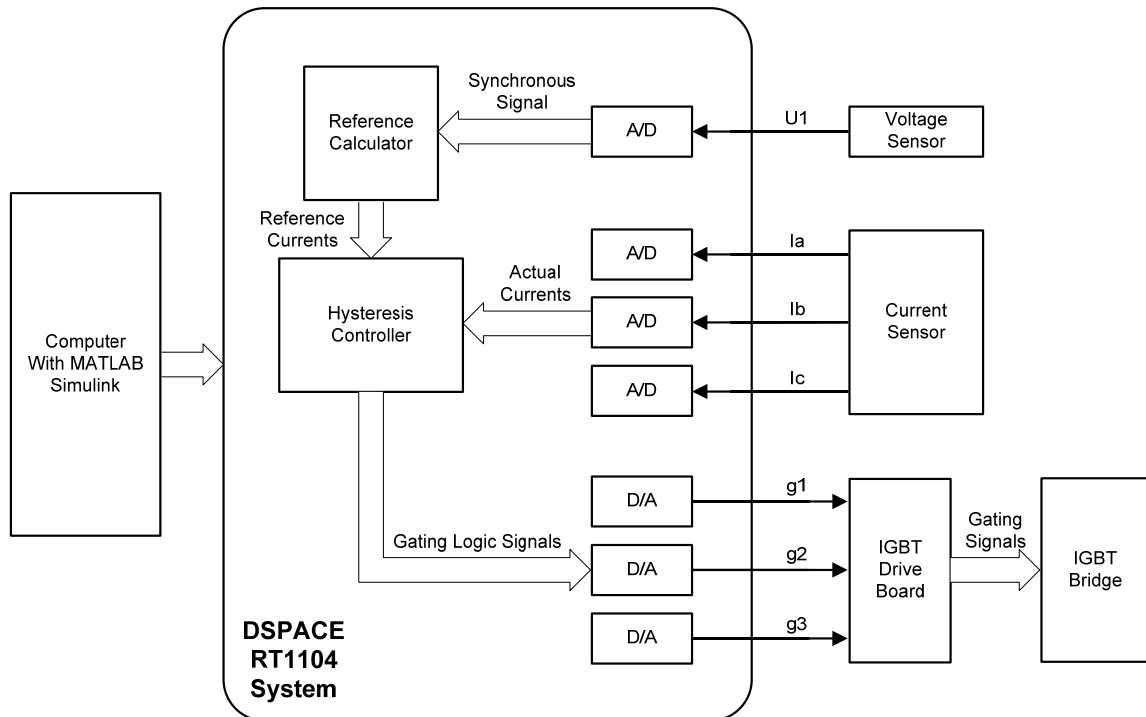


Figure 30: Diagram of hardware configuration

One voltage sensor is used to measure phase A input voltage which is used as a zero crossing detector. Three current sensors are used to capture actual three-phase currents. Four A/D converters on the DSPACE master control board convert these four analog signals to four digital signals.

In this thesis, reference currents are calculated and generated using MATLAB Simulink. Three independent hysteresis controllers are adopted to compare three-phase

actual currents with three reference currents. Hysteresis controllers' outputs are switching logic signals that determine the status of six switches of the PWM bridge. A converter drive board is designed and built using IR21091S drive chip, which has programmable dead time at the transient of switching. This dead time prevents two switches in one leg from conducting at the same time (see Fig. 31 [24]). Fig. 32 and Fig. 33 show the schematic of one phase circuit and the photo of the IGBT drive board. It converts three switching logic signals to six gating signals and supplies them to the converter bridge to control six switches. The list of hardware devices is shown in Table VII.

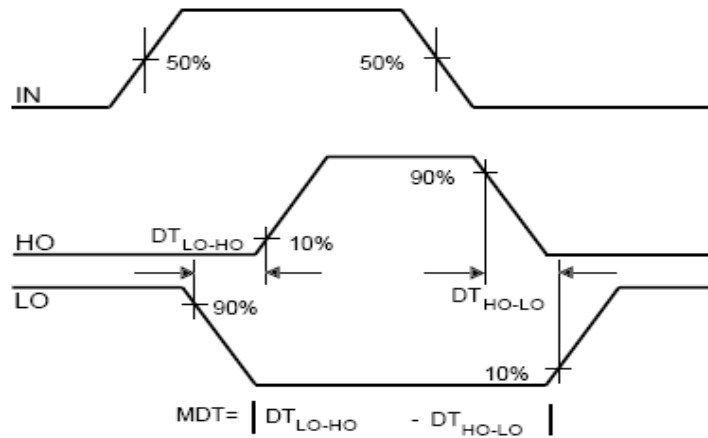


Figure 31: Dead time waveform definition

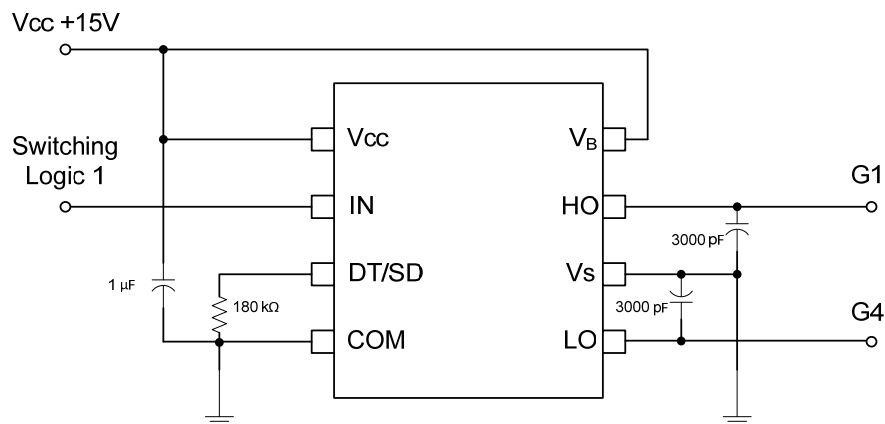


Figure 32: Schematic of one phase IGBT drive circuit

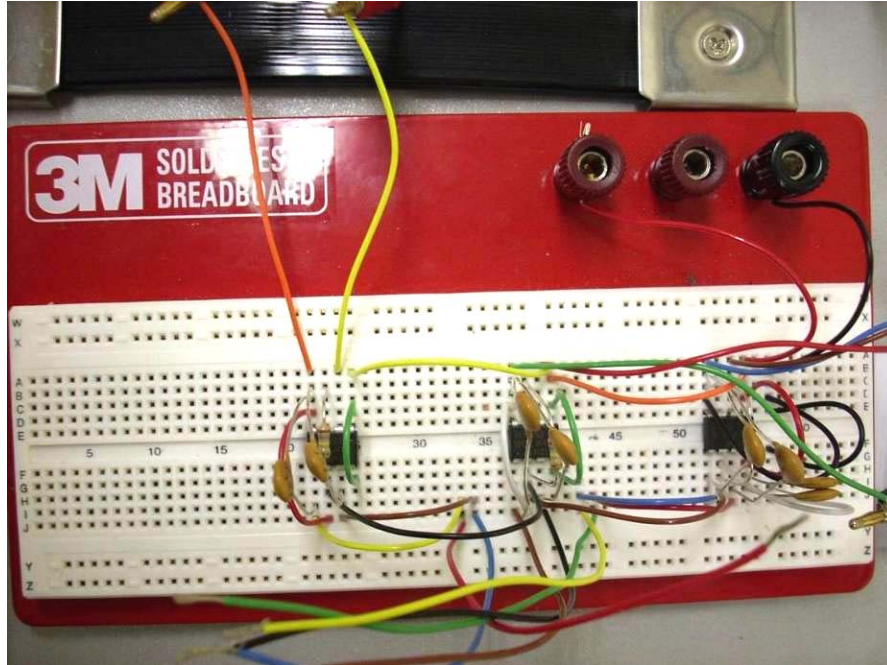


Figure 33: Designed IGBT drive board

TABLE VII: LIST OF APPARATUS AND EQUIPMENT

Item	Description	Manufacturer	Model or S/N
1	Input AC Voltage Source	Lab-Volt	EMS 8321
2	Input Series Inductor	Hammond Reactor	195J20
3	Three-phase IGBT Bridge	Lab-Volt	EMS 8837-A0
4	Center-tapped Transformer	Acme Transformer	T-2-53013-S
5	DC Power Supply	BK Precision	1730A
6	Power Quality Analyzer	Fluke	43B
7	Voltage Isolator	Tektronix	P5200
8	Current Probe	Fluke	80i-110s
9	Current Probe (2)	Hewlett Packard	1146A
10	Current Probe Amplifier	Tektronix	TM502A
11	Multi-meter	Fluke	87
12	Oscilloscope	Tektronix	TDS2014

#### 4.1.4 Software Configuration

In this thesis, MATLAB Simulink is used to design the control loop for PWM boost type rectifier. Several functional blocks in the Simulink model calculate input current references and generate switching logic signals. The DSPACE RT1104 controller is embedded in MATLAB Simulink using the Real Time Workshop (RTW) toolbox, which converts the control logic and algorithm of the Simulink model into C code and downloads the code to DSPACE controller's memory. Then the DSPACE controller board can run the code in real time and achieve the functions designed in Simulink.

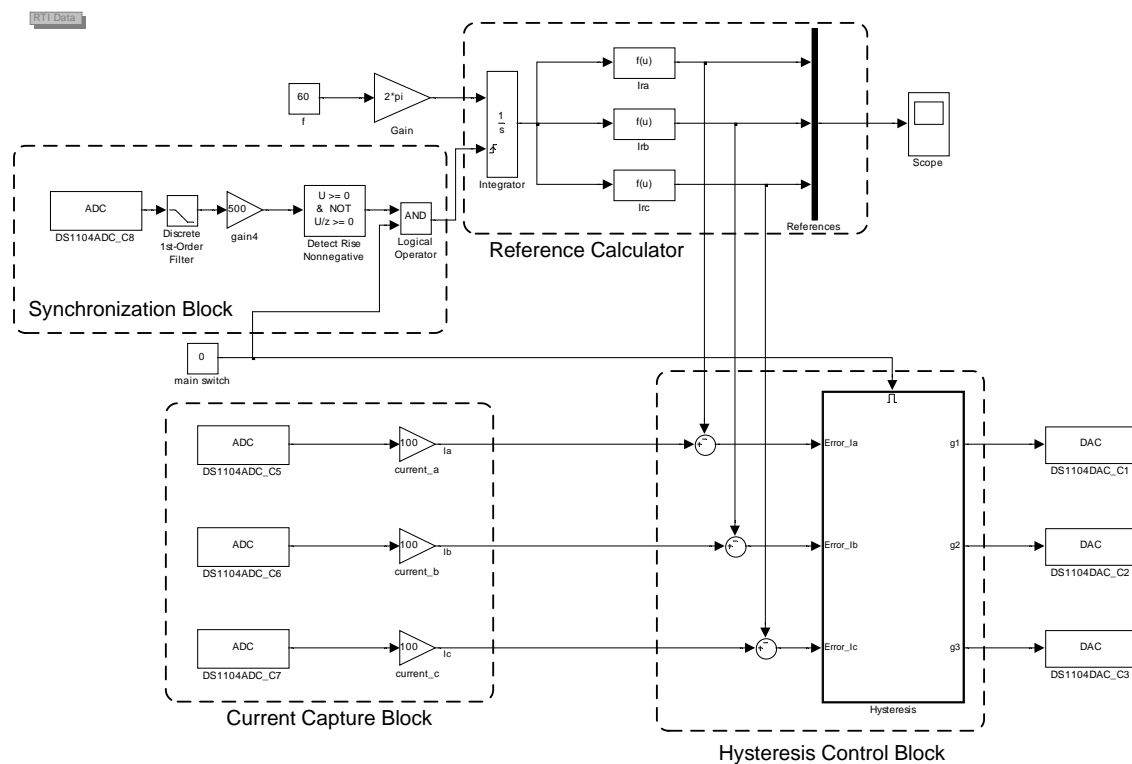


Figure 34: Diagram of Simulink model for open-loop operation

In the open-loop operation mode, the three-phase input voltages and impedances are pre-determined and used as known variables. This means the three-phase input

reference currents can be calculated in advance which reduces the complexity of implementation. As a result, smaller sampling time can be applied to obtain more accurate reference tracking. The MATLAB program for reference calculation is provided in appendix A.

The diagram of Simulink model in open-loop operation mode is shown in Fig. 34. Synchronization block measures phase A input voltage and gives reset signal every cycle through a zero-cross detection module. This signal resets the reference currents every cycle to avoid possible phase shift caused by frequency deviation. Reference calculator block reads the pre-calculated data from system memory and generates three-phase input reference currents in real time. Then, hysteresis control block will compare the actual currents to the references and supply gating logic signals to drive the converter.

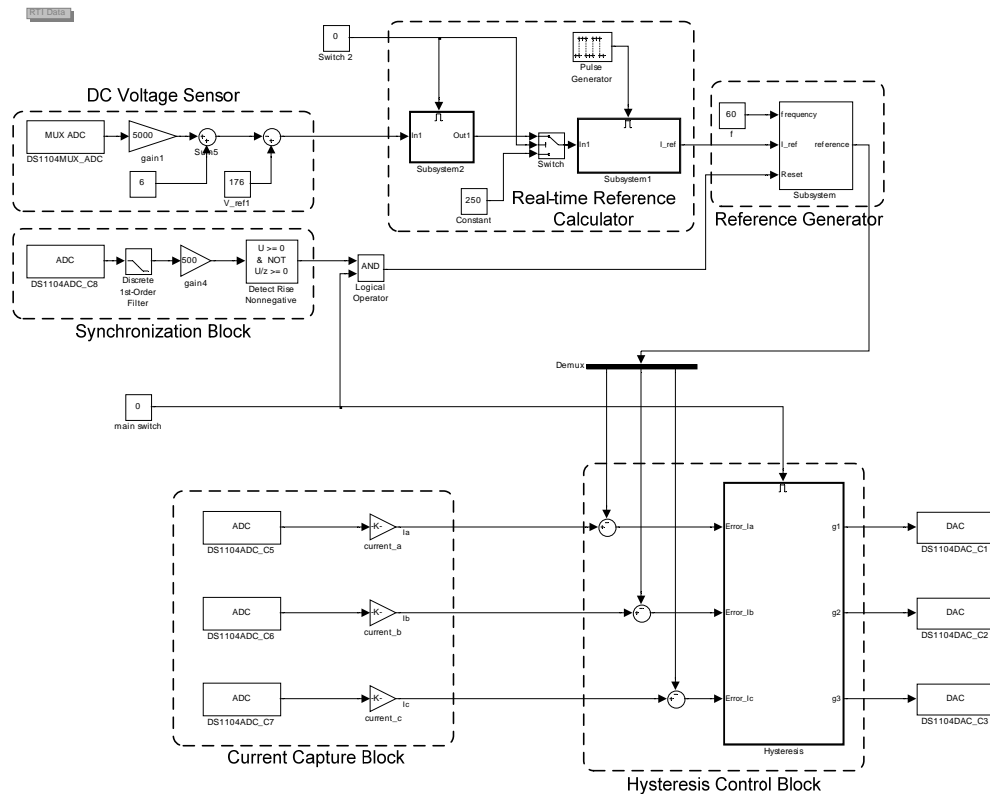


Figure 35: Diagram of Simulink model for closed-loop operation



In the closed-loop operation mode, a feedback loop is added to the Simulink model to make the DC link voltage controllable. Since the load resistance is fixed, desired DC link voltage can be obtained by updating the setting of transferred real power. This requires the Simulink model to handle a series of nonlinear calculations in real time and requires a bigger sampling step.

Fig. 35 shows the diagram of Simulink model with DC link voltage control. DC voltage sensor block takes care of the measurement of the actual DC link voltage. The difference between actual voltage and reference is sent to the real-time reference calculator. To reduce the burden of real-time calculation, a programmable trigger module is added, which prevents unnecessary calculations in each single time step. Then, the real-time updated reference currents are obtained and used to drive the rectifier system. The MATLAB program file and the detailed diagram of each functional block in closed-loop operation mode are provided in appendix B.

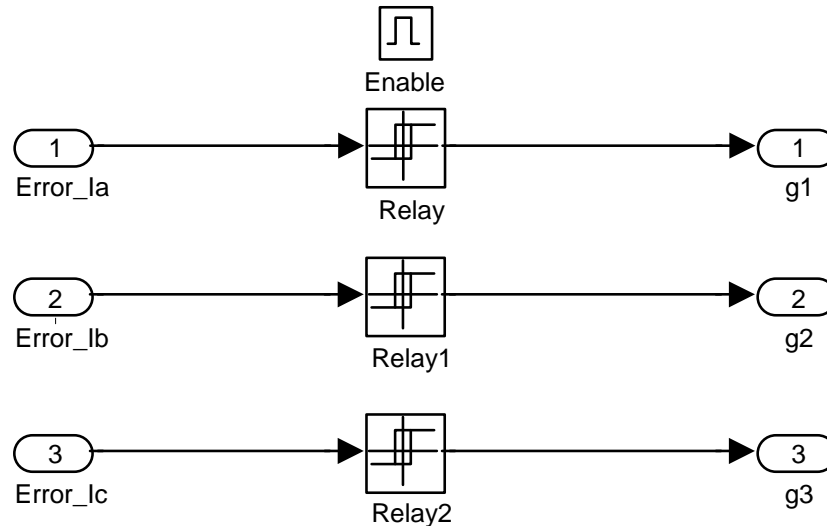


Figure 36: Digital hysteresis controllers in Simulink

Actual voltages and currents can be captured by A/D converters on the DSPACE RT1104 Master board. These actual values are compared with the reference currents. The digital hysteresis controller is defined in Simulink (see Fig. 36). Three relay blocks generate logical gating signals from the comparison between the currents' actual and the reference values. The logical signals are converted to analog signals through a set of D/A converters on the RT1104 Master board.

After the control loop is designed, DSPACE will convert the control schemes described in Fig. 34 and 35 into C codes using the Real Time Workshop (RTW) toolbox. Then, DSPACE processor can execute the codes and apply the control method in real time.

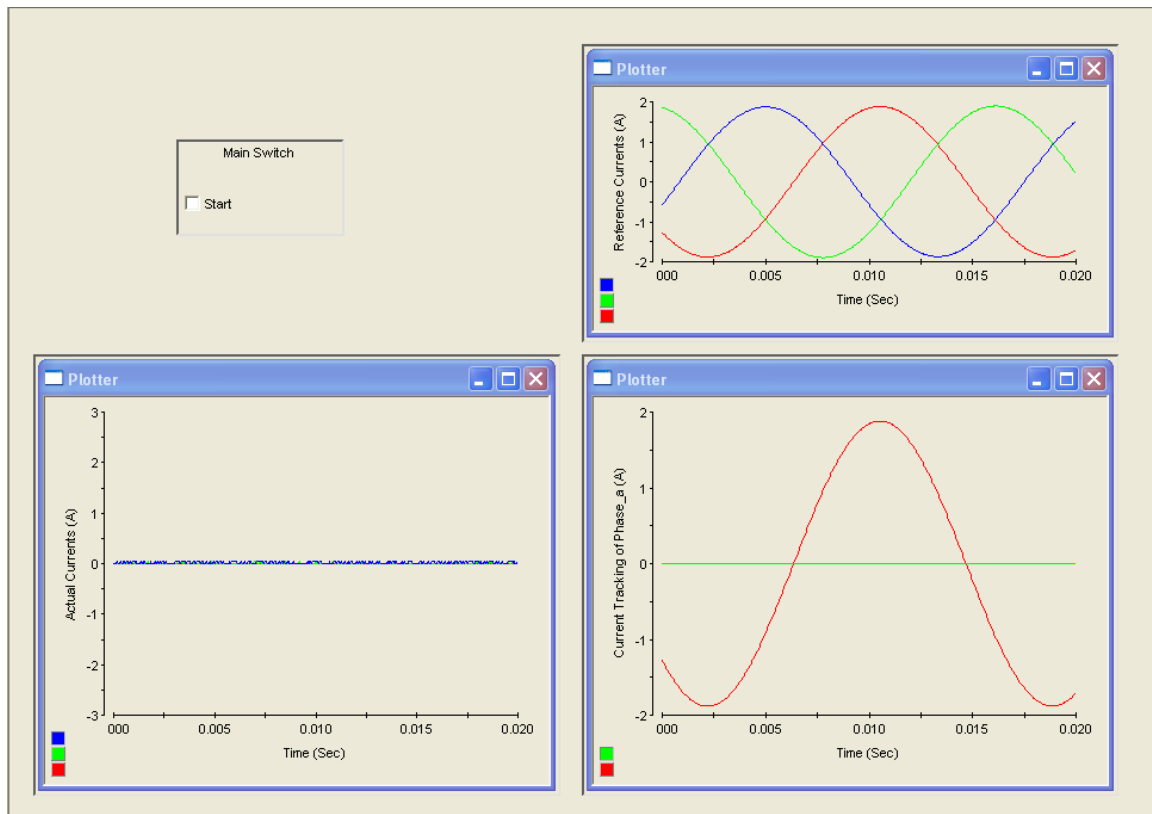


Figure 37: Diagram of the DSPACE control desk

The DSPACE control system provides a graphical user interface “DSPACE Control Desk” to achieve most of its control functions. Fig. 37 shows the user interface for DSPACE Control Desk. By clicking the “main switch”, the synchronization block and hysteresis controllers start working. The waveform of calculated reference currents is shown in the upper right corner. The bottom two plots show actual three-phase input currents and a comparison of actual and reference currents respectively.

## **4.2 Experimental Results**

Laboratory prototype of the three-phase PWM boost type rectifier has been built to implement the proposed harmonic elimination control scheme. It uses the DSPACE digital control system and Lab-Volt test bench.

Experimental results prove that the input-output harmonics can be effectively eliminated under extremely unbalanced operating conditions.

### **4.2.1 Open-Loop Operation Results**

Seven different simulation cases were selected in Chapter III. The same seven cases are selected in this experiment to test the proposed harmonic elimination method. A balanced case with balanced three-phase input voltages and impedances is performed as a reference case. Other six cases with different levels of unbalanced three-phase input

conditions are examined. Table VIII shows the list of all experiment cases performed on Lab-Volt IGBT bridge.

TABLE VIII: EXPERIMENT CASES ON LAB-VOLT IGBT BRIDGE

CASE	Input Conditions		Power Setting (W)	DC Load Resistance ( $\Omega$ )
	Voltage (V)	Impedance		
1	$U_1 = 60\angle 0^\circ$ $U_2 = 60\angle -120^\circ$ $U_3 = 60\angle 120^\circ$	$L_1 = L_2 = L_3 = 10\text{mH}$	250	114
2	$U_1 = 60\angle 0^\circ$ $U_2 = 60\angle -120^\circ$ $U_3 = 60\angle 120^\circ$	$L_1 = L_3 = 10\text{mH}$ $L_2 = 0$	250	114
3	$U_1 = 60\angle 0^\circ$ $U_2 = 60\angle -120^\circ$ $U_3 = 0$	$L_1 = L_2 = L_3 = 10\text{mH}$	250	114
4	$U_1 = 60\angle 0^\circ$ $U_2 = 60\angle -120^\circ$ $U_3 = 0$	$L_1 = L_3 = 10\text{mH}$ $L_2 = 0$	250	114
5	$U_1 = 60\angle 0^\circ$ $U_2 = 0$ $U_3 = 0$	$L_1 = L_2 = L_3 = 10\text{mH}$	100	342
6	$U_1 = 60\angle 0^\circ$ $U_2 = 0$ $U_3 = 0$	$L_1 = 0$ $L_2 = L_3 = 10\text{mH}$	100	342
7	$U_1 = 60\angle 0^\circ$ $U_2 = 60\angle -180^\circ$ $U_3 = 0$	$L_1 = L_2 = L_3 = 10\text{mH}$	100	400

The current probe and voltage isolator are set at the numbers listed in Table IX for all seven experiment cases.

TABLE IX: MEASUREMENT SETTING

Item	Setting
Current Probe	100 mV/A
Voltage Isolator	2 mV/V

The results of case 1 indicate that the proposed method works for three-phase balanced conditions. Fig. 38 shows the measured waveforms of three-phase line currents and DC link voltage.

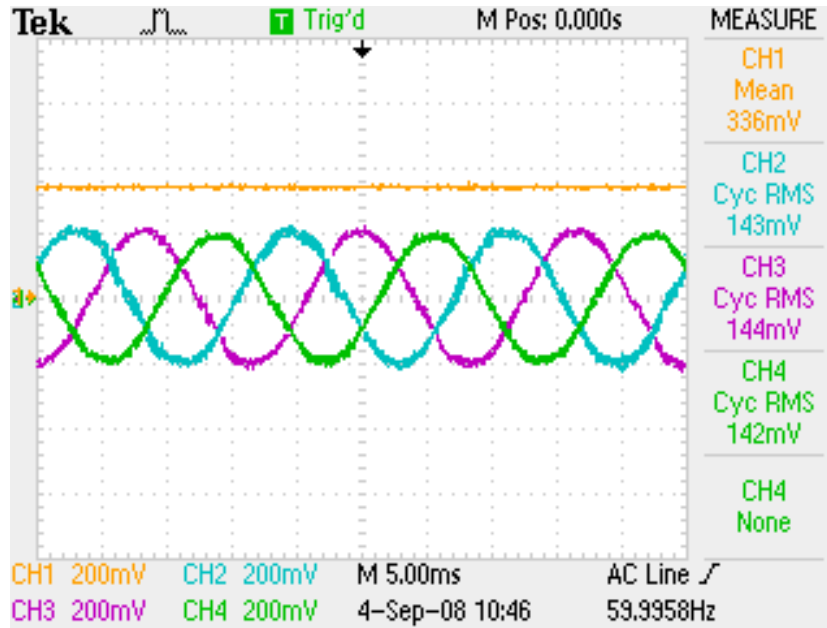


Figure 38: Line currents and DC link voltage of case 1

From case 2 to case 7, different levels of unbalanced operating conditions appear at the input of three-phase PWM boost type rectifier. Results are shown in Fig. 39 to 44. Each figure shows waveforms of input line currents and DC link voltage.

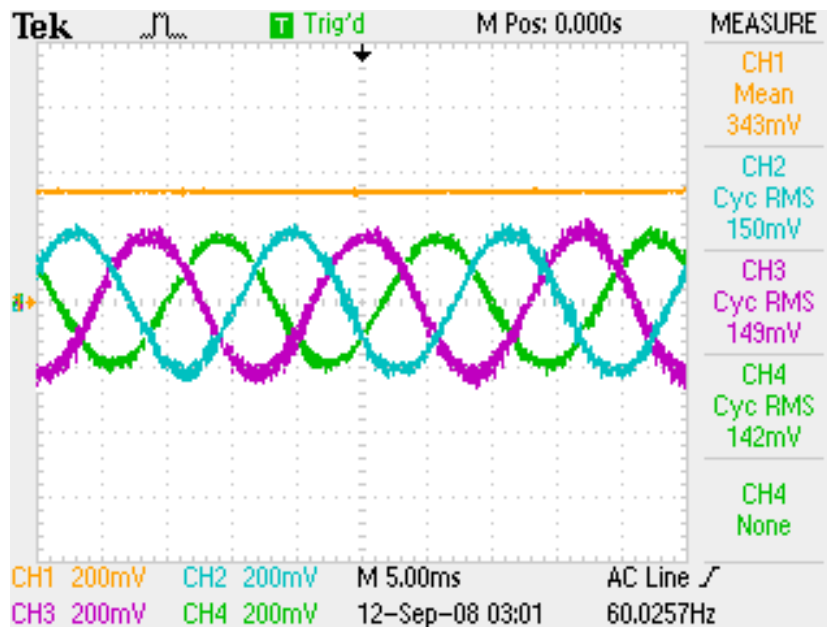


Figure 39: Input voltages, DC link voltage and line currents of case 2

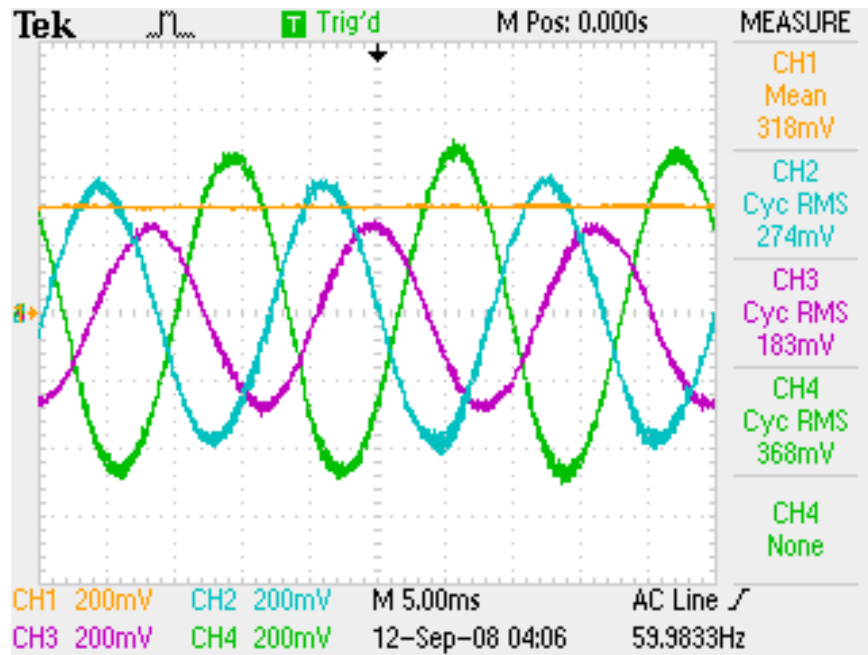


Figure 40: Input voltages, DC link voltage and line currents of case 3

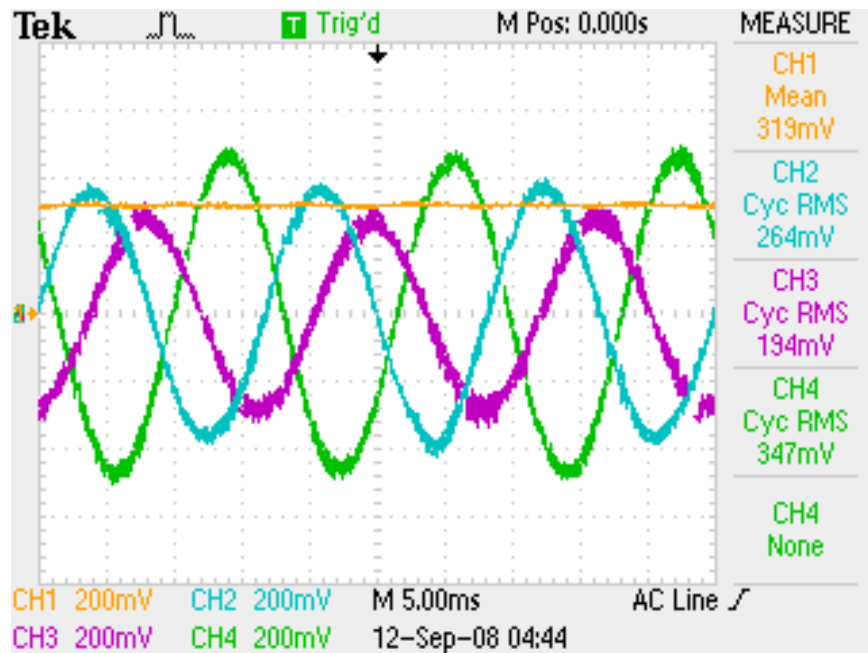


Figure 41: Input voltages, DC link voltage and line currents of case 4

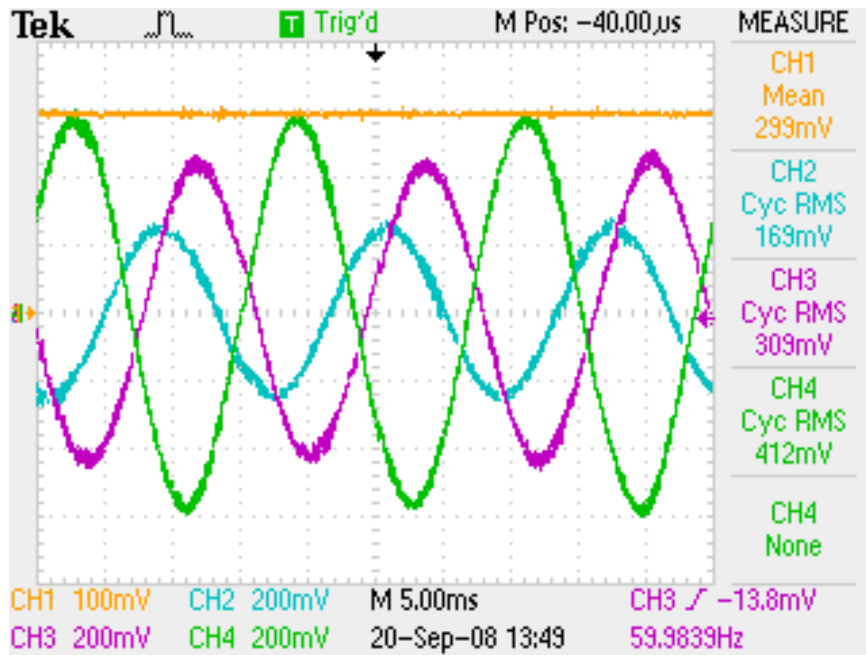


Figure 42: Input voltages, DC link voltage and line currents of case 5

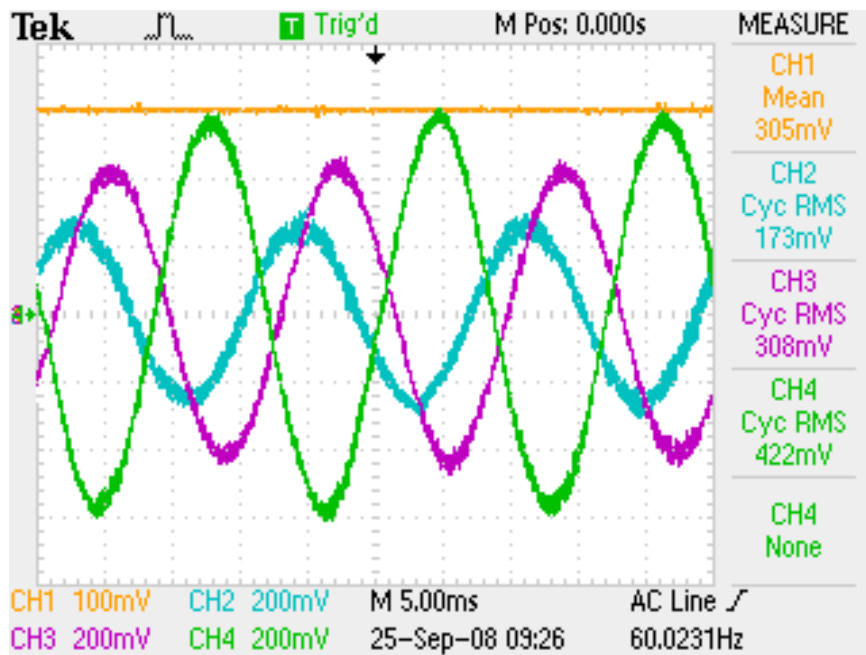


Figure 43: Input voltages, DC link voltage and line currents of case 6

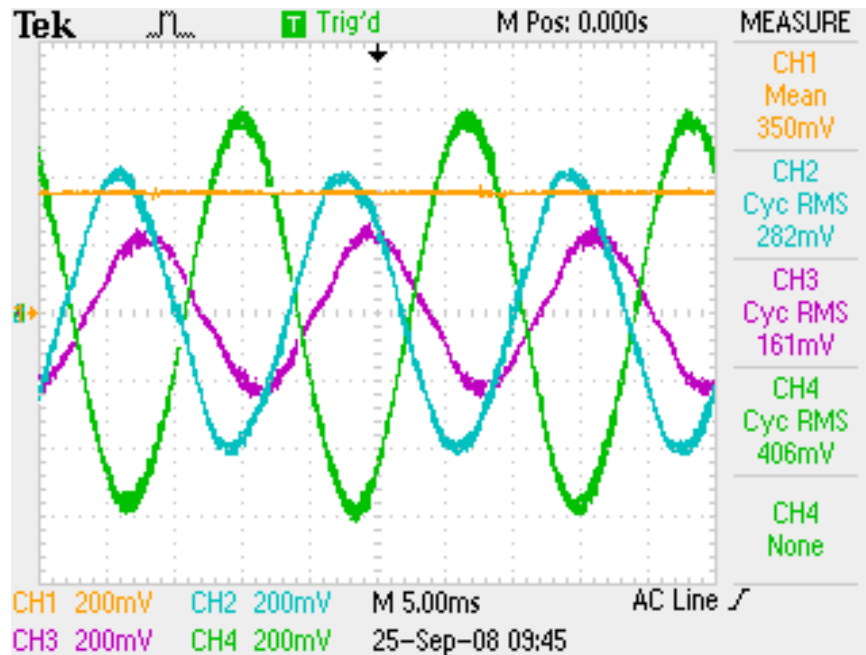


Figure 44: Input voltages, DC link voltage and line currents of case 7

In open-loop operation mode, the sampling time is set at  $T_s = 20 \mu\text{S}$ , therefore, the theoretical maximum switching frequency  $f_{\text{max}} = 25 \text{ kHz}$ . Fig. 45 below shows the measured maximum switching frequency  $f_{\text{max}} = 25 \text{ kHz}$ .

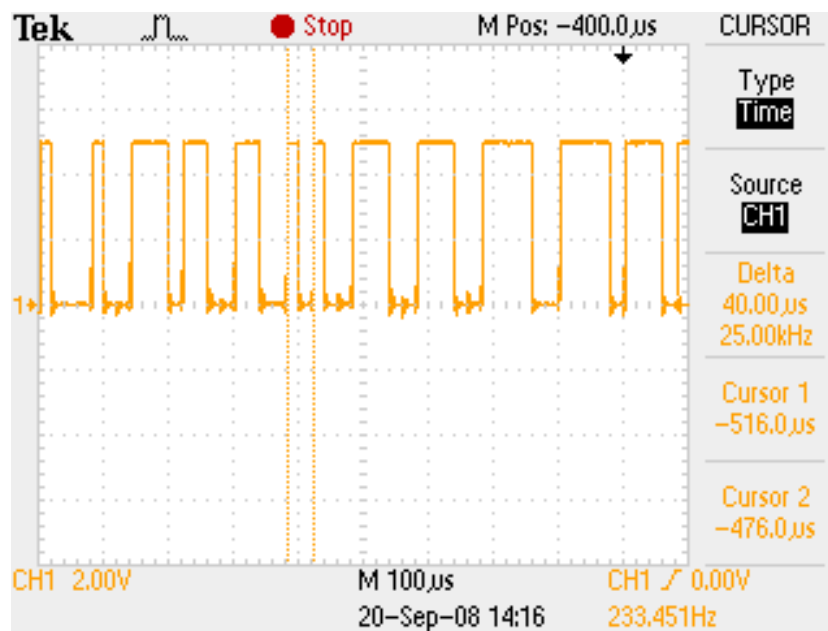


Figure 45: Measured switching frequency in open-loop operation



The comparisons of simulation and experimental results are summarized in Table X and XI. Table X gives the rms values of three-phase input line currents in all seven cases. And Table XI lists the results of DC link voltages.

TABLE X: COMPARISON SIMULATION AND EXPERIMENTAL CURRENTS (MAGNITUDE)

CASE	Simulation Currents rms (A)			Experiment Currents rms (A)		
	a	b	c	a	b	c
1	1.429	1.429	1.43	1.43	1.44	1.42
2	1.507	1.494	1.438	1.50	1.49	1.42
3	2.737	1.816	3.629	2.74	1.83	3.68
4	2.684	1.894	3.512	2.64	1.94	3.47
5	1.697	3.174	4.258	1.69	3.09	4.12
6	1.761	3.109	4.293	1.73	3.08	4.22
7	2.78	1.625	4.201	2.82	1.61	4.06

TABLE XI: COMPARISON OF REFERENCE, SIMULATION AND EXPERIMENTAL VOLTAGES

CASE	DC Link Voltage (V)		Case Description
	Simulation	Experiment	
1	168.3	168	Balanced condition
2	171.1	171.5	3 voltages, 2 impedances
3	162.6	159	2 voltages, 3 impedances
4	164.7	159.5	2 voltages, 2 impedances
5	156.2	149.5	Single voltage, 3 impedances
6	161.2	152.5	Single voltage, 2 impedances
7	177.1	175	Center tapped voltages, 3 Impedances

From Table X, it can be seen experimental results of input currents are consistent with the simulation results. According to Table XI, the error of DC link voltages between simulation and experimental result increases when the level of imbalance increases, which indicates an efficiency drop of the system under extreme conditions. Table XII lists the comparison of simulation and experimental efficiencies.

TABLE XII: COMPARISON OF SIMULATION AND EXPERIMENTAL EFFICIENCY

CASE	Simulation					Experiment				
	INPUT			OUTPUT	Efficiency	INPUT			OUTPUT	Efficiency
	P (W)	Q (Var)	pf	P (W)		P (W)	Q (Var)	pf	P (W)	
1	257.2	0.7731	1.0	248.2	96.5%	256	0.0	1.0	247.6	96.7%
2	265.5	0.7073	1.0	256.8	96.7%	268	0.4	1.0	258.0	96.3%
3	254.2	1.208	1.0	231.1	90.9%	245	12.5	0.999	221.8	90.5%
4	259.5	2.11	1.0	236.8	91.2%	250	0.0	1.0	223.2	89.3%
5	101.9	0.3532	1.0	71.3	70.0%	99	0.0	1.0	65.4	66.1%
6	105.0	0.7049	1.0	76.0	72.3%	101	6.6	0.998	68.0	67.33%
7	105.5	0.4098	1.0	78.7	74.5%	105	0.0	1.0	79.2	72.9%

The measurement indicates that the PWM boost type rectifier operates under the unity power factor for all seven cases. One particular case 6, in which the rectifier is supplied from a center-tapped transformer, is selected to demonstrate the unity power factor. In case 6, phase A draws reactive power from the input while phase B supplies the same amount of reactive power so that the net input reactive power is equal to zero. Fig. 46 shows phase A current lags the voltage. Fig. 47 shows phase B current leads the voltage.

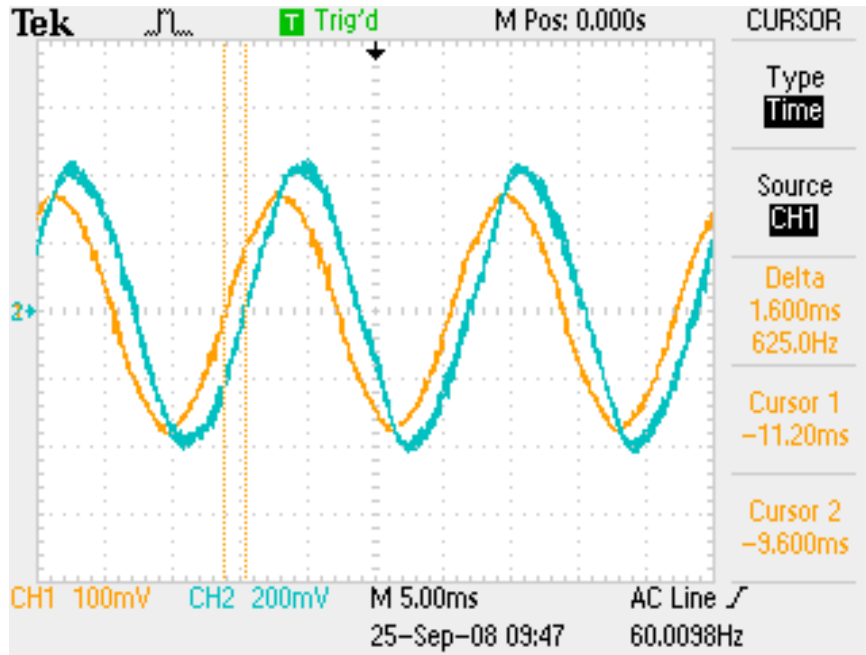


Figure 46: Angle between phase A voltage and current

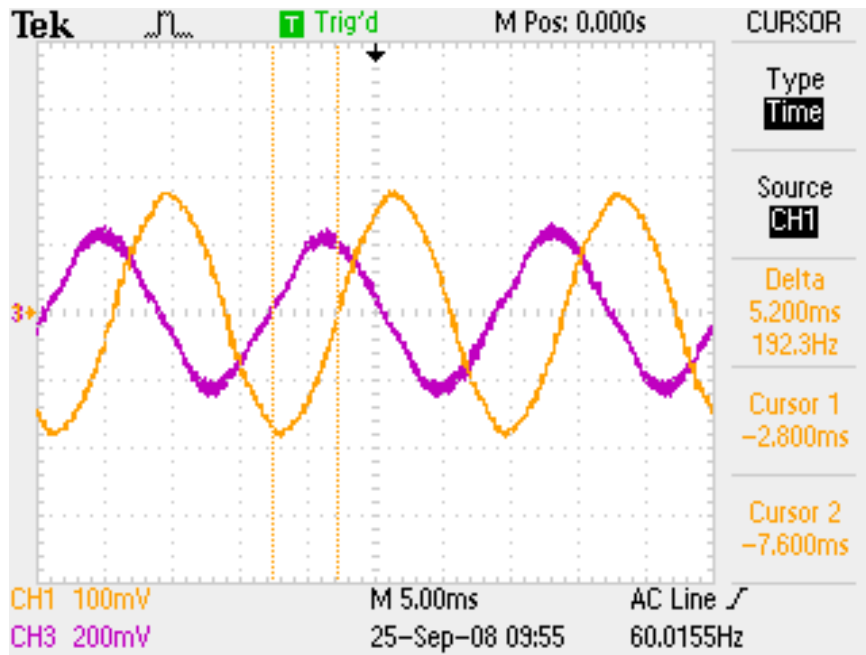


Figure 47: Angle between phase B voltage and current

According to Fig. 38 to Fig. 44, there is no obvious low-order harmonic component in line currents and DC link voltage when the three-phase PWM boost type rectifier is operating under unbalanced conditions. The spectrums of three-phase currents of all cases are shown in Fig. 48 to Fig. 68.

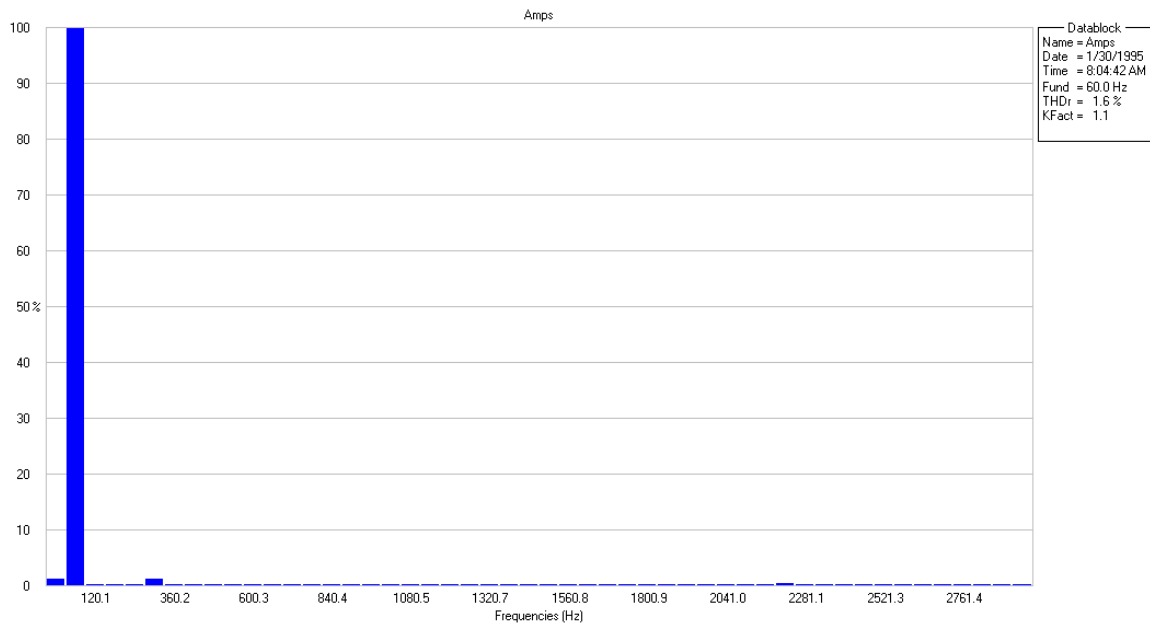


Figure 48: Spectrum of phase A current of case 1

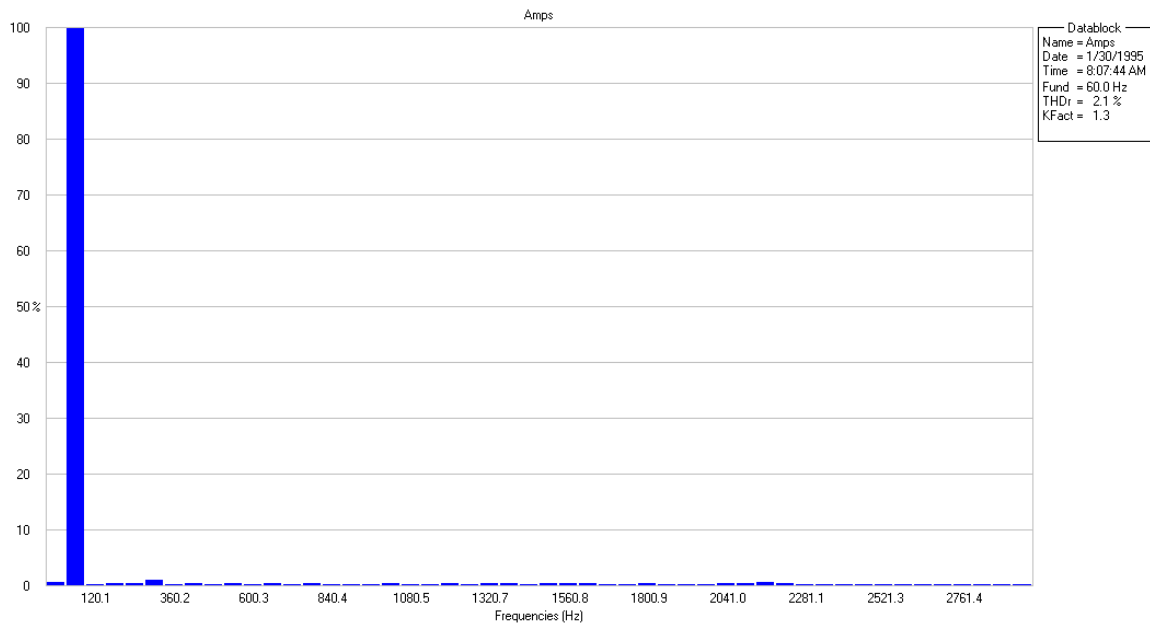


Figure 49: Spectrum of phase B current of case 1

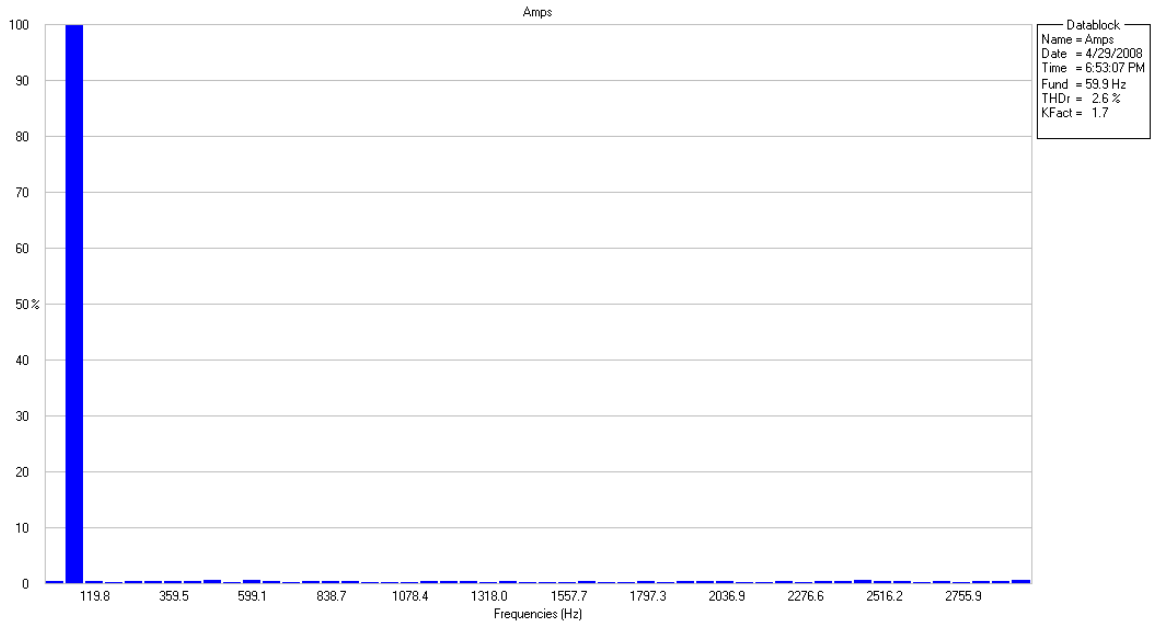


Figure 50: Spectrum of phase C current of case 1

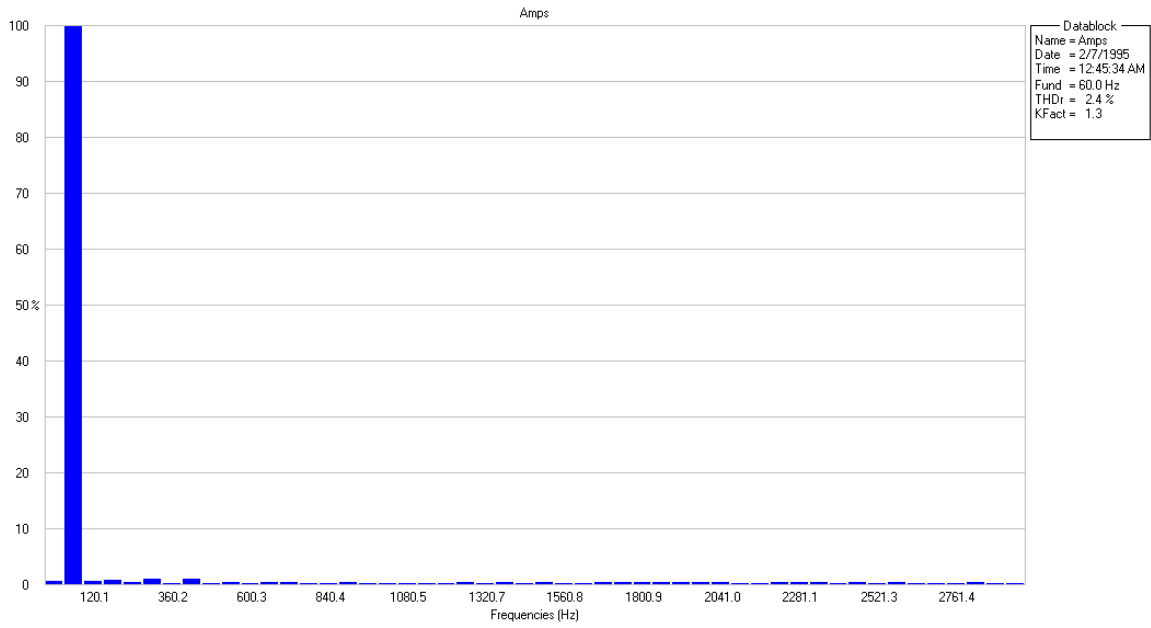


Figure 51: Spectrum of phase A current of case 2

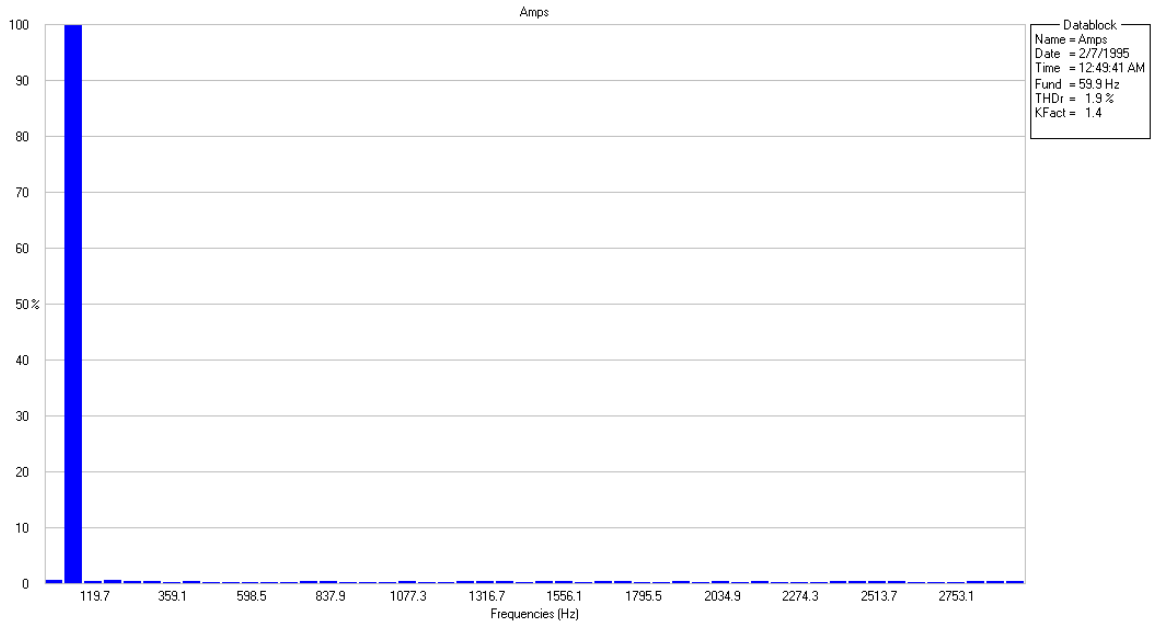


Figure 52: Spectrum of phase B current of case 2

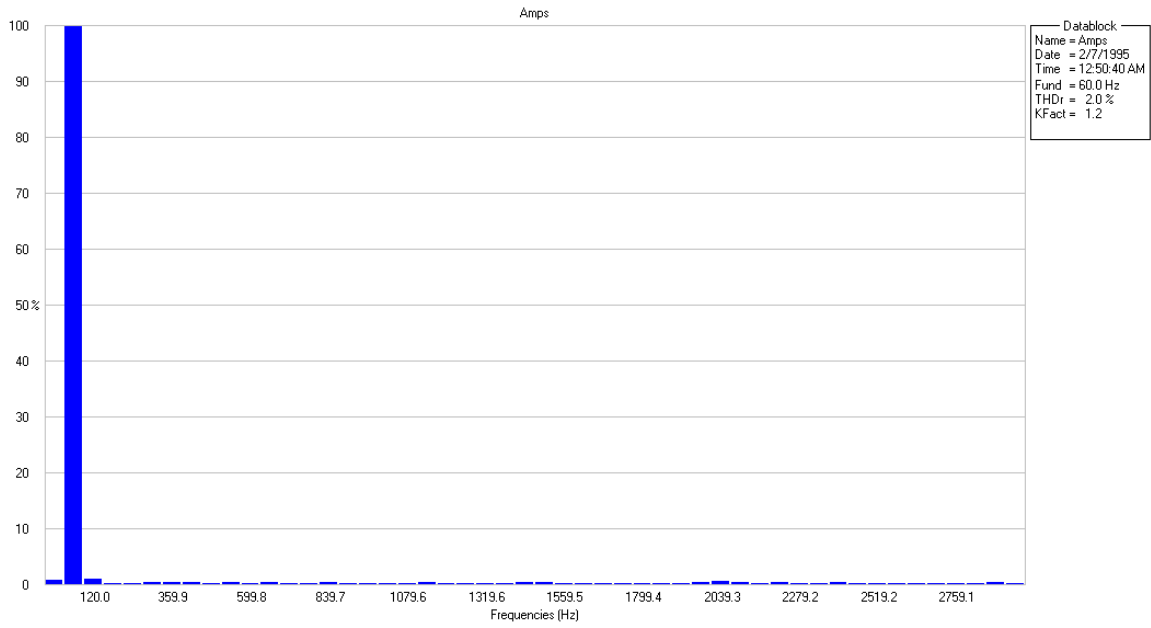


Figure 53: Spectrum of phase C current of case 2

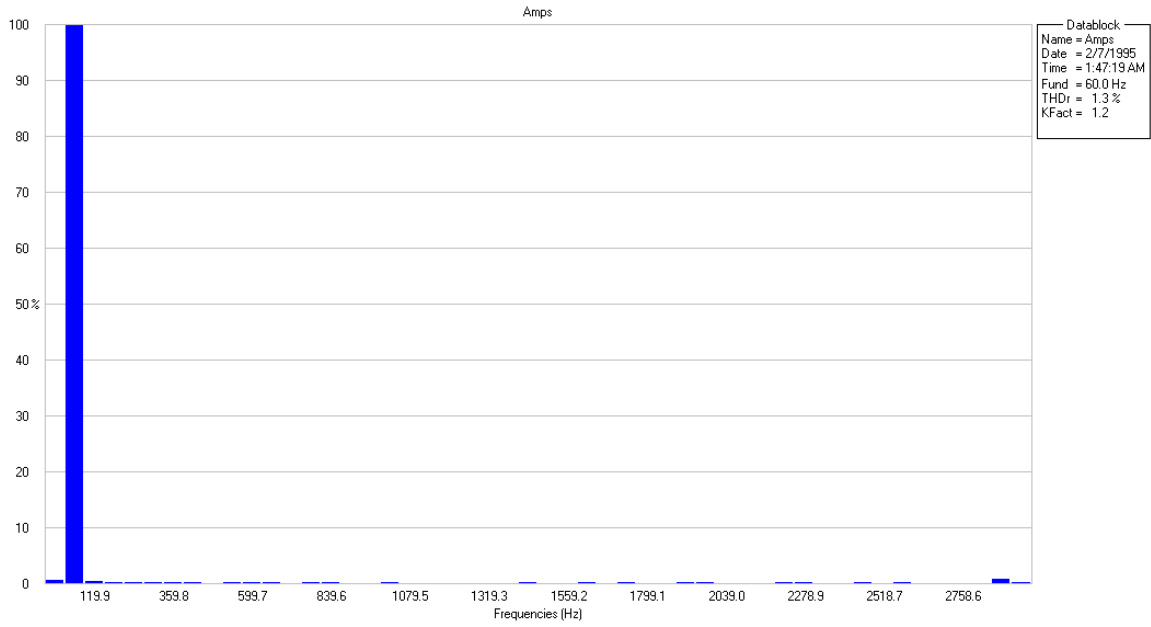


Figure 54: Spectrum of phase A current of case 3

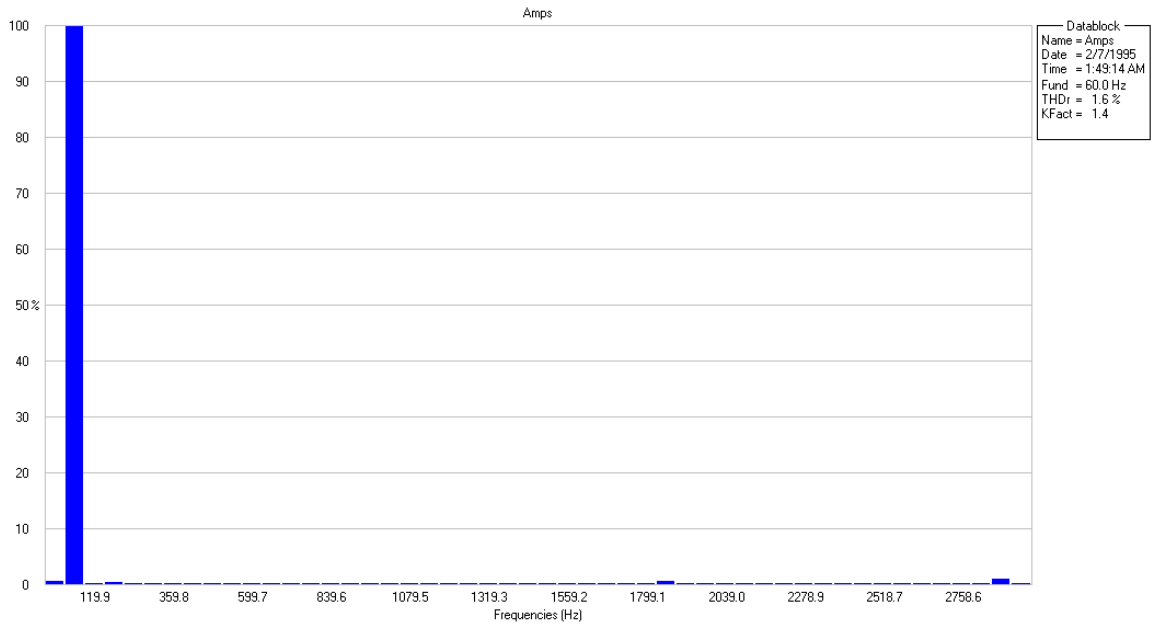


Figure 55: Spectrum of phase B current of case 3

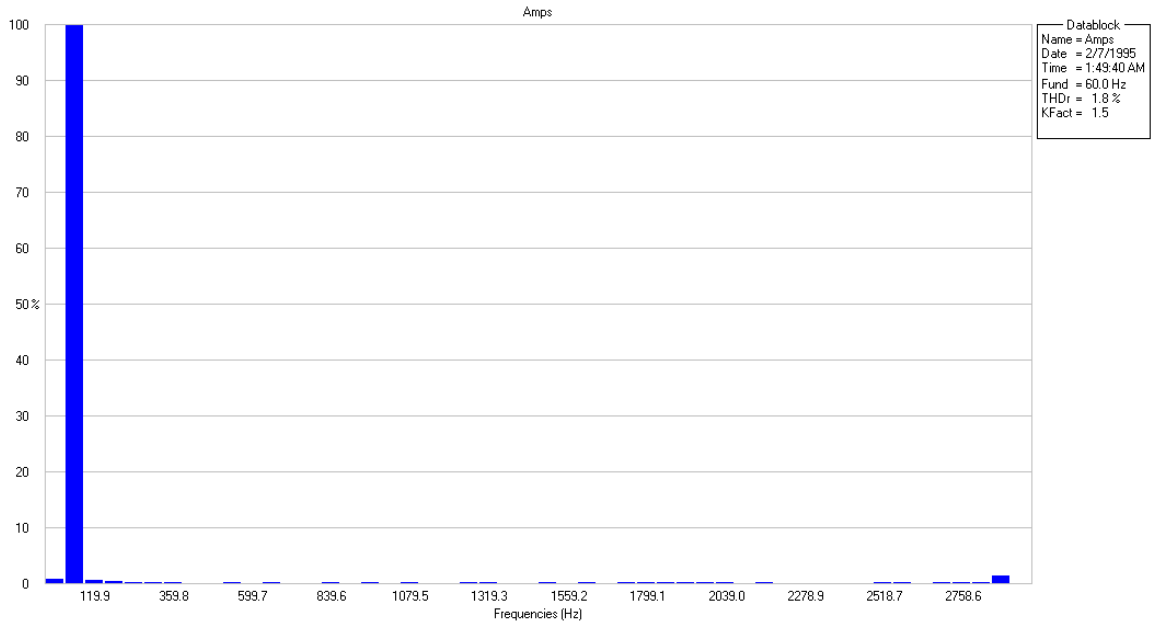


Figure 56: Spectrum of phase C current of case 3

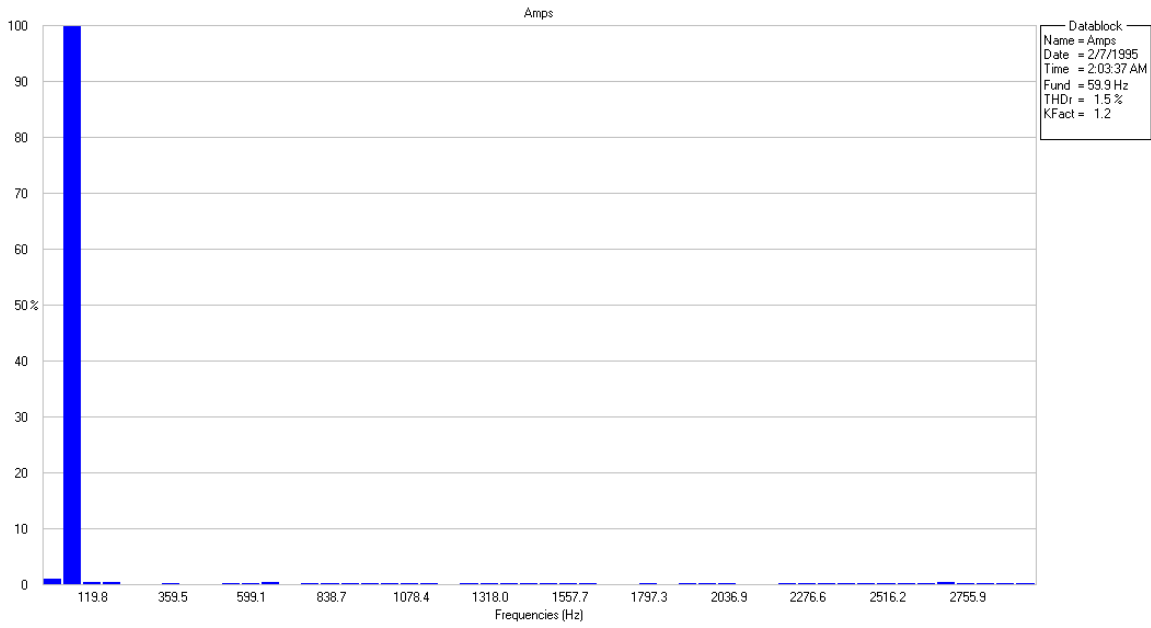


Figure 57: Spectrum of phase A current of case 4



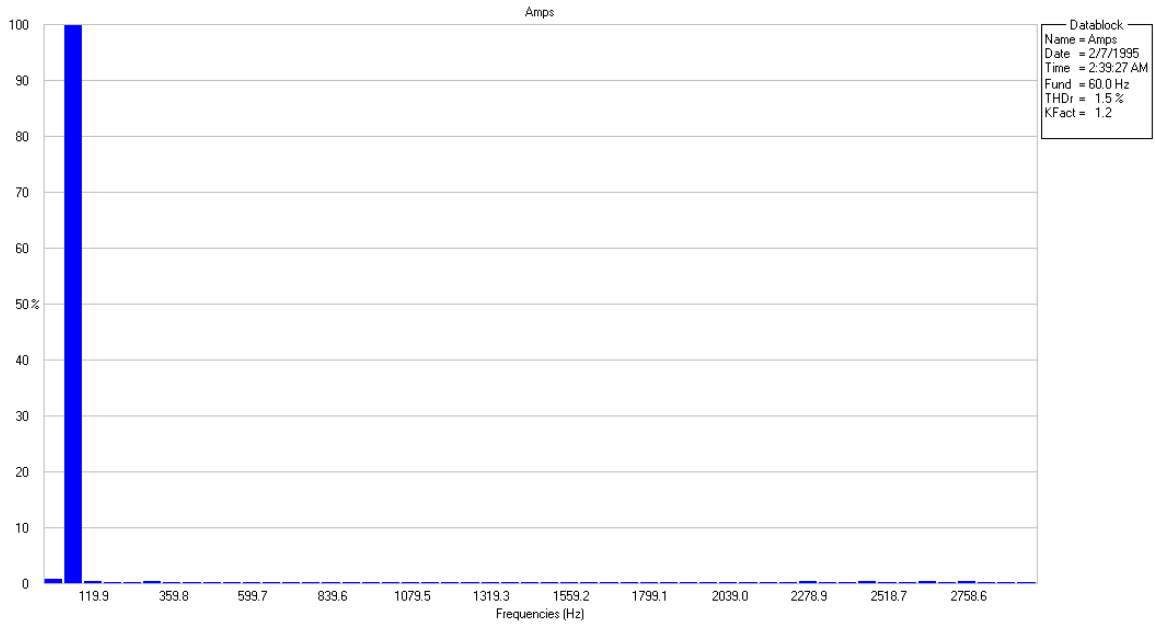


Figure 58: Spectrum of phase B current of case 4

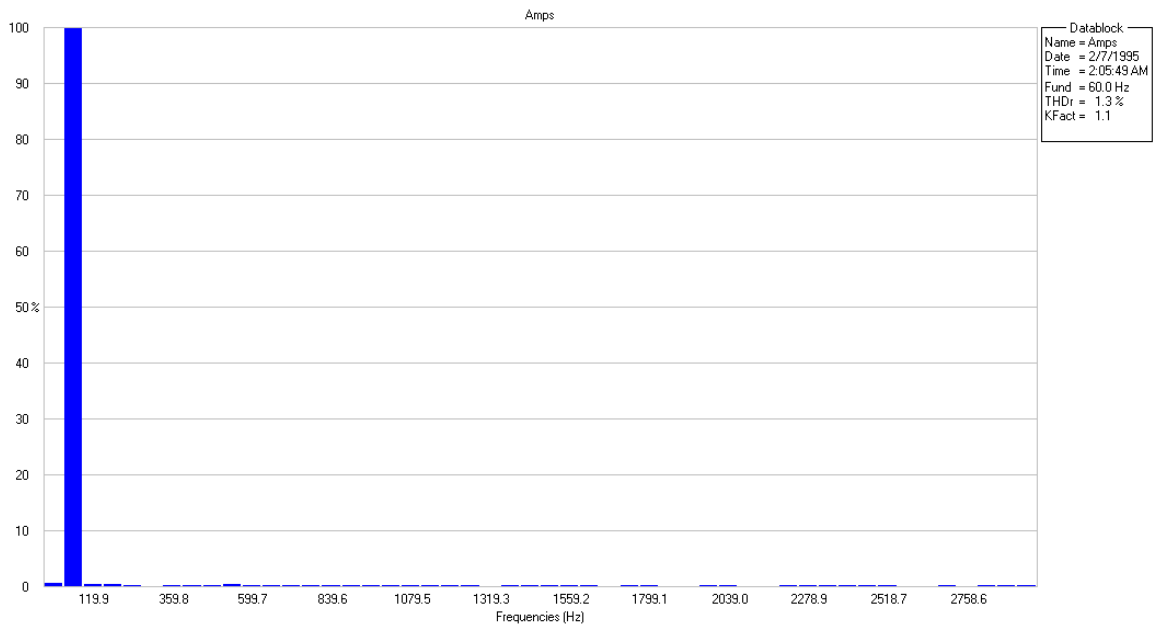


Figure 59: Spectrum of phase C current of case 4

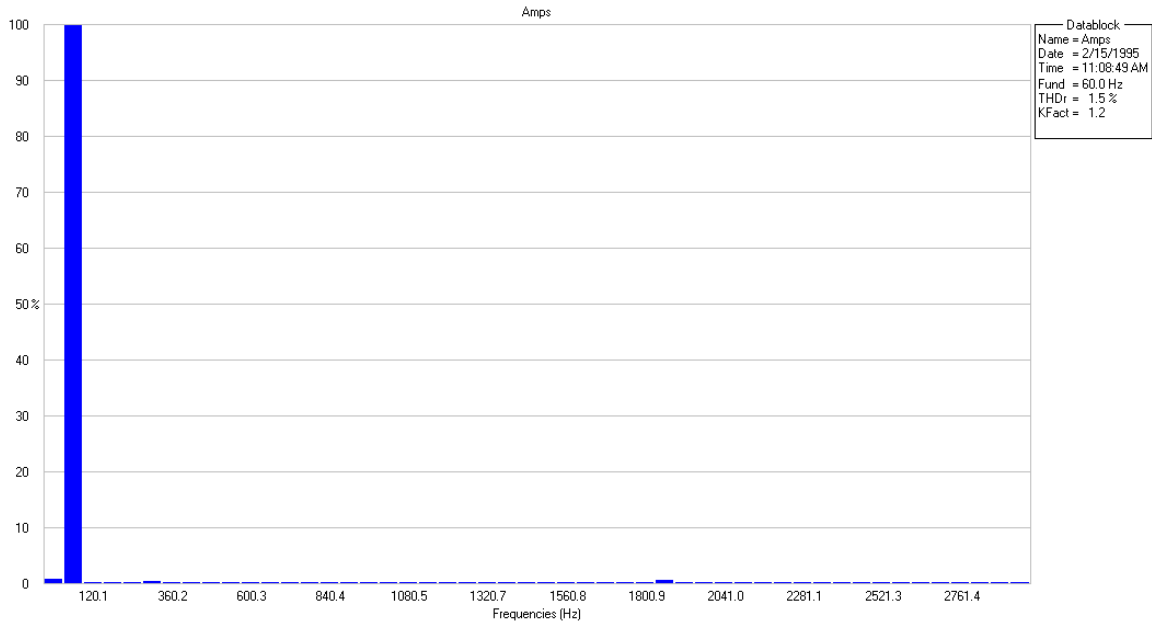


Figure 60: Spectrum of phase A current of case 5

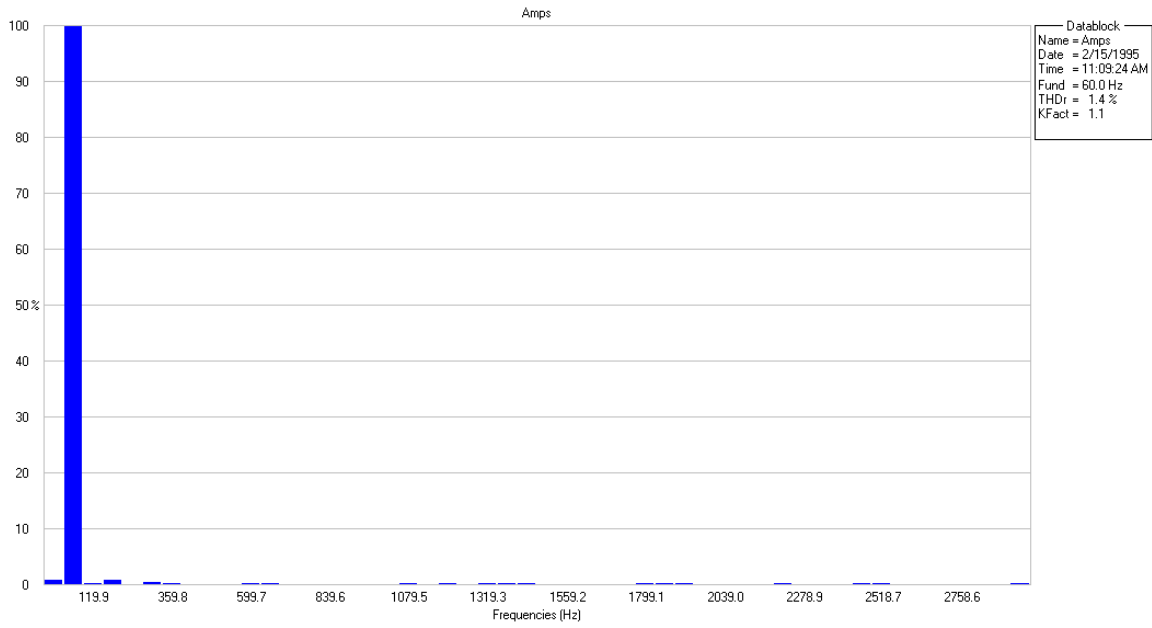


Figure 61: Spectrum of phase B current of case 5

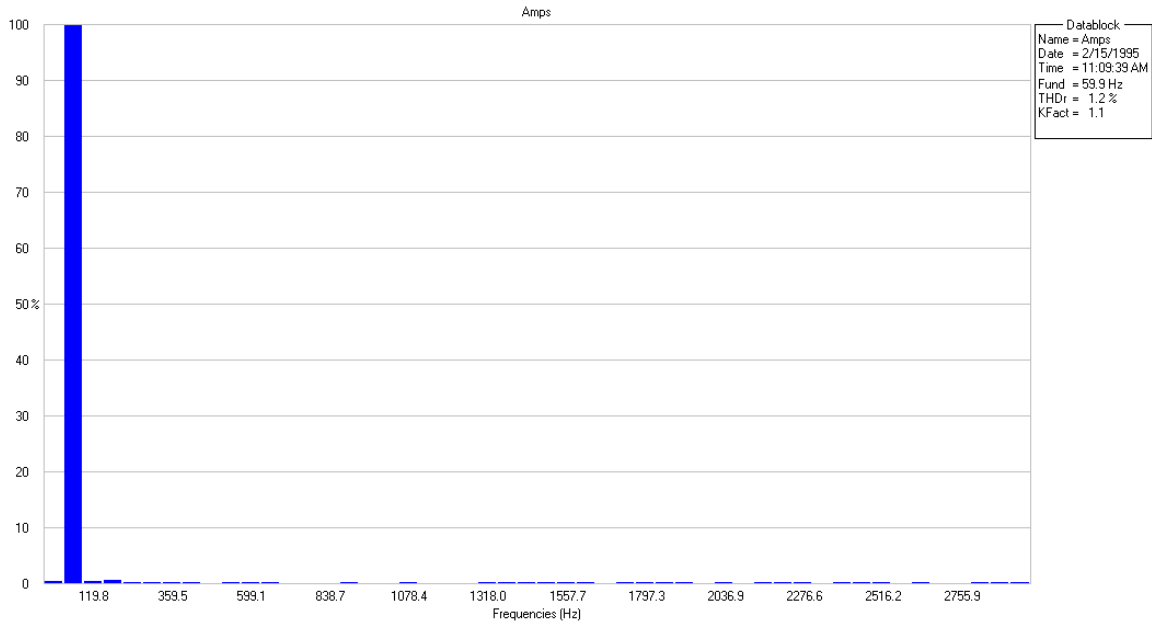


Figure 62: Spectrum of phase C current of case 5

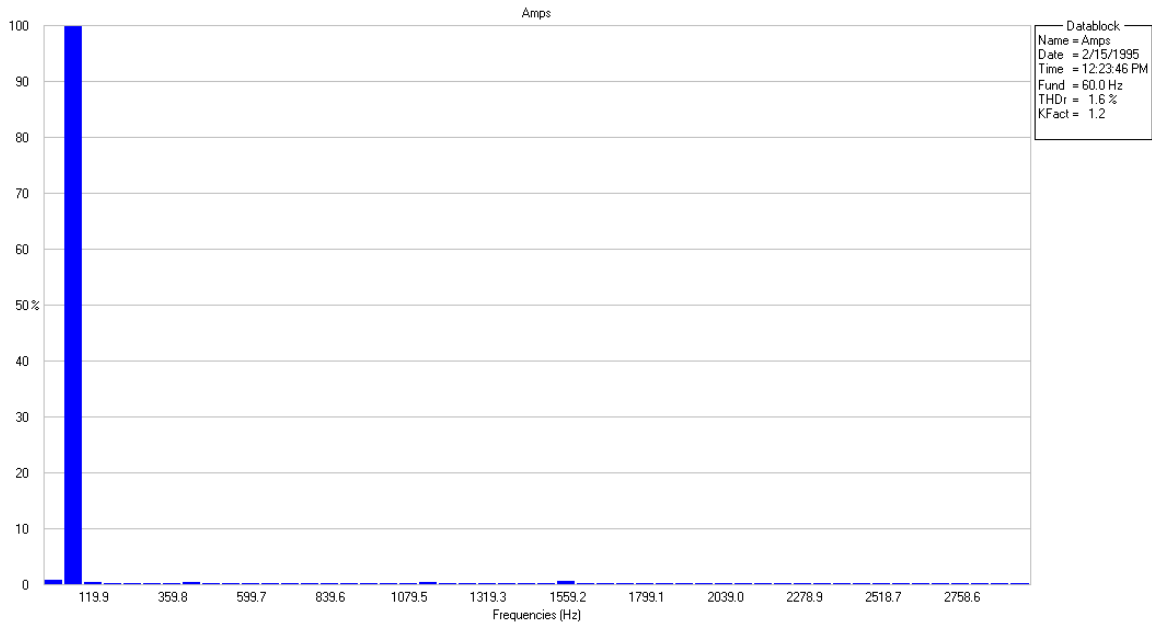


Figure 63: Spectrum of phase A current of case 6

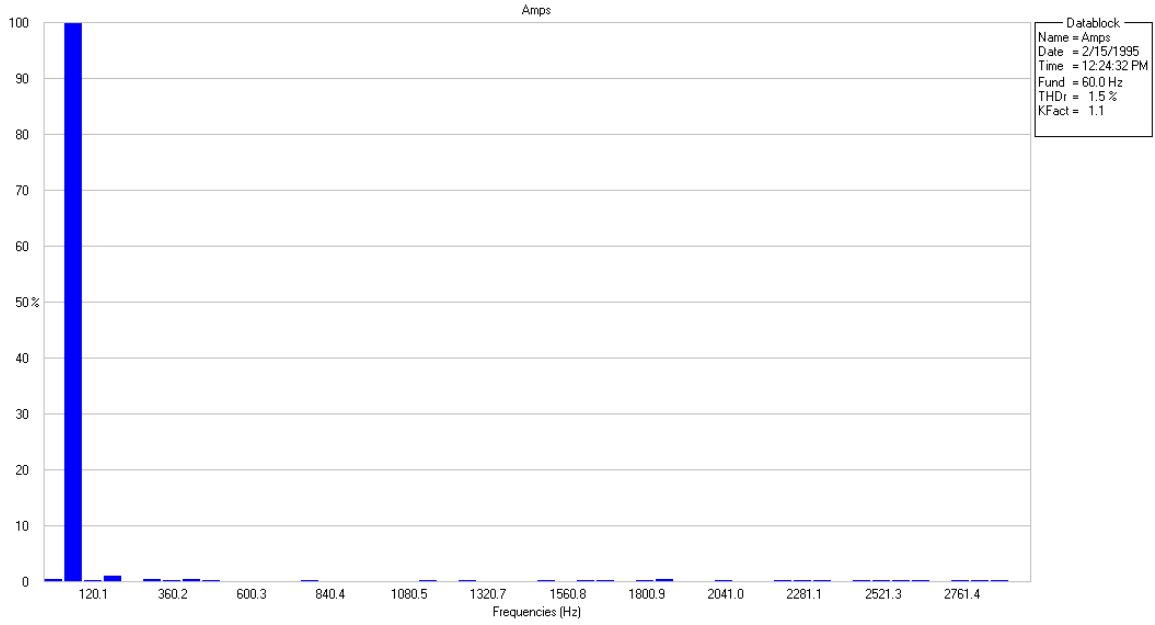


Figure 64: Spectrum of phase B current of case 6

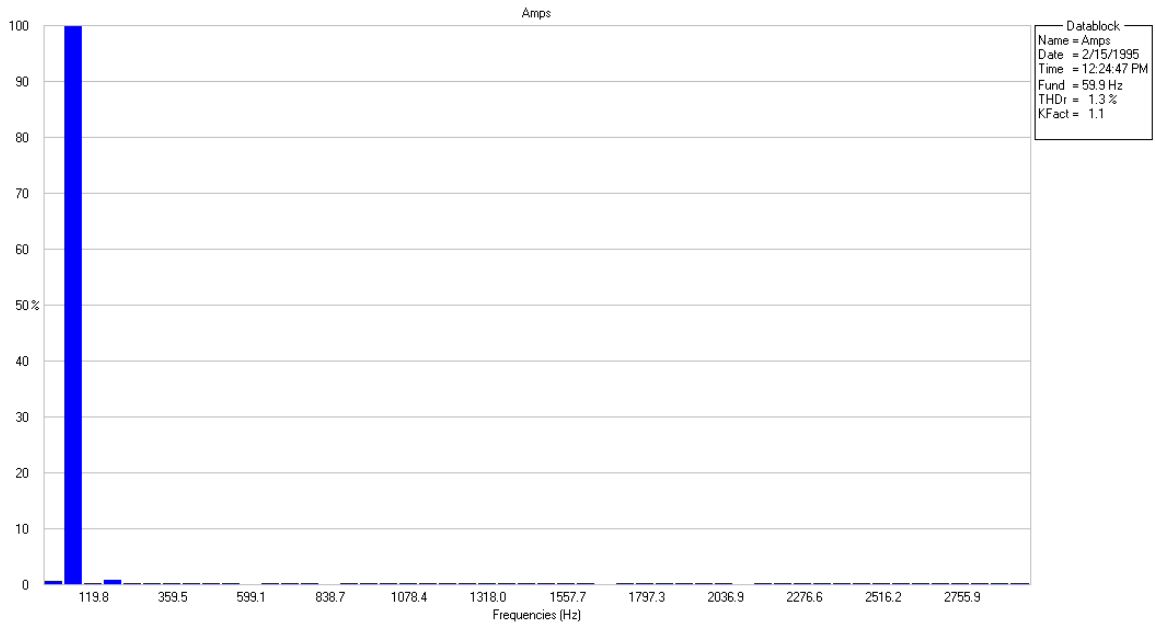


Figure 65: Spectrum of phase C current of case 6

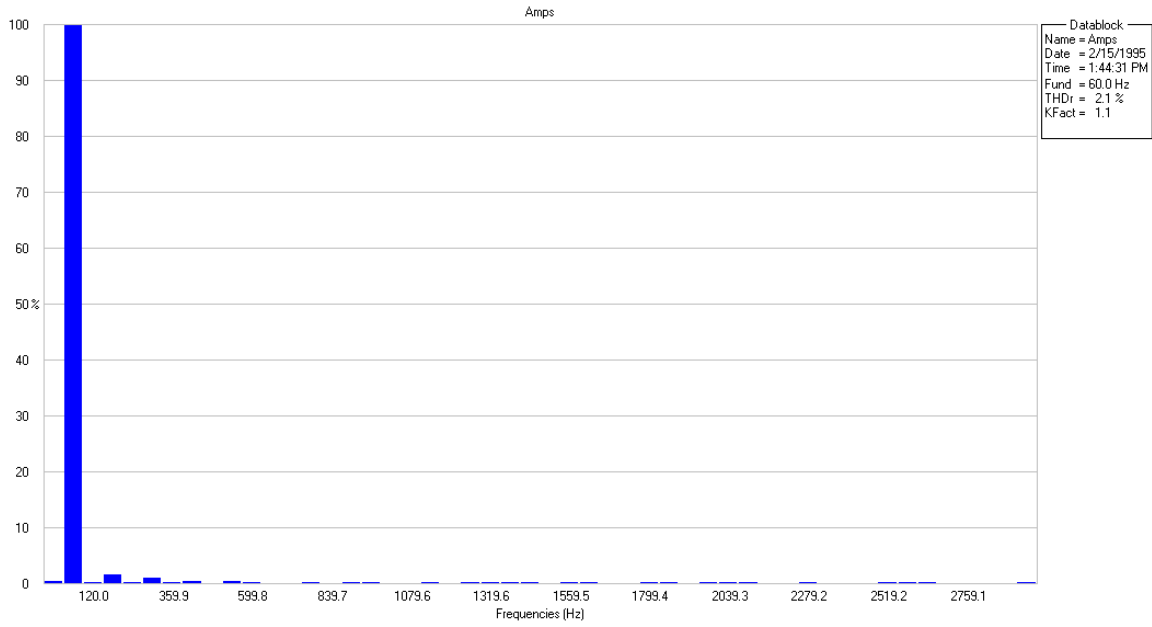


Figure 66: Spectrum of phase A current of case 7

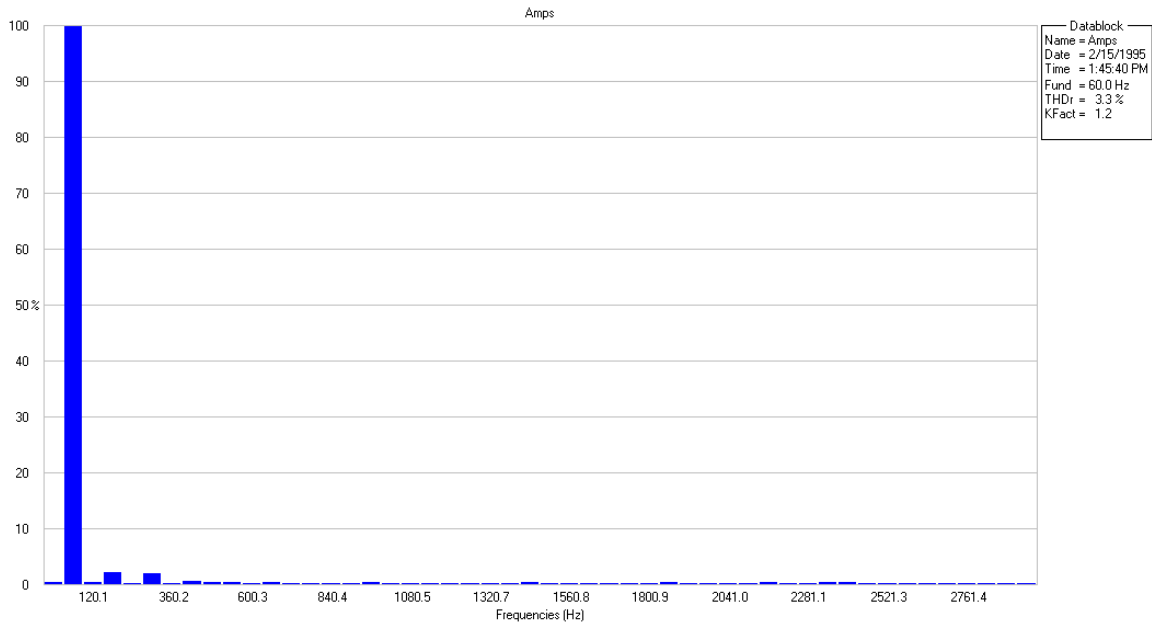


Figure 67: Spectrum of phase B current of case 7

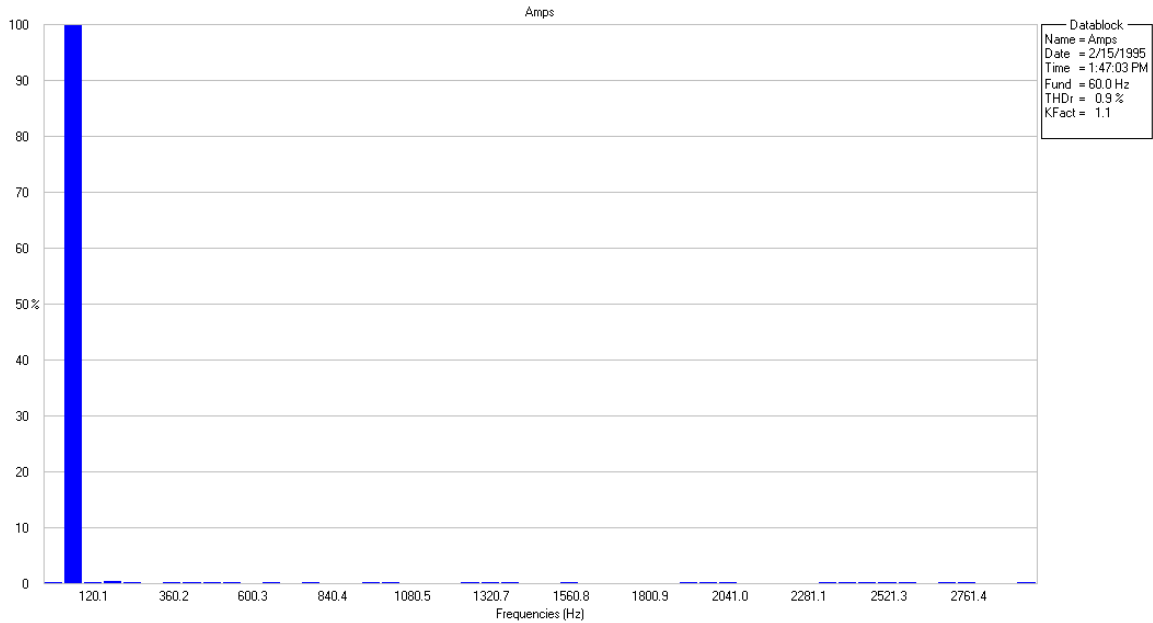


Figure 68: Spectrum of phase C current of case 7

Table XIII summarizes the total harmonic distortion of line currents in all seven cases. Results show that the proposed method effectively eliminated the harmonics even under extreme conditions.

TABLE XIII: LIST OF TOTAL HARMONIC DISTORTION OF LINE CURRENTS

CASE	THD of Input Line Currents			Case Description
	Phase A	Phase B	Phase C	
1	1.6%	2.1%	2.6%	Balanced condition
2	2.4%	1.9%	2.0%	3 voltages, 2 impedances
3	1.3%	1.6%	1.8%	2 voltages, 3 impedances
4	1.5%	1.5%	1.3%	2 voltages, 2 impedances
5	1.5%	1.4%	1.2%	Single voltage, 3 impedances
6	1.6%	1.5%	1.3%	Single voltage, 2 impedances
7	2.1%	3.3%	0.9%	Center tapped voltages, 3 Impedances

#### 4.2.2 Closed-loop Operation Results

The closed-loop operation is performed on case 3 to control the DC link voltage while harmonic elimination. Using the control model in Fig. 35, desired DC link voltage can be obtained. The DC reference is initially set to be 180V and has a step change to 200V. After a while, the DC reference changes back to 180V. The actual voltage tracks the reference in real time. In steady state, the waveforms of input line currents and DC link voltage are similar to those obtained in the open-loop operation. Figures 69, 70 and 71 show the actual DC link voltage change.

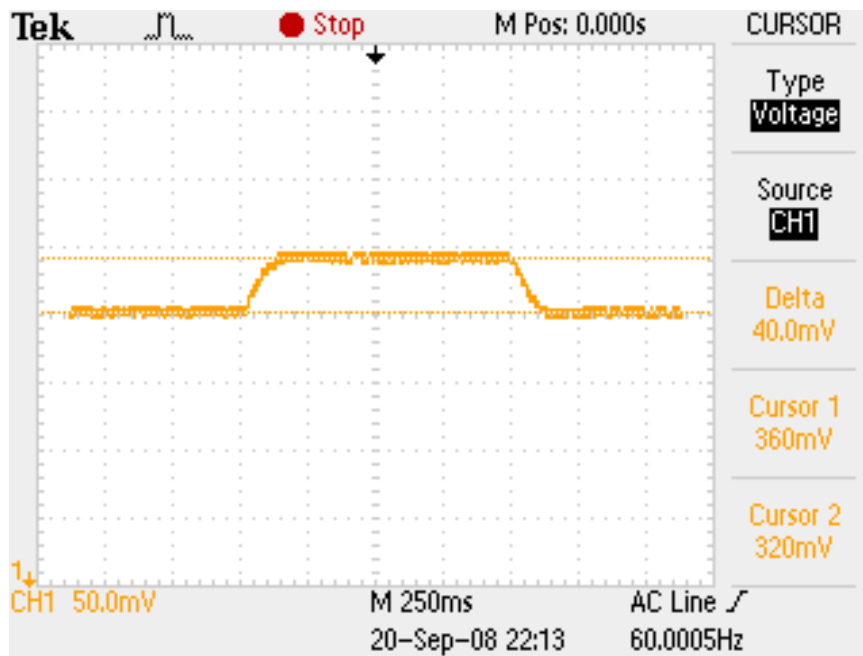


Figure 69: Experimental result of closed-loop operation, 20V voltage change

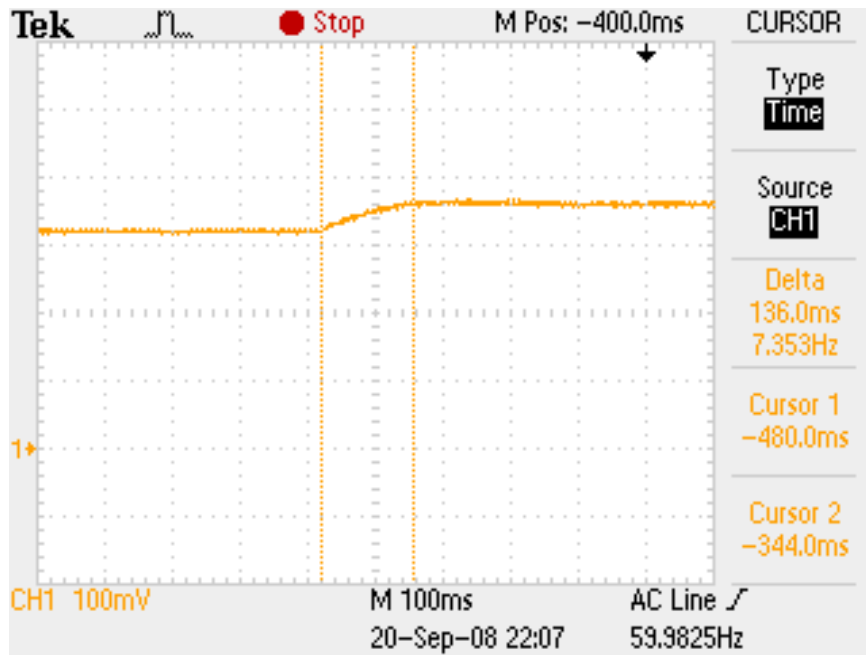


Figure 70: Experimental result of closed-loop operation, first step change

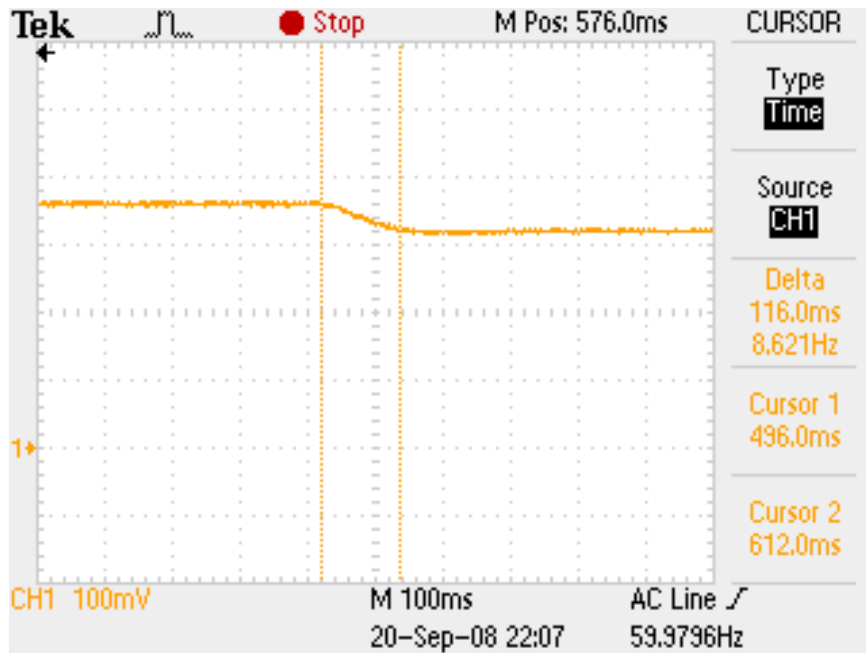


Figure 71: Experimental result of closed-loop operation, second step change



The calculation time consumptions of each functional block in the closed-loop control diagram (see Fig. 35) are estimated from the experiment and shown in Table XIV.

TABLE XIV: FUNCTION BLOCK TIME CONSUMPTION

Function	Time
Reference Calculator	10~20 $\mu$ S
Reference Generator	$\approx$ 25 $\mu$ S
Hysteresis Control	<10 $\mu$ S
Synchronization	<2 $\mu$ S
Voltage/Current Capture	<2 $\mu$ S
Total	50~60 $\mu$ S

According to the results in Table XIV, the minimum feasible sampling time is 60  $\mu$ S. Therefore, the theoretical maximum switching frequency  $f_{\max} = 8.33$  kHz. Fig. 72 shows the measured maximum switching frequency  $f_{\max} = 8.33$  kHz.

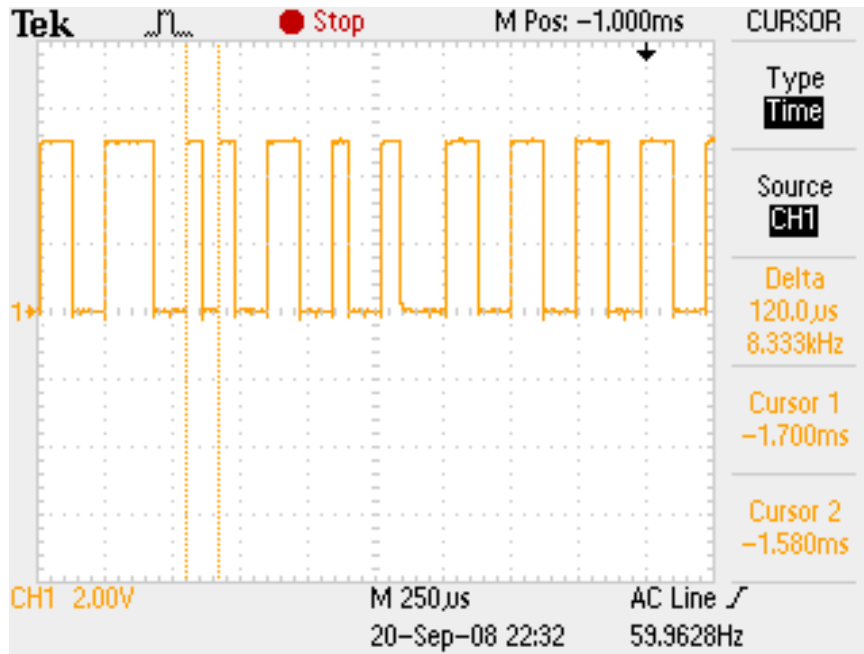


Figure 72: Measured switching frequency in closed-loop operation

### 4.2.3 Analysis of the Experimental Results

Experimental results from the Lab-Volt IGBT bridge prove the effectiveness of harmonic elimination using the proposed control method. The closed-loop operation is performed by adding a feedback loop and updating reference currents in real time. As a result, controllable DC link voltage is obtained. In the steady state, there are no low-order harmonic components in the input line currents and DC link voltage under unbalanced operating conditions.

To conclude, the proposed control method is a generalized method. The three-phase PWM boost type rectifier can achieve low-order harmonic elimination as well as unity input power factor even under extreme operating conditions.

## **CHAPTER V**

### **CONCLUSIONS AND FUTURE WORK**

This thesis implements a proposed generalized control method on a three-phase PWM boost type rectifier to achieve harmonic elimination under extremely unbalanced operating conditions. When the input is not balanced, low-order harmonics appear at the input and output of the three-phase PWM boost type rectifier. A proposed method of harmonic elimination under general input conditions is presented and analyzed. The proposed algorithm and control method are implemented on a DSPACE digital control system coupled with MATLAB Simulink. The results of simulation and experimentation prove that with the proposed method, high quality input and output waveforms of three-phase PWM boost type rectifier are obtained under unbalanced operating conditions.

The method is valid in general cases as long as the following two requirements are satisfied:

- Input voltage and input impedance of one phase are not equal to zero at the same time.
- Switching functions must be equal to or less than one to ensure practically valid analytical solutions.

Simulation results demonstrate the PWM boost type rectifier can achieve stable operation with effective harmonic elimination under unbalanced operating conditions when the proposed method is applied. A laboratory prototype is designed to verify the analysis and simulation results. Experimental results show this method removes low-order harmonics at the input-output sides of the PWM boost type rectifier and provides almost unity power factor. DC link voltage can be adjusted by updating the reference currents in real time through a feedback loop.

It is shown that the three-phase PWM boost type rectifier can be operated using a single-phase power supply or a center-tapped transformer (two extremely unbalanced cases) when the proposed method is applied. This is a very meaningful observation. It means the PWM boost type rectifier can still obtain high quality input and output characteristics when a three-phase voltage source is not available.

For the same power level and the same input voltage, the losses in the PWM boost type rectifier (semiconductor devices) increase as the level of imbalance in input voltages and input impedances increase. This is to be expected since the current level in all three phases increase with the level of imbalance. This should be considered when the PWM boost type rectifier is designed to operate under fault conditions or if it is supplied from the center-tapped transformer. The fact that losses increase during the abnormal operation of the rectifier is not an issue since the fault will be eliminated and the rectifier will return to its normal operation. The load will not be affected during the fault condition.

The dynamic response of the PWM boost type rectifier under unbalanced operating conditions should be investigated and experimentally verified. Only steady-state performance is studied in this thesis.

## REFERENCES

1. R. Rocha and L. de Siqueira Martins Filho, "A discrete current control for PWM rectifier," *Proc. IEEE Intl. Sym. on Industrial Electronics*, vol. 2, pp. 681-686, Jun. 2005.
2. X. Wu, S. K. Panda, and J. Xu, "Analysis and Experimental Validation of the Output Voltage and Input Current Performances in Three Phase PWM Boost Rectifiers Under Unbalanced and Distorted Supply Voltage Conditions," *2007 Intl. Conf. on Control Applications*, pp. 605-610, Oct. 2007.
3. P. Tenti, L. Malesani, L. Rossetto, D. Ciscato, G. L. Basile, M. Pasti, and F. Voelker, "PWM rectifier with low voltage ripple for magnet supply," in *Proc. IEEE-IAS Annual Meeting*, Seattle, WA, 1990, pp. 1017-1023.
4. L. Rossetto and P. Tenti, "AC/DC PWM converter with sinusoidal ac currents and unity power factor for dc motor drives," in *Proc. Int. Conf. Electrical Machines*, (ICEM 88), Pisa, Italy, Sept. 1988, pp. 313-318.
5. T. A. Lipo, "Recent progress in the development of solid-state ac motor drives," *IEEE Trans. Power Electron.*, vol. 3, no. 2, pp. 105-117, Apr. 1988.
6. S. Nonaka, K. Kesamaru, K. Yamasaki, and M. Nishi, "Interconnection system with single phase IGBT PWM CSI between photovoltaic arrays and the utility line," in *Proc. IEEE-IAS Annual Meeting*, Seattle, WA, 1990, pp. 1302-1307.
7. E. Muljadi, R. Schiferl, and T. A. Lipo, "Induction machine phase balancing by unsymmetrical thyristor voltage control," *IEEE Trans. Ind. Appl.*, vol. IA-21, pp. 669-678, May/June 1985.
8. L. Moran, P. D. Ziogas, and G. Joos, "Design aspects of synchronous PWM rectifier-inverter systems under unbalanced input voltage conditions," *IEEE Trans. Industry Applications*, vol. 28, issue 6, pp. 1286-1293, Nov.-Dec. 1992.
9. P. N. Enjeti and S. A. Choudhury, "A new control strategy to improve the performance of a PWM AC to DC converter under unbalanced operating conditions," *IEEE Trans. Power Electronics*, vol. 8, issue 4, pp. 493-500, Oct. 1993.
10. P. Verdelho, "Voltage type reversible rectifiers control methods in unbalanced and nonsinusoidal conditions," *Proc. Conf. Rec. IECON'98*, pp. 479-484, 1998.
11. P. Rioual, H. Pouliquen and J. P. Louis, "Regulation of a PWM rectifier in the unbalanced network using a generalized model," *IEEE Trans. Power Electron.*, vol. 11, pp. 495-502, May, 1996.
12. H. Song and K. Nam, "Dual current control scheme for PWM converter under unbalanced input voltage conditions," *IEEE Trans. Ind. Electron.*, vol. 46, pp. 953-959, Oct, 1999.

13. A. V. Stankovic and T. A. Lipo, "A generalized control method for input-output harmonic elimination for the PWM boost rectifier under simultaneous unbalanced input voltages and input impedances," *Proc. IEEE Conf. PESC 2001*, vol. 3, pp. 1309-1314, Jun. 2001.
14. A. V. Stankovic, "Input-Output Harmonic Elimination of the PWM Boost Type Rectifier Under Unbalanced Operating Conditions," Ph.D. dissertation thesis, at the University of Wisconsin-Madison, 1998.
15. Y. S. Suh, V. Tijeras, and T. A. Lipo, "A control method in dq synchronous frame for PWM boost rectifier under generalized unbalanced operating conditions," in *Proc. IEEE PESC*, 2002, pp. 1425-1430.
16. Y. Suh, V. Tijeras, and T. A. Lipo, "A nonlinear control of the instantaneous power in dq synchronous frame for PWM AC/DC converter under generalized unbalanced operating conditions," *Proc. IEEE-IAS Annual Meeting 2002*, vol. 2, pp. 1189-1196, Oct. 2002.
17. Y. Suh and T. A. Lipo, "Control scheme in hybrid synchronous stationary frame for PWM AC/DC converter under generalized unbalanced operating conditions," *IEEE Trans. Industry Applications*, vol. 42, issue 3, pp. 825-835, May-Jun. 2006.
18. B. Yin, R. Oruganti, S. K. Panda, A. K. S. Bhat, "An Output-Power-Control Strategy for a Three-Phase PWM Rectifier Under Unbalanced Supply Conditions," *IEEE Trans. Industrial Electronics*, vol. 55, issue. 5, pp. 2140 - 2151, May 2008.
19. X. Wu, S. K. Panda, and J. Xu, "Development of a New Mathematical Model of Three Phase PWM Boost Rectifier Under Unbalanced Supply Voltage Operating Conditions," *Proc. IEEE Conf. PESC 2006*, vol. 3, pp. 1-7, Jun. 2006.
20. P. Xiao, K. A. Corzine and G. K. Venayagamoorthy, "Cancellation Predictive Control for Three-Phase PWM Rectifiers under Harmonic and Unbalanced Input Conditions," *Proc. IEEE Conf. IECON 2006*, pp. 1816-1821, Nov. 2006.
21. O. Ojo and Zhiqiang Wu, "A new controller for three-phase boost rectifiers lacking balance in source voltages and impedances," *Applied Power Electronics Conference and Exposition*, vol. 1, pp. 508 - 514, March 2005.
22. D. M. Brod and D. W. Novotny, "Current Control of VSI-PWM Inverters," *IEEE Trans. Industry Applications*, vol. IA-21, issue 3, pp. 562-570, May 1985.
23. Ke Chen, and A. V. Stankovic, "Building a Modern Power Electronics and Electric Machines Laboratory", American Society for Engineering Education (ASEE) Annual Conference, June, 2007.
24. *IR21091(s) & (PbF) data sheet*, data sheet no. PD60191 revD, International IOR rectifier, inc., EI Segundo, CA.

## **APPENDICES**

### A. MATLAB Program for Reference Calculation (open-loop operation)

```

clc
clear

%%%%%%%%%%%%%%%%%%%%%%%%%%%%%%%%%%%%%%%%%%%%%%%%%%%%%%%%%%%%%%%%%%%%%%%%%
%Define three-phase input voltages
U1=60;
U2=60*(cos(-2*pi/3)+j*sin(-2*pi/3));
U3=60*(cos(2*pi/3)+j*sin(2*pi/3));
%Define the three-phase input impedances
f=60;%Default system frequency.
Z1=2*pi*f*0.01j+0.000001j;
Z2=2*pi*f*0.01j;
Z3=2*pi*f*0.01j-0.000001j;
%Define the power setting
S=250;
%%%%%%%%%%%%%%%%%%%%%%%%%%%%%%%%%%%%%%%%%%%%%%%%%%%%%%%%%%%%%%%%%%%%%%%%%
%Reference currents calculation%%%%%%%%%%%%%%%%%%%%%%%%%%%%%%%%%%%%%%%%%%%%%%%%%%%%%%%%%%%%%%%%%%%%%%%%%
%Define the sampling time for the real-time operation.
Ts=0.00002;
%Giving the initial condition
I=zeros(1,3);
%Calculation
Up1=conj(U1);
Up2=conj(U2);
Up3=conj(U3);
Sp=conj(S);

a=((2*Z1*(Up3-Up1)/(Up2-Up1))-((Z1+Z2)*(Up3-Up1)^2/(Up2-Up1)^2)-(Z1+Z3));
b=((U3-U1)-(Up3-Up1)*(U2-U1)/(Up2-Up1))-(2*Z1*Sp/(Up2-Up1))+
(2*Sp*(Z1+Z2)*(Up3-Up1)/(Up2-Up1)^2);
c=(Sp*(U2-U1)/(Up2-Up1))-((Z1+Z2)*Sp^2/(Up2-Up1)^2);

I(3)=(-b-sqrt(b^2-4*a*c))/(2*a);
I(2)=(Sp-I(3)*(Up3-Up1))/(Up2-Up1);
I(1)=-I(2)-I(3);

%Check phase sequence
if angle(I(3))<angle(I(1)) || angle(I(2))>angle(I(1))
    I(3)=(-b+sqrt(b^2-4*a*c))/(2*a);
    I(2)=(Sp-I(3)*(Up3-Up1))/(Up2-Up1);
    I(1)=-I(2)-I(3);
end

%Solve for the reference current
IM=abs(I)*sqrt(2);
IA=angle(I);

```



## B. MATLAB Program for Reference Calculation (closed-loop operation)

```

clc
clear
%%%%%%%%%%%%%%%%%%%%%%%%%%%%%%%%%%%%%%%%%%%%%%%%%%%%%%%%%%%%%%%%%%%%%%%%%
%Define three-phase input voltages
U1=60;
U2=60*(cos(-2*pi/3)+j*sin(-2*pi/3));
U3=60*(cos(2*pi/3)+j*sin(2*pi/3));
%Define the three-phase input impedances
f=60;%Default system frequency.
Z1=2*pi*f*0.01j-0.0001j;
Z2=2*pi*f*0.01j;
Z3=2*pi*f*0.01j+0.0001j;
%Define the power setting
S=250;
%%%%%%%%%%%%%%%%%%%%%%%%%%%%%%%%%%%%%%%%%%%%%%%%%%%%%%%%%%%%%%%%%%%%%%%%%
%Reference currents calculation%%%%%%%%%%%%%%%%%%%%%%%%%%%%%%%%%%%%%%%%%%%%%%%%%%%%%%%%%%%%%%%%%%%%%%%%%
%Define the sampling time of the real-time operation.
Ts=0.00006;
%Giving the initial condition
I=zeros(1,3);
%Calculation
Up1=conj(U1);
Up2=conj(U2);
Up3=conj(U3);
Sp=conj(S);

a=((2*Z1*(Up3-Up1)/(Up2-Up1))-((Z1+Z2)*(Up3-Up1)^2/(Up2-Up1)^2)-(Z1+Z3));

%t1,t2,t3,t4 are interim variables used for real-time calculation
t1=((U3-U1)-(Up3-Up1)*(U2-U1)/(Up2-Up1));
t2=(2*Z1/(Up2-Up1))-((2*(Z1+Z2)*(Up3-Up1)/(Up2-Up1)^2);
t3=(U2-U1)/(Up2-Up1);
t4=((Z1+Z2)/(Up2-Up1)^2);

b=((U3-U1)-(Up3-Up1)*(U2-U1)/(Up2-Up1))-((2*Z1*Sp/(Up2-Up1))+((2*Sp*(Z1+Z2)*(Up3-Up1)/(Up2-Up1)^2);

c=(Sp*(U2-U1)/(Up2-Up1))-((Z1+Z2)*Sp^2/(Up2-Up1)^2);

I(3)=(-b+sqrt(b^2-4*a*c))/(2*a);
I(2)=(Sp-I(3)*(Up3-Up1))/(Up2-Up1);
I(1)=-I(2)-I(3);

%Solve for the reference current
IM=abs(I)*sqrt(2);
IA=angle(I);

```

### C. Simulink Model of DC Link Voltage Control

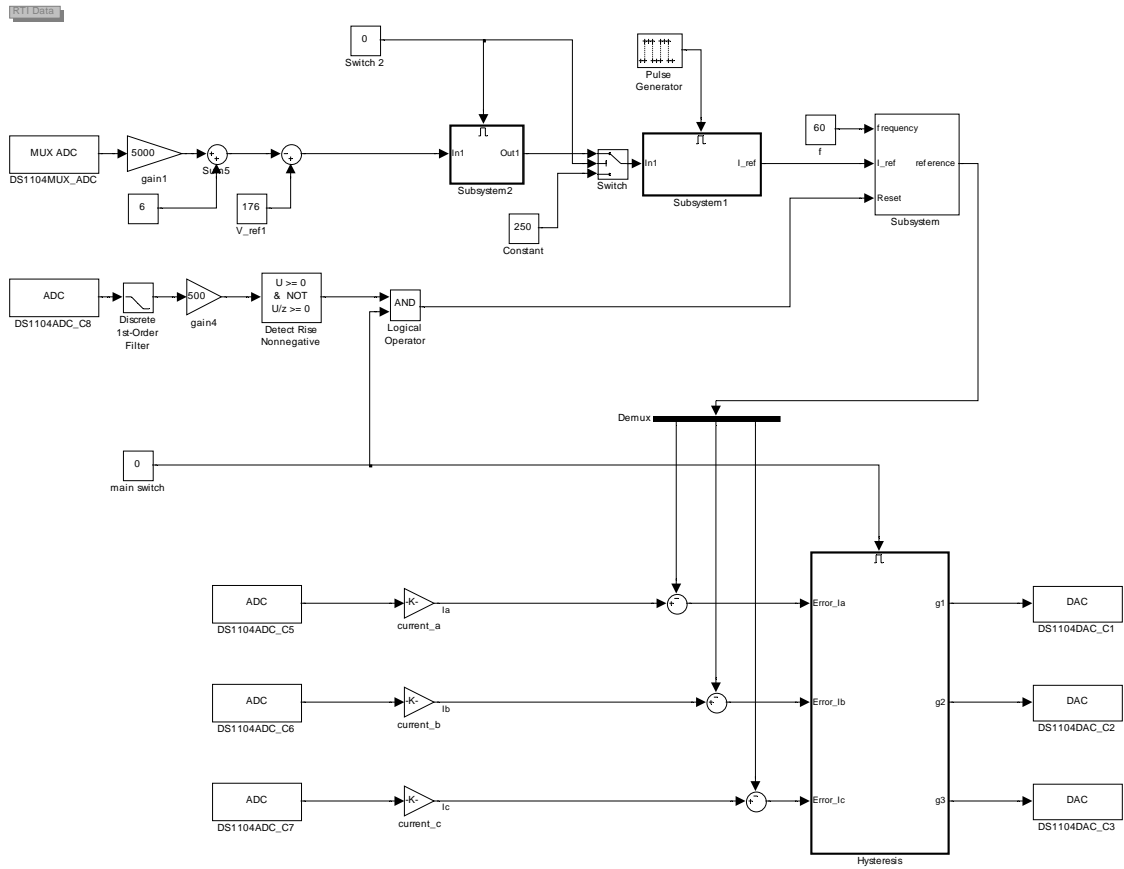


Figure 73: Diagram of main model for DC link voltage control

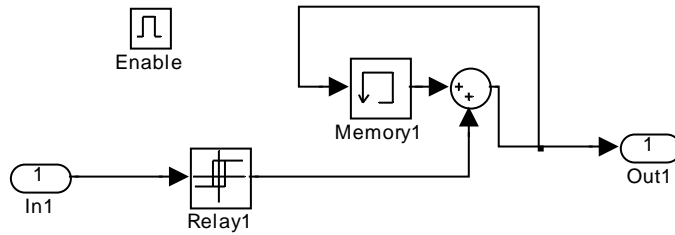


Figure 74: Diagram of DC voltage error feedback block

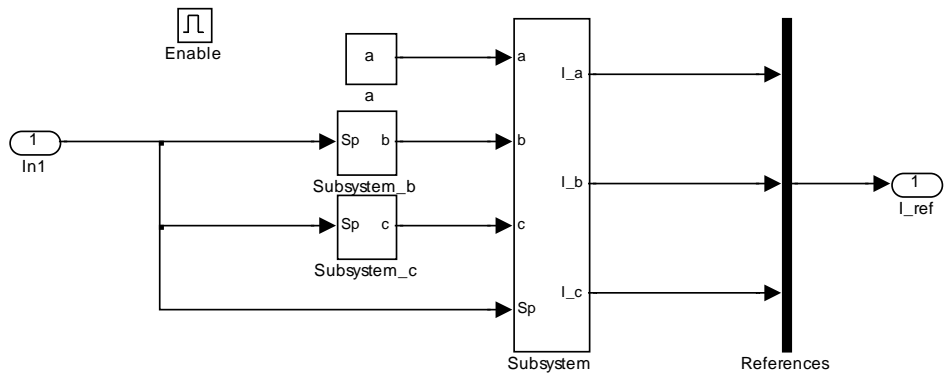


Figure 75: Diagram of real-time reference calculation block

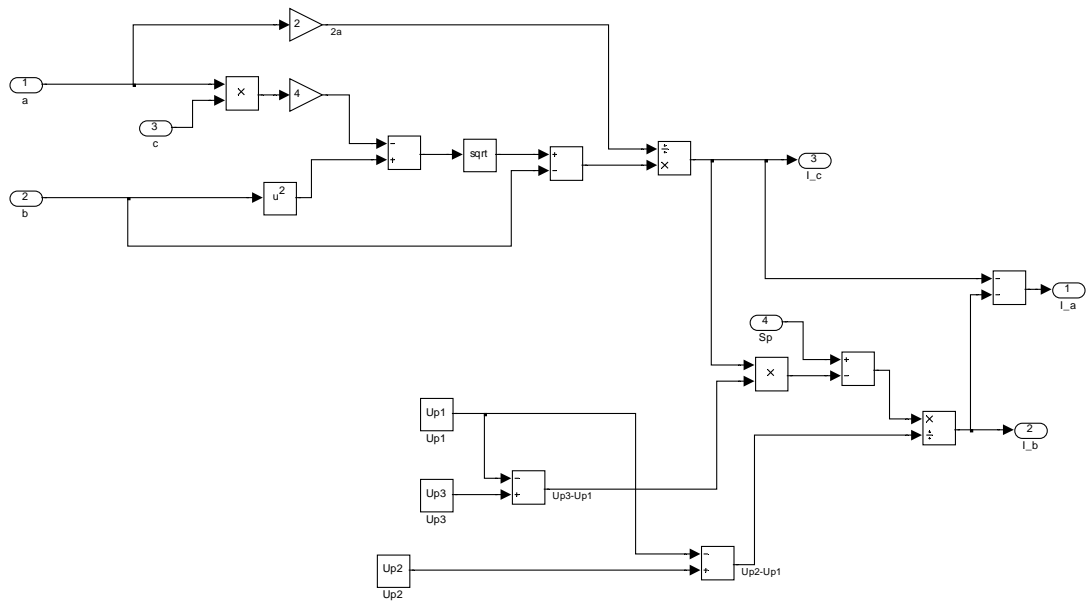


Figure 76: Diagram of real-time reference currents generation block